Dissertation zur Erlangung des Doktorgrades
der Fakultät für Chemie und Pharmazie
der Ludwig-Maximilians-Universität München

Measuring mechanical tension across the focal adhesion protein talin-1

Katharina Anneliese Austen

aus
München, Deutschland

2016

Erklärung

Diese Dissertation wurde im Sinne von § 7 der Promotionsordnung vom 28. November 2011 von Herrn Prof. Dr. Reinhard Fässler betreut.

Eidesstattliche Versicherung

Diese Dissertation wurde eigenständig und ohne unerlaubte Hilfe erarbeitet.

München, 31. Mai 2016

.....

(Katharina Anneliese Austen)

Dissertation eingereicht am …03.06.2016.....

1. Gutachter: …Prof. Dr. Reinhard Fässler.....

2. Gutachter: …Prof. Dr. Martin Biel.....

Mündliche Prüfung am …19.07.2016.....

Table of contents

Summary

Cell adhesion is an essential mechanism involved in many cellular processes, such as migration, proliferation and differentiation. The mechanical linkage between extracellular matrix and the f-actin cytoskeleton is mediated in specialized protein complexes, called focal adhesions. Key components of these cellular compartments are members of the integrin protein family; transmembrane proteins that connect to ligands in the extracellular matrix and recruit intracellular focal adhesion proteins. However, integrins have no catalytic function and cannot bind cytoskeletal components. The association with f-actin is mediated by intracellular adaptor molecules that link integrin tails and the cytoskeleton. These adhesion complexes not only mediate association with the extracellular matrix, but also serve as the mechanosensitive units of the cell. It has been known for some time that mechanical stimuli – as for example tissue rigidity – are epigenetic factors, regulating processes like organ development and stem cell differentiation. However, even though single components of the adhesion complex have been demonstrated to be involved in mechanosensitive processes, central mechanisms in mechanosensing through focal adhesions remained unknown.

One of the major components responsible for the integrin-f-actin connection is the focal adhesion protein talin-1. Talin-1 directly binds intracellular integrin tails but also carries three f-actin binding sites and thus directly mediates the connection between extracellular matrix and the cytoskeleton. Besides its important role as integrin activator – and thus important promotor of integrin mediated adhesion – talin-1 has long been suspected as a mechanosensitive component in focal adhesions. Still, evidence of a regulatory role of talin-1 in mechanosensing in adhesive cells is still missing due to the lack of appropriate techniques.

Using two single-molecule-calibrated FRET (Förster resonance energy transfer) based tension sensors, it could be demonstrated in this work that talin-1 is indeed subject to low-piconewton (pN) forces in integrin mediated adhesion processes. When localized in focal adhesion talin−1 bears forces of 7-10 pN. Regulation of talin-1 forces occurs through association with f-actin, either direct or indirect via binding of vinculin, a talin−1 interactor that strengthens the connection of talin−1 with the actin cytoskeleton. Disturbing the mechanical linkage of integrins to f-actin via talin−1 does not prevent integrin activation, but leads to defects in cell spreading and focal adhesion reinforcement. Furthermore, it could be shown that mechanical resilient linkages through talin−1 in focal adhesions are important for extracellular rigidity sensing.

Taken together this work provides strong evidence that talin-1 mediated mechanical linkage between the extracellular matrix and the actin cytoskeleton is essential in mechanosignaling processes. For the first time it could be shown that talin-1 is subject to pN forces in living cells and that the force transmission is indeed dependent on f-actin and vinculin association with talin-1.

Zusammenfassung

Adhäsion von Zellen mit Komponenten der extrazellulären Matrix ist eine wichtige Eigenschaft für viele zelluläre Prozesse wie Migration, Proliferation und Differenzierung. Die Verbindung zwischen extrazellulärer Matrix und dem Aktin Cytoskelett wird in spezialisierten Proteinkomplexen, so genannten fokalen Adhäsionen, vermittelt. Eine zentrale Rolle in diesen Adhäsionen stellen Mitglieder der Integrin-Proteinfamilie dar. Integrine sind Transmembranproteine, die einerseits extrazelluläre Liganden binden, sowie intrazellulär die Rekrutierung von Komponenten des Adhäsionskomplexes anregen. Integrine haben keine intrinsische katalytische Funktion und können nicht direkt mit dem Cytoskeletts interagieren. The Verbindung zu Aktinfilamenten wird daher durch Adaptermoleküle hergestellt, die die intrazellulären Anteile von Integrinen mit dem Cytoskelett verbinden. Diese Adhäsionskomplexe sind hierbei nicht nur verantwortlich für die Verbindung zwischen extrazellulärer Matrix und dem Cytoskelett, sondern dienen auch als mechanosensitive Einheiten der Zelle. Es ist schon länger bekannt, dass mechanische Reize – zum Beispiel die Steifigkeit des umliegenden Gewebes – epigenetische Faktoren darstellen, die wichtige Prozesse wie Organentwicklung oder Stammzelldifferenzierung regulieren. Obwohl bereits gezeigt wurde, dass einzelne Komponenten von Adhäsions-komplexen in mechanosensitive Prozesse involviert sind, blieben die zentralen Mechanismen, wie mechanische Reize in der Zelle verarbeitet werden, bislang unbekannt.

Eine Hauptkomponente in fokalen Adhäsionen ist Talin-1. Es stellt eine direkte Verbindung zwischen Integrinen und dem Aktin Cytoskelett her, da es sowohl Integrin- als auch Aktinbindestellen besitzt. Neben seiner wichtigen Rolle als Integrinaktivator wurde eine mechanosensitve Funktion von Talin-1 in fokalen Adhäsionen schon länger vermutet. Dennoch war, vor Allem aufgrund fehlender Analysetechniken, bisher kein Beweis für die regulatorische Rolle von Talin-1 in mechanosensitiven Prozessen in fokalen Adhäsionen lebender Zellen vorhanden. Mithilfe zweier kalibrierter, FRET (Förster-Resonanzenergietransfer) basierter Kraftsensoren konnten in dieser Studie zum ersten mal direkt Kräfte auf Talin-1 im unteren Piconewton (pN) Bereich nachgewiesen werden. Ist Talin-1 in Integrin positiven fokalen Adhäsionen verankert, lasten Kräfte von 7-10 pN auf dem Protein. Diese Kräfte werden durch die Bindung zum Cytoskelett reguliert, die sowohl direkt als auch indirekt durch die Verbindung über Vinculin etabliert wird. Durch Vinculin, einem Protein das sowohl Talin-1 als auch Aktin bindet, wird die Interaktion der beiden Moleküle noch verstärkt. Wird die mechanische Kopplung von Integrinen mit Aktin durch

Talin-1 zerstört, bleibt die Aktivierung von Integrinen unbeeinflusst, allerdings sind zelluläre Prozesse wie beispielsweise das Ausbreiten der Zelle auf ihrem Untergrund stark beeinträchtig. Weiterhin konnte gezeigt werden, dass mechanisch stabile Verbindungen durch Talin-1 in fokalen Adhäsionen eine wichtige Rolle in der zellulären Wahrnehmung ihrer extrazellulären Rigidität spielen.

List of abbreviations

Abbreviation	full name
µg	micro gram
µl	micro litre
aa	amino acid
ABS	actin binding site
APS	ammonium peroxisulfate
ATP	adenosine-triphosphate
BCA	bicinchoninic acid
Bis	Bisacrylamide
bp	base pair
BSA	bovine serum albumine
CCD	charge coupled device
cDNA	complementary DNA
cTS	C-terminal tension sensor
DNA	deoxyribonucleic acid
DAPI	4', 6-Diamidin-2-phenylindol-dihydrochloride
DD	dimerization domain
DMEM	Dulbecco's Modified Eagle Medium
DMSO	dimethylsulfoxide
dNTP	deoxynucleotide-triphosphate
ECM	extracellular matrix
EDTA	ethylene-diamine-tetraacetic acid
EGF	epidermal growth factor
F40	flagelliform peptide
FA	focal adhesion
f-actin	filamentous actin
FAK	focal adhesion kinase
FCS	fetal calf serum
FERM	four-point-one, ezrin, radixin, moesin
FN	fibronectin
FRET	Förster resonance energy transfer
g	gram
GFP	green fluorescent protein
h	hour
HCl	hydrochloric acid
IBS	integrin binding site
iTS	internal tension sensor
KO	knock out
LZ	leucine zipper
M	molar
Mg	Magnesium
min	minute
MLC	myosin light chain
mM	millimolar

Abbreviation	full name
Mn	Manganese
NaCl	sodium chloride
nm	nanometer
NMR	nuclear magnetic resonance
O/N	over night
OD	optical density
PAA	polyacrylamide
PBS	phosphate buffered saline
PCR	polymerase chain reaction
PFA	paraformaldehyde
PH	pleckstrin homology
PIP2	phosphatidylinositol (4,5) bisphosphate
PIP3	phosphatidylinositol (3,4,5) trisphosphate
PIPK1γ	PIP kinase type 1γ
PVDF	polyvinylidene fluoride
RFP	red fluorescent protein
RNA	ribonucleic acid
ROCK	Rho kinase
RPM	rotations per minute
RT	room temperature
SDS	sodium dodecyl sulphate
SDS-PAGE	SDS polyacrylamid gel electrophoresis
shRNA	short hairpin RNA
siRNA	small interfering RNA
TAE	Tris-acetic acid-EDTA buffer
Taq	Thermophilus aquaticus
TBS	Tris-buffered saline
TCSPC-FLIM	Time-correlated single photon counting - fluorescence lifetime microscopy
TE	Tris-EDTA buffer
TEMED	N,N,N',N'-Tetramethylethylenediamine
TFM	traction force microscopy
TMD	transmembrane domain
Tris	Tris (hydroxymethyl) aminomethane
U	Unit
UV	ultra violet
V	Volt
VBS	vinculin binding site
VH	Villin headpiece
WT	wild type
YPet	yellow fluorescent protein for FRET

1 Introduction

1.1 Mechanotransduction

1.1.1 Mechanotransduction is a universal cell feature

Sensing of and responding to mechanical stimuli is a fundamental property of cells that is central to many developmental, homeostatic and pathological processes. Forces in biological systems are manifold and occur in many forms such as stretch, shear or compression. Many of these mechanical signals are detected by specialized cell surface receptors or ion-channels and propagated into the cell to be converted into biochemical signaling cascades that regulate fundamental processes like migration, proliferation or differentiation. Not surprisingly, misregulation in mechanosensing and mechanotransduction have been associated with pathologic processes during tumor formation, Atherosclerosis, Osteoporosis and Rheumatoid arthritis[1]. As a result, the field of mechanobiology engulfs a wide range of disciplines, ranging from cell biology and developmental biology to clinical research. Common to these very different research fields is that the underlying biological processes are, in most cases, occurring on the cellular level and share the same physical principles. Therefore, the analysis of mechanosensitive processes and thus subcellular forces has become of great interest. However, owing to the lack of suitable techniques to measure mechanical forces within cells, very little is known about the molecular mechanisms that govern cellular mechanotransduction.

1.1.2 Physical forces trigger cellular functions

Cells react to changes in their mechanical environment in various ways, depending on the cell type and extracellular stimulus.

A well-studied example is the mechanotransduction of hair cells in the inner ear. Bundles of 50-60 stereocilia protrude from the apical hair cell membrane of the sensory macula and are dislocated through acoustic waves that arrive at the inner ear. The stereocilia in one bundle are connected via so called tip-link proteins, including cadherin 23 and proto-cadherin 15, to potassium ion channels of the neighboring cell such that dislocation of the bundle results in a deflection of the stereocilia and opening of the ion channels.

Other stretch activated ion channels have functions in the retention of hydrostatic pressure in bacteria, they mediate the sense of touch in C. elegans and regulate blood pressure regulation in vertebrates[2]. Mechano-sensitive ion-channels can be activated by deformations of the plasma membrane resulting in conformational changes within the ion channel that

permeabilize the pore for their corresponding carrier[3]. Other channels might be directly anchored to intra- or extracellular force bearing structures and respond to displacements of these anchor-proteins[4].

But also other transmembrane proteins serve as a platform for mechanical signaling cascades. In cardiac myocytes, for example, changes in blood flow and pressure are sensed through diverse pathways including G-protein coupled receptors, growth factor receptors and integrin receptors, all leading to the activation of specific transcription factors and driving the expression of mechano-responsive genes that results in proliferation, migration and differentiation of the cardiac tissue[5].

In addition to extrinsically applied forces, cells generate mechanical signals that can be transduced to the extracellular environment such as traction forces generated during cell migration[6]. These forces, generated by contractility of the actomyosin network, can vary between cell types and are furthermore influenced by external factors like substrate rigidity.

Altogether, signal recognition and transmission of the mechanical information into, within and out of cells is complicated involving numerous signaling cascades that are cell type and -function dependent.

1.1.3 Mechanical stimuli are converted into intracellular signaling pathways

As mentioned before, mechanical stimuli are not exclusively external signals but can also be derived from intra- or intercellular events. The process of cellular rigidity sensing and mechanosignaling, for instance, involves numerous pathways and can be generally divided into two partially overlapping processes: a passive outside–in and an active inside–out signaling. Whereas in the former case cells respond to externally generated forces[7], they can also actively modulate their environment in the latter case [8], e. g. by changes in protein surface expression and activation[9].

Interestingly, mechanosignaling often involves a close interaction between outside–in and inside–out signaling. A well-studied example for the complex interaction between both is the substrate-rigidity dependent relocalization of YAP (Yes-associated protein) and TAZ (transcriptional co-activator with PDZ-binding motif), effectors of the Hippo pathway, from the cytosol into the nucleus. Substrate rigidity information e. g. is transduced via the f-actin cytoskeleton, triggers downstream kinase activity that influences the phosphorylation state of YAP and TAZ. This phosphorylation, in turn, determines affinity states for cytosolic interaction partners and the translocation of these transcription factors into the nucleus. Here, YAP and TAZ trigger the expression of force related genes that affect proliferation, survival and differentiation processes[10].

1.1.3.1 Coupling of intra- and extracellular force responses occurs in specialized cellular compartments

In order to sense and respond to mechanical stimuli, cells need to connect the contractile elements of the cytoskeleton with extracellular components. By the formation of the extracellular-intracellular linkage, cells generate traction forces, a direct consequence of motor protein activity that is distributed over a large protein network[11]. F-actin filaments are coupled with intracellular adaptor proteins in complexes called focal adhesions. Proteins embedded in those anchoring networks were shown to bear piconewton (pN) forces[12-14], stretch ECM proteins[15] and change interaction partners in a stretch dependent manner[16]. In most cases, proteins under moderate forces show a modified structure-function relationship by reaching an intermediate unfolding conformation. As a consequence, mechanosignaling proceeds either by the exposure of cryptic binding sites or masking of interaction sites in mechanosensitive proteins and thus translation of the mechanical signal into specific biochemical pathways[11]. However, underlying mechanisms of how mechanical information is propagated through focal adhesions remain only poorly understood. This study focuses on the unraveling of force propagation in a specific adhesion protein, called talin-1, to investigate the process of mechanotransduction in these structures in more detail.

1.2 Focal adhesions: Mechanosensitive compartments of the cell

Cell adhesion to the extracellular matrix is established in subcellular compartments called focal adhesions (FAs). FAs are complex structures, connecting the extracellular matrix (ECM) with, in most cases, the f-actin network of the cytoskeleton. Although the general structure of FAs has been studied intensively, mechanistic insight into force propagation across those protein complexes was still missing.

1.2.1 Focal adhesions are complex structures established by integrins

1.2.1.1 Integrin are heterodimeric transmembrane receptors without intrinsic enzymatic activity

The cellular connections between the intracellular cytoskeleton and ECM components are established by the integrin receptors family, a set of heterodimeric transmembrane domain (TMD) proteins composed of an α and a β subunit. Depending on the α/β subunit composition, integrins engage specific extracellular ligands and intracellularly connect to the cytoskeleton. Importantly, integrins lack intrinsic enzymatic activity[17,18] and cannot directly bind f-actin or myosins[19,20]. . Instead, a set of downstream adaptor molecules serves as intracellular signaling platform that mediate the physical linkage to the cytoskeleton, but also administer ligand affinity states of integrins [21].

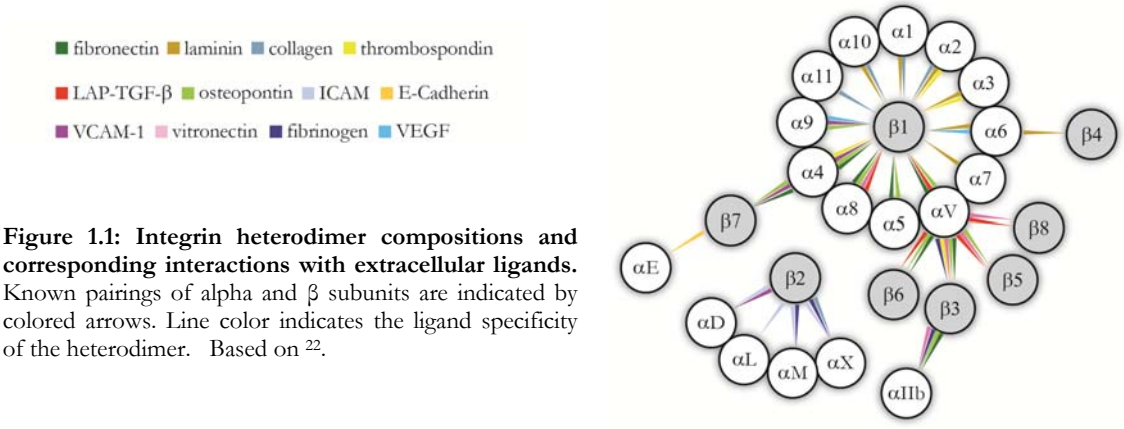

Figure 1.1: Integrin heterodimer compositions and corresponding interactions with extracellular ligands. Known pairings of alpha and β subunits are indicated by colored arrows. Line color indicates the ligand specificity of the heterodimer. Based on [22].

In vertebrates, the integrin superfamily comprises 8 β and 18 α subunits forming 24 sets of heterodimers with specificity to various types of extracellular ligands e. g. ECM components such as fibronectin (FN), laminins or collagens but also other cell surface receptors like VCAM-1 or ICAM for heterotypic cell-cell adhesion (Figure 1.1). Knockout studies of single integrin subunits revealed widespread, nonredundant functions of integrins ranging from defects in preimplantation development, to affected leukocyte function, bone remodeling and

angiogenesis[23]. All integrins heterodimers connect to the f-actin cytoskeleton, apart from α6β4, which is establishing the laminin-keratin filament connection in epithelial cells. In addition, integrins do not only serve as attachment sites for extracellular ligands but also act as (co-)receptors in adhesion related signaling cascades[20] thus they are involved in many different cellular functions such as survival, proliferation and transcriptional control.

1.2.1.2 Integrin activation is mediated by talins and kindlins

Integrin heterodimers are thought to exist in at least 3 different affinity states (low-, intermediate-, and high affinity) characterized by the conformation of the ectodomain, the transmembrane domain (TMD) and the cytoplasmic tail. The low affinity state is characterized by a 'bent' conformation of the ectodomains and a close association of the TMD. The process of 'integrin activation' involves a series of conformational changes of the ligand-binding ectodomains as well as the TMDs of both subunits (Figure 1.2) , induced by either intracellular binding proteins of talin or kindlin families or extracellular binding of cations (Mg^{2+}, Ca^{2+} or Mn^{2+})[18,24].

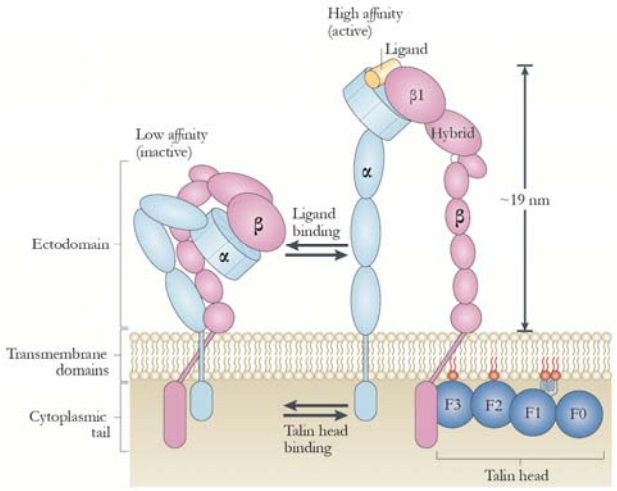

Figure 1.2 Schematic model for integrin activation by the talin FERM domain. In the low affinity state, ectodomains of both integrin subunits (α and β) exist primarily in a bent conformation with interaction between residues in the TMDs. Upon binding of the F3 binding site in the talin head domain (and also kindlin) TMDs get separated and consequently ectodomains adopt an extended conformation with high affinity for ligand binding. (Adapted from [25])

Both TMDs of α and β subunit interact at two distinct sites within the membrane, the inner and the outer membrane clasp, resulting in a characteristic angle of the β subunit TMD (~ 25° relative to the normal axis of the membrane), as shown for β3 integrins[21]. The rather short cytoplasmatic tails of β subunits (40-60 aa[20]) contain two phosphotyrosine-binding (PTB) motifs: a membrane distal NxxY and a proximal NPxY motif[19]. Whereas kindlins interact with the distal NxxY motif, talins bind the integrin β tail in the proximal NPxY (except β4, β6, and β8)[20,26]. Even though both proteins were shown to act as direct integrin activators, kindlins seem to form a signaling platform through paxillin[27] whereas talins serve as scaffolding proteins for other important FA components[26]. Both proteins seem to act synergistically, as it

was shown that in the absence of kindlin-2 in embryonic stem cells[61] and kindlin-3 in platelets[62], talin-1 is insufficient to fully activate integrins[28,29]. Conversely, depletion of talin-1 cannot be compensates by the presence of kindlins[27]. For most subunits the actual mechanism of integrin activation has not been analyzed, but structural as well as FRET and biochemical cross linking studies have provided evidence for activation of αvβx or αIIbβ3 integrins[30,31]. In almost all proposed models, intracellular binding of talin or kindlin 'primes' integrin ectopic domains for ligand binding into the intermediate affinity state conformation. Ligand binding itself further separates both subunits, leading to increased stabilization of the extended high affinity state.

An interesting feature of integrins is their potential ability to form mechanically resilient linkages. For α5β1 heterodimers it has been shown that integrin-ligand interaction was strengthened by the application of force and thus was among the first 'catch-bond' - linkages that are characterized by an increase in bond-lifetime under mechanical load[32]. Altogether, integrin activation is central to many cellular processes such as cell migration[33], platelet activation[34], leukocyte recruitment[35] and the formation of integrin-based adhesion structures is strictly regulated and tightly coupled with the functionality of integrin-associated proteins.

1.2.1.3 FAs are assembled in function related layers

FAs comprise a large number of proteins. Whereas conventional pull down and in silico studies suggested a number of approximately 160 proteins in the adhesome [36], proteomics studies revealed an interactome containing hundreds to more than thousand proteins that are at least transiently associated with FAs[37]. Besides the integrin activators talin and kindlin, a complex network of interacting proteins is assembled downstream of integrins that regulates adhesion complex formation and maturation as well as diverse signaling events triggered by cell adhesion, migration or rigidity sensing. Though mature adhesions can be stable for minutes up to several hours, protein turnover of single components within the complexes can be very fast[38]. Still, individual components are immobilized differentially due to their individual function.

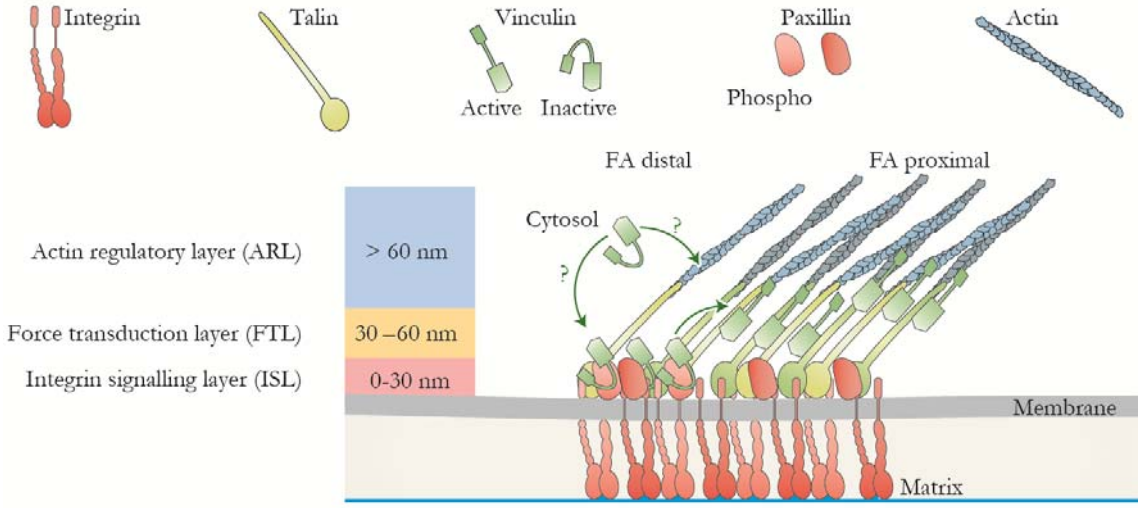

Figure 1.3: Lateral organization of FAs. Integrin positive adhesions are organized in function related layers. Membrane proximal, talin heads as well as inactive vinculin and paxillin accumulate at the integrin cytoplasmic tails in the integrin signaling layer (ISL). In the medial layer (FTL), talin rod domains and other force transducing proteins, like active vinculin, accumulate, whereas in the actin regulatory layer (ARL) processes involved in cytoskeletal reorganization take place. (Image was modified from [39])

Among key players of adhesion formation and maturation are vinculin and paxillin. These FA resident proteins can be localized to early adhesion structures (called nascent adhesions) and influence FA dynamics[38]. Tightly regulated cooperation of scaffolding and mechanosensitive proteins with FA-associated kinases like Src and FAK conveys adhesion dependent signaling[40]. Data from high resolution imaging experiments (e. g. interferometric PALM) suggest an axial layered FA sub-structure where different processes of integrin mediated signaling take place in different FA compartments (Figure 1.3). Binding of integrins to the ECM occurs in the extracellular layer, followed by an integrin signaling layer composed of the talin head subunits that mediate recruitment of FAK as well as paxillin and inactive vinculin. Force transduction subsequently takes place in a layer enriched for talin rods and active vinculins that passes into an f-actin regulatory layer enriched for VASP and zyxin[41]. Components of the inner layers, like talin C-terminal domains and vinculin are actively pulled by the f-actin (retrograde) flow and therefore localized rearward compared to integrin cytoplasmic tails, suggesting that these elements of FA protein complexes are presumably under force. These findings underline the importance of FAs not only in cell adhesion pathways but also force sensing and transmission processes of the cell. However, mechanistic insight in force-related signaling remains sparse.

1.2.1.4 The f-actin cytoskeleton is anchored to integrins in FAs

Anchoring of ECM components to the f-actin cytoskeleton is one of the main functions of FAs. Furthermore, sensing and transmission of intracellularly generated forces, exerted by the actin cytoskeleton is an essential factor for many cellular processes, such as attachment and migration. Thus, architecture and protein composition of the cytoskeleton are important for mechanosensitive processes in the cell and will be shortly introduced below.

Actin filaments (f-actin) are large fibrous complexes comprised of globular but asymmetrical actin subunits (g-actin). The filaments are helical bundles of 5-9 nm in diameter and 166.15° axial rotation between subunits[42] with an intrinsic polarity, a plus (barbed) and a minus (pointed) end[43]. Through interaction with various interaction partners – such as the Arp2/3 complex, formins[44] or ADF/cofilin – f-actin fibers are assembled and disassembled in a ATP dependent manner (Figure 1.4).

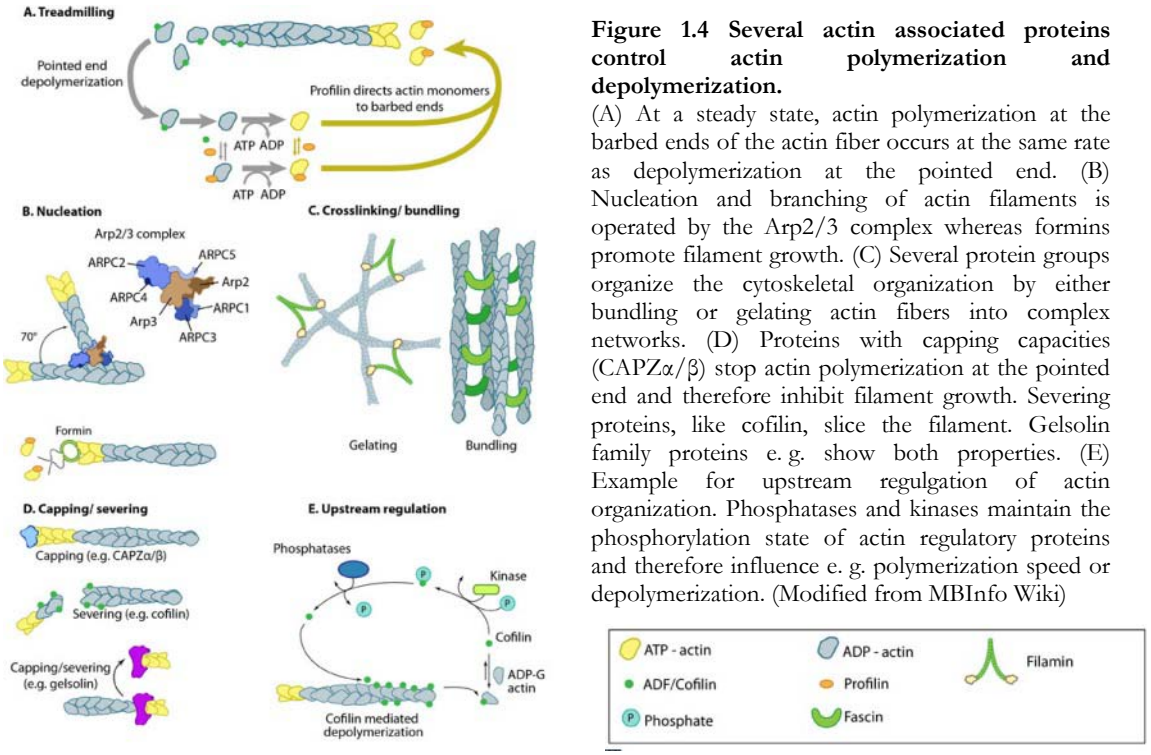

Figure 1.4 Several actin associated proteins control actin polymerization and depolymerization.
(A) At a steady state, actin polymerization at the barbed ends of the actin fiber occurs at the same rate as depolymerization at the pointed end. (B) Nucleation and branching of actin filaments is operated by the Arp2/3 complex whereas formins promote filament growth. (C) Several protein groups organize the cytoskeletal organization by either bundling or gelating actin fibers into complex networks. (D) Proteins with capping capacities (CAPZα/β) stop actin polymerization at the pointed end and therefore inhibit filament growth. Severing proteins, like cofilin, slice the filament. Gelsolin family proteins e. g. show both properties. (E) Example for upstream regulgation of actin organization. Phosphatases and kinases maintain the phosphorylation state of actin regulatory proteins and therefore influence e. g. polymerization speed or depolymerization. (Modified from MBInfo Wiki)

Under steady state conditions, f-actin polymerization at the barbed end and depolymerization at the pointed end result in a constant f-actin flow that can occur because the critical concentrations of G-actin at barbed and pointed end are different[45].

This f-actin flow is important for cell protrusion and lamellipodia formation and can be regulated by a group of capping proteins that control polymerization at the barbed end and in some cases, like gelsolin, carry intrinsic severing capacity to disassemble the f-actin fiber[45].

Besides polymerization, other processes like crosslinking (filamin, α-actinin) as well as bundling (fascin) of f-actin fibers by specialized actin binding proteins modulate the organization and hence force bearing capacity of the actin cytoskeleton within the cell[46]. The architecture of the actin network can be influenced by internal signals as well as external stimulations, as it was shown that the application of external stresses leads to a re-orientation of adhesion sites and thus the actin cytoskeleton perpendicular to the stress axis[47,48].

1.2.1.5 Intracellular force generation by the actomyosin network

Force generation at the actin cytoskeleton is established via at least two independent pathways. First, protrusive forces are directly generated by assembly of the f-actin network. The f-actin flow resulting from the polymerization processes actively pushes the plasma membrane in lamellipodia[49,50]. The plasma membrane forms a physical barrier that (together with myosin II contractions within lamellar cortical f-actin network) is accountable for the so called 'retrograde f-actin flow' that occurs with a velocity of about 0.5-1.5 μm min^{-1} at the lamellipodium[51]. Anchorage of these f-actin filaments within FAs and formation of a 'molecular clutch' by membrane associated adaptor molecules is necessary for directed cellular movements and generation of cellular traction forces[52].

Second, contractile forces are exerted on the cytoskeleton by molecular motor proteins [53]. A large number of motor proteins acting on the f-actin cytoskeleton belong to the myosin family and especially myosin II A and B are important in contractile force generation[54]. Through stepwise ATP hydrolysis, myosin-head subunits undergo conformational changes leading to a displacement of two oppositely oriented filaments against each other[55]. ATP hydrolysis dependent stepping of each myosin II motor subunit causes deformations of the F-actin fiber, by displacing it towards the pointed end; hence myosin II uses chemical energy to generate forces along the cytoskeleton. Anchorage of the protrusive end of the fiber in adhesion sites will therefore generate pulling forces in direction of the myosin-displacement[51].

The activity of myosin is tightly regulated through phosphorylation of the light chain subunit through various kinases and phosphatases including myosin light chain kinase, myosin light chain phosphatase[56] as well as other kinases acting downstream of Rho family GTPases and Rho kinase (ROCK); thus inhibition of myosin-related kinases results in reduction of myosin activity and therefore cell contractility[57]. ROCK dependent myosin activity however does not only determine cell contractility but also triggers formation of large f-actin stress fibers[58]. These fibers are anchored in adhesion sites and oriented parallel to an applied force field (e. g. by shear flow[59]) but can also react to changes in tension by reorganization of the actomyosin network[60].

Disrupted functionality of the cytoskeleton has been linked with implications in mechanical signaling pathways[61-63]. Moreover, stress fiber formation and f-actin organization are dependent on substrate rigidity[64]. Mechanical stimuli like substrate rigidity are converted into biochemical signaling cascades that modulate f-actin network associated factors, thus the actomyosin network is thought to act as a mechanosensitive system itself. This hypothesis has been tested theoretically by computational modeling which proposed an inherent mechanosignaling capacity of the cytoskeleton for a distinct force range that is tunable through changes in single components[65].

Altogether, the actomyosin network acts as active and passive mechanosensitive element of the cell that senses external loads but also exerts forces intracellularly. The organization of the actin cytoskeleton and modifications by its associated interaction partners modulates force transmission properties of the system and thus plays a critical role in different force-related cellular functions[66].

1.2.1.6 FA associated kinases trigger downstream signaling cascades

ince FAs are very complex structures with hundreds of different associated proteins, also chemical signaling responses are manifold. A set of kinases was described to be associated with FA dependent signaling events: Rho/ROCK mediated contractility of the f-actin network but also extracellular stimuli are transmitted into different signals; FAK phosphorylation by Src kinase results in activation of Ras and enhances cell proliferation signaling routes; activation of PI3K and the Akt pathway leads to the expression of anti-apoptotic genes and thus triggers cell survival. The Src associated p130Cas on the other hand regulates cell migration through activation of the Rac pathway or triggers cell cycle progression through JNK[67]. Altogether, integrin-dependent signaling in FAs engulfs a large number of proteins affecting various signaling cascades. Still, it is not fully understood how mechanical signals are sensed and propagated into the cell even though it has been shown that FAs play a critical role in these processes.

1.2.2 FAs are multifunctional signaling hubs in mechanotransduction

Maturation of FAs from early nascent adhesion sites is a complex process that depends on many extra- and intracellular factors. For fibroblasts seeded on FN or immobilized RGD ligand clusters, it has been shown that establishment of integrin mediated adhesion but also migration speed are limited by the presence of sufficient anchorage site clusters in the ECM[68]. Limiting factors for adhesion formation are ligand density, as at least 3 RGD sites in the ECM are required for FN dependent integrin attachment[68], the assembly of at least 3 FN binding integrins in a cluster[69], as well as spacing between those integrins at a maximum distance below ~70 nm[70]. Early adhesion sites within certain proximity can fuse and further mature into focal complexes or FAs[71]. This process seems to be load-dependent as immobilization of integrins within the FA complex requires mechanical anchorage at both sides: extracellular coupling to the ECM as well as intracellular association to the cytoskeleton. Unbound integrin heterodimers in contrast show free diffusion within the plasma membrane[72].

I In mature adhesions, single integrin-ligand bonds, measured on immobilized ligands, were shown to experience a wide range of forces up to 40 pN [73], whereas single myosin motors generate forces of about 3-4 pN[74]. This suggests that forces in adhesion structures are highly diverse and mechanotransduction pathways can be tightly regulated. The process of integrin clustering itself, however, was shown to be a force-independent process, even though integrin clustering stimulates f-actin polymerization from early adhesion sites. Myosin II activity further drives the recruitment of integrins together with adaptor molecules in a Src-kinase-dependent manner, thus inducing adhesion maturation and strengthening[75].

Another signaling route influencing myosin II activity and thus FA assembly and disassembly is the RhoA/ROCK dependent pathway. Besides MLC phosphorylation, effectors of RhoA/ROCK inhibit MLC phosphatase and regulate the activity of f-actin organizing factors like ADF/cofilin and LIM Kinase[76,77]. Hence, the process of FA reinforcement seems to involve several processes including tension-dependent myosin II activity.

In contrast to early adhesion sites, the mechanical engagement of integrins in mature adhesions was shown to be critical for the functionality of downstream interactors in the adhesion complex. The tyrosine phosphorylation of a set of FA proteins such as paxillin, FAK and p130Cas by Scr-kinase is upregulated at FA sites after the application of external forces[14]. Additionally, p130Cas was shown to be stretch activated and trigger a signaling cascade of MAP Kinases[14]. Mechanical engagement of FAs is therefore not only required in cellular adhesion but also an important factor in many other cellular processes like motility, proliferation and differentiation[36].

Besides the function of FA resident proteins in mechanosensing, opening of stretch activated ion channels and subsequent changes in local ion concentration have been suggested to influence cellular contractility through MLCK as well as the f-actin binding protein calmodulin[8]; enhanced contractility in consequence promotes the formation of adhesion structures. Downstream of force induced adhesion maturation, f-actin polymerization is driven by formins such as mDia1 and mDia2[78-80], which further increase the stability of the adhesive bond. Additionally it has been suggested, that the f-actin polymerizing zyxin-ena/VASP complex is involved in stress fiber elongation as a consequence of mechanical load on FAs[81-83].

Altogether, establishment and stabilization of the load bearing adhesion complexes are achieved by several factors. First, force induced clustering of extracellular ligands (FN) with integrins induces nascent adhesion assembly. In a second step, FA maturation is accompanied by f-actin stress fiber formation from single actomyosin bundles[84]. Crosslinking of f-actin stress fibers through various f-actin binding proteins distributes over several molecules in the complex and therefore prolongs the lifetime of the adhesive bond[85] (Figure 1.5).

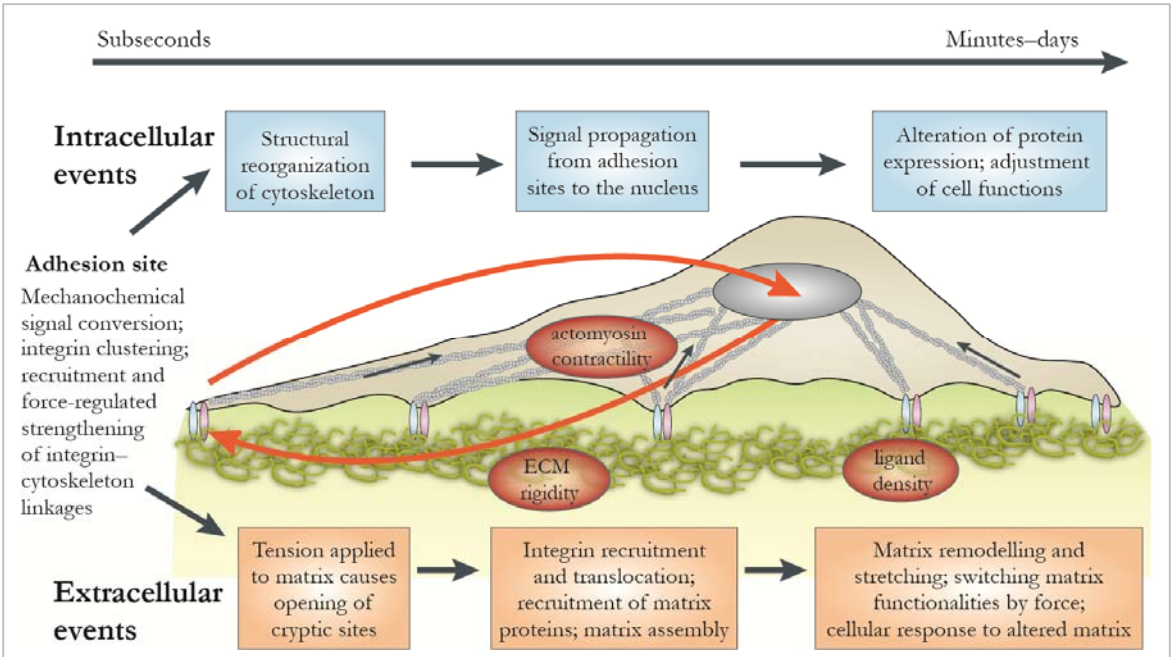

Figure 1.5: Overview of intra- and extracellular events involved in mechanotransduction processes. Intracellular processes reach over the immediate local reorganization of the cytoskeleton over signal transduction to the nucleus to altered protein expression by transcription of force-related genes. Extracellularly, force applied to FAs leads to increased integrin recruitment (followed by intracellular FA maturation) and long-term matrix remodeling. Mechanical stimuli are indicated in red circles. (Adapted from [86])

All these processes suggest a positive-feedback loop, where load upon single components of the force-bearing adhesion complex leads to recruitment of additional molecules and interaction partners that ease the mechanical load across force bearing proteins and thus stabilization of the whole complex. Furthermore, assembly of FAs and adhesion maturation also enlarge loads upon the adhesion through increased ligand binding of integrin clusters and f-actin polymerization, resulting in formation of further ligand-integrin-cytoskeleton linkages. Still, the full process of mechanotransduction through FAs remains unclear due to the enormous complexity of the system. Even though integrin dependent adhesion was studied intensively over the last years, forces applied on the ECM-cytoskeleton linkage could not be determined in living cells. Single myosin motors generate 3-4 pN forces[74], but forces across integrin subunits are expected to be significantly higher, as αvβ3 integrins were demonstrated to generate forces about 33-43 pN during cell adhesion[73]. Linkage of an integrin ligand peptide to a force sensitive DNA hairpin structure revealed traction forces of up to 30 pN in single FAs[87]. However, both methods only reported extracellular forces but information about the forces acting on proteins within these linkages is important to understand the mechanobiology of processes like cell migration.

1.2.3 Talin-1 is a central FA resident protein

1.2.3.1 Talins play a central role in organ function and development

The crucial importance of talin-1 for all kinds of cellular functions became evident in various knockout studies:

Talin-1 knockout mice die at E8.5 due to defects in gastrulation[88], whereas a conditional knockout of talin-1 in endothelia cells leads to defects in angiogenesis as well as endothelial cell spreading at E10.5[89]. Other conditional knockouts also show severe defects in tissue development that can be ascribed to inaccurate integrin-mediated cellular processes[90,91]. Cell based studies on talin-1 knockout cells revealed compensatory upregulation of talin-2[92], thus talin-2 knockdown in talin-1 deficient cells led to defects in integrin activation, FAK phosphorylation (Y397), FA assembling and strengthening as well as exerted traction forces. Knockdown of talin-1 in HUVEC cells, which do not seem to upregulate talin-2, reduced spreading and migration of the cells underlining the important role of talin-1 for these processes[93].

1.2.3.2 Protein structure of talin-1 reveals two main structure elements

Talin-1 is a 270 kDa protein comprised of the talin head, containing a four-point-one, ezrin, radixin, moesin homology (FERM) domain and an elongated rod with 14 helix bundles (R1-R13, dimerization domain)[94]. Head and rod domain are separated by an unstructured linker region (~80 aa) containing, besides numerous phosphorylation sites, recognition sites for a set of proteases including calpain-II [95,96] (Figure 1.6).

The talin-1 head FERM domain, comprised of F0, F1, F2 and F3 subdomains, carries several interaction motifs that mediate FA localization. Binding to integrins occurs between the PTB-like fold in talins F3 domain and the membrane proximal NPxY motif of the β integrin tail[94,97,98], resulting in conformational changes and thus a ligand affinity increase of the integrin heterodimer (see 1.2.1.2). Other interactions with the talin-1 head domain were shown for f-actin[99], PIP kinase type 1γ[100], the hyaluronate receptor layilin[101] and FAK[102].

Assembling various crystal and nuclear magnetic resonance (NMR) studies of individual parts of the talin-1 rod domain led to the conclusion that the 62 helices in the talin-1 rod domain form 13 helical bundles (R1-R13) and a C-terminal dimerization domain (DD), allowing the formation of an antiparallel homodimer[26]. Carrying 11 vinculin binding sites (VBS), two additional f-actin and one integrin binding site, along with interaction domains for RIAM, synemin and DLC1[94], the talin-1 rod acts as a signaling hub for downstream cascades, as well as platform for direct and indirect connection to the f-actin cytoskeleton.

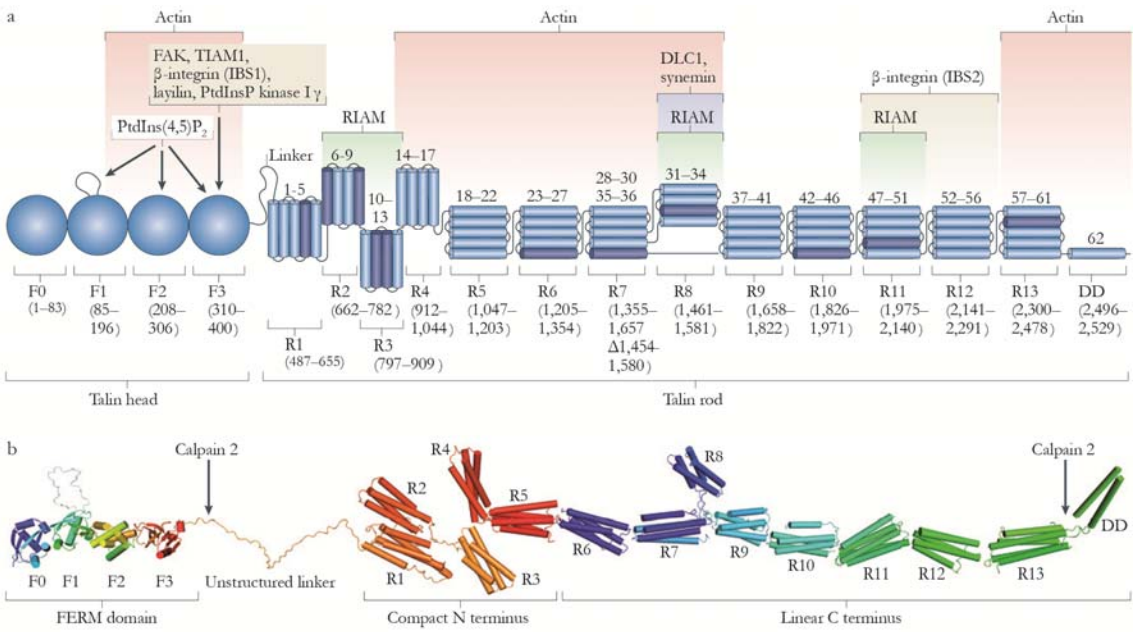

Figure 1.6: Schematic representation of the talin-1 structure.
(a) The talin-1 head domain comprises of an atypical FERM domain with F0, F1, F2 and F3 domains and carries binding motifs for several interaction partners such as integrins, actin, focal adhesion kinase (FAK), layilin and PIP Kinase 1 γ but also PIP_2. The talin-1 rod is composed of 13 helix bundles (R1-R13) as well as a DD. Here, binding sites for vinculin, RIAM and actin but also other interaction partners are located. (b) Proposed domain structure of talin-1 from NMR and crystallization studies. Calpain 2 cleavage sites are indicated with arrows. Image was modified from [94].

1.2.3.3 Two talin isoforms display tissue specific expression pattern

Vertebrates express two talin isoforms, namely talin-1 and talin-2. While talin-1 is ubiquitously expressed, talin-2 shows highest expression in heart muscle as well as brain and also exists in various tissue specific splice-isoforms[103]. Studies of heart development in mice revealed a stage-specific expression pattern for both isoforms; talin-1 and talin-2 are both expressed in embryonic cardiac myocytes but talin-2 was the abounded form in the adult heart. It was also shown, that hypertrophy of cardiac tissue upon external stress caused increased expression of both talin isoforms, indicating close relation between mechanical load and talin function in heart muscle tissue[104]. However, even though numerous biochemical, *in vitro* and *in vivo* studies exist for talin-1, little is known about the structure and function of talin-2. In cell culture experiments using MEFs, loss of talin-1 can be compensated by upregulation of talin-2; moreover talin-2 knockdown in those cells reveals the importance of the talin family members for integrin association with the f-actin cytoskeleton as cells exhibit defects in adhesion and downstream signaling[92]. Still, talin-2 knockout mice are viable and fertile, showing only a mild muscle dystrophy[105].

1.2.3.4 Cytoplasmic talin-1 exists in an autoinhibited conformation

Talin-1 was shown to adopt a compact, globular conformation in low salt buffers[106] that is ascribed to close interactions between the talin-1 head F3 and rod R9 domains[107,108]. This intermolecular interaction conceals the PTB binding site for β integrin tails and thereby sterically blocks talin-integrin interaction[109]. In the current model, auto-inhibited talin-1 forms a 12.5 nm x 11 nm x 9.5 nm donut shaped dimer with the heads incorporated in the center of the structure[109]. Also, these NMR studies showed several other inter-domain associations within talin-1 apart from the F3-R9 connection that seem to stabilize the intramolecular association. Those autoinhibitory interactions were shown to be released upon talin-1 connection with $PI(4,5)P_2$ as a consequence of talin-1 localization from the cytoplasm to the plasma membrane[108]. The shift in talin-1 localization might be caused by the interaction with the PIP kinase type 1γ (PIPK1γ) as deletions of the talin-1 F3 binding domain in the PIPK1γ declined β1 mediated cell adhesion due to defects in talin-1 and vinculin recruitment to adhesions sites[110]. Furthermore, talin-1 membrane- and αIIbβ3 association occurs upon activation by RAP1A GTPase and its effector RIAM[111] but the actual mechanism of this activation pathway remains elusive[94].

1.2.3.5 NMR studies correlate talin-1 dimerization with protein function

The NMR data showing an autoinhibited state for talin-1 also suggest that talin-1 forms a homodimer through interaction between two-helix bundles at the C-terminus[94]. While in the autoinhibited state, the dimer adopts a donut-like shape in the cytoplasm, the activated and elongated molecules that may span the distance between two integrin heterodimers[109]. Molecular dynamics modeling recently suggested a mechanical regulation of dimer orientation, that depend on the quantity and quality of external stresses[112], thus altering integrin density and clustering at the plasma membrane. Nevertheless, *in vitro* or *in vivo* data about the function of talin-1 homo-dimerization are still missing.

1.2.3.6 Talin-1 directly links integrins with the f-actin cytoskeleton

Talins association with f-actin filaments influences adhesion stability and is rate-limiting in cell migration [113]. So far, three distinct f-actin binding sites (ABS) have been identified within talin, one in the F2-F3 domain of the talin-1 head[99] and two in the talin-1 rod domain[85,114,115]. All three binding sites are adjacent but not overlapping with binding sites for vinculin[116] suggesting that the establishment of the integrin-actin connection via talin-1 and vinculin can occur independently. The C-terminal ABS was characterized as THATCH domain (talin/HIP1R/Sla2p actin-tethering C-terminal homology) and closer studies on this domain

suggested that talin-1 homo-dimerization is essential for efficient f-actin binding of this particular helix bundles[85]. Yet the actual mechanisms behind f-actin binding and dimerization remain unresolved.

1.2.3.7 Vinculin binding enhances the talin-1- f-actin connection

Vinculin is one of the major interaction partners of talin family proteins in FAs but was also shown to be involved in other adhesion processes[117]. Similar to talin-1, vinculin is comprised of a series of αhelical bundles forming three distinct domains, a 91 kDa head domain and a 21 kDa tail region that are interconnected via a 4.6 kDa proline-rich linker [118,119]. In contrast to talin-1 knockout cells that show severe adhesion defects, vinculin cells can still form FAs, even though they feature several changes compared to their wildtype counterparts that can be related to an increased motility and reduced cell adhesion[120,121]. Vinculin was shown to exist in an autoinhibited globular conformation characterized by a tight head-tail interaction [119] masking the talin-1 binding site in the vinculin head. Activation of vinculin is regulated by talin-1, f-actin and probably other interaction partners[122,123] as well as phosphorylation[124]. Inactive vinculin could be directly translocated from the cytoplasm or stored in the FA, e. g. in the upper actin regulating layer[39] (Figure 1.3). The talin-vinculin interaction occurs between the vinculin head and the 11 vinculin binding sites (VBS) in the talin-1 rod domain[125-127] (Figure 1.6).

Earlier studies also suggested talin-1 activation by vinculin, as the expression of vinculins talin-1 interaction domain led to FA expansion in a talin-1 but not myosin II dependent fashion[128]. Interestingly, vinculin binding to talin-1 depends on talin-1 stretching through actomyosin contractions[127], whereas bound vinculin inhibits the refolding of talins R2-R3 domains. This suggests that vinculin stabilizes the integrin-actin connection via talin[129]. *In vitro* data also confirmed that vinculin binding to talin-1 locks talin-1 R1-R3 domains in an unfolded conformation[130].

Taken together, vinculin-talin interactions are suggested to play a critical role for cellular mechanosensing and mechanotransduction but quantitative evidence for the importance of the interaction in cells is missing.

1.2.4 Talin-1 shows characteristics of a mechanosensitive protein

Over the last years, it has been recognized that talin-1 is not only an efficient integrin activator but also plays an important role in the assembly and disassembly of FAs. Moreover, *in vitro* experiments strongly suggested a role of talin-1 during mechanosensing and force transduction. As an arrangement of helical bundles in a rather linear chain (Figure 1.6), the

talin-1 rod was predicted to unfold in response to mechanical forces after the engagement of talin-1 to integrins and f-actin[13]. The characterization of the C-terminal ABS in the talin-1 rod revealed that mutations which negatively influence the binding affinity to f-actin decrease the rescue capability of talin-1 in knockdown experiments and force exerted on the R13 domain might increase the binding affinity to f-actin[93,131]. Other studies provided evidence that the N-terminal VBS in R1-R3 domains unfold upon application of 2-12 pN leading to vinculin recruitment[132]. Hence vinculin association with talin-1 in FAs is believed to – at least partially – dependent on myosin II activity[133]. This observation was supported by single molecule studies *in situ* and *in vitro*, demonstrating stretching of talin-1 molecules in direction of the f-actin flow[134,135]. Furthermore, the force extension curve of talin-1 modeled from single molecule applications suggests a three-state behavior for the talin-1 rod unfolding between 5 – 30 pN: an unbound state, an intermediate state with unbundling of individual helix bundles and a disordered peptide chain[136].

Interestingly, VBS in R2-R3 overlap with a RIAM binding site pointing towards a mutually exclusive recruitment of both proteins[136]. RIAM was also detected in nascent adhesions whereas vinculin seems to be more abundant in mature FAs[137]. In a recent model[138], RIAM localizes talin-1 to the plasma membrane and facilitates interaction with PI(4,5)P2, after GTP dependent activation of RIAM through RAP1A. The close proximity to the plasma membrane is necessary for the interaction of talin-1 with β integrin tails and subsequent activation of integrins. In addition, RIAM drives f-actin polymerization through the recruitment of vasodilator-stimulated phosphoprotein (VASP) in talin-positive adhesions. The mechanical engagement and resulting forces above 5 pN across talin-1, promoted by the f-actin binding in these early adhesions, disable the RIAM binding to talin, exposing the cryptic VBSs in the R2-R3 domains. The talin-vinculin interactions in R1-R3 stabilize the unfolded conformation of talin[130], subsequently the integrin-talin-actin connection is further enhanced, leading to FA maturation, recruitment of further FA proteins and activation of downstream signaling pathways[139].

All these data suggest that talin-1 recruitment and function are regulated in a force-dependent manner, but direct evidence from *in vivo* or cell culture based studies is still missing. This study will analyze forces across talin-1 and elucidate the importance of interactions with f-actin and vinculin for a subset of cellular functions.

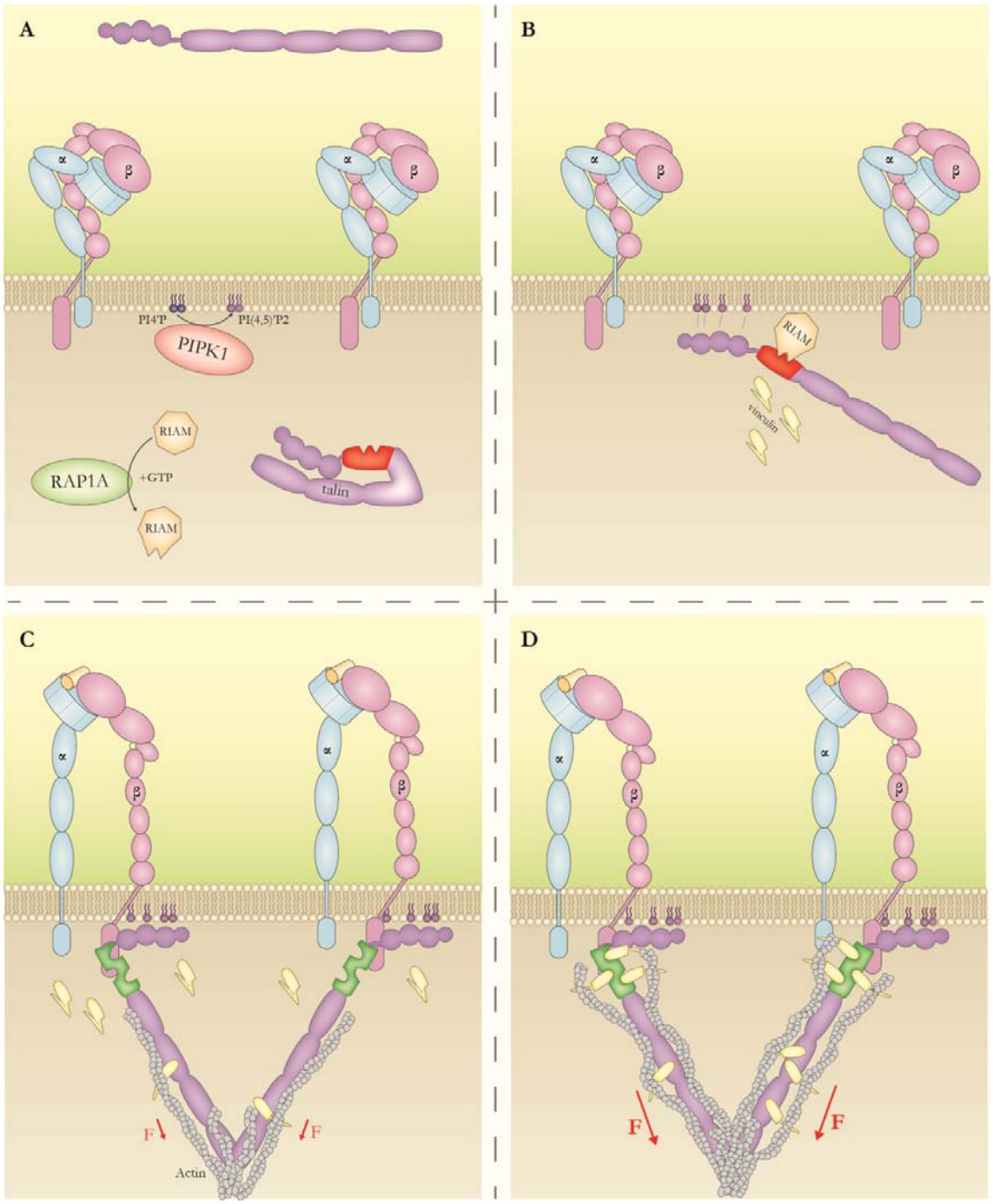

Figure 1.7 Proposed model for talin activation and force related functionality.
(**A**) Autoinhibited talin is localized in the cytoplasm with VBSs buried within the helical bundles in the talin rod but exposed RIAM binding sites. RAP1A activates RIAM in a GTP consuming manner and PIPK1 converts PI4'P into PI(4,5)'P2. (**B**) Activated RIAM localizes talin to the plasma membrane where the talin head domain interacts with PI(4,5)'P2, releasing the head-tail interaction of talin. (**C**) Interaction of the talin F3 domain and integrin cytoplasmic tails triggers integrin activation thus ligand binding in the ectopic domain of the heterodimers. Furthermore, the elongated talin rod connects with the actin cytoskeleton; this interaction is further stabilized by initial vinculin binding to C-terminal VBSs and actin. Forces generated by actin polymerization enhance the load upon talin and lead to accessibility of cryptic VBSs and the release of RIAM. (**D**) Vinculin recruitment to talin stabilizes the integrin-talin-actin connection and enhances force propagated across the complex, leading to recruitment of downstream interactors and FA maturation.

1.3 Common techniques to measure cellular and subcellular forces

With the growing interest in mechanical force propagation in cells, several techniques to measure forces extra- and intracellular have been developed and were used for the analysis of mechanical forces across talin-1.

1.3.1.1 Force response measurements of individual proteins in vitro

Studying the mechanical properties of individual proteins or protein subunits, several techniques such as AFM as well as optical and magnetic tweezers setups emerged over the last years. The common principle of these methods is to trap the molecule of interest between functionalized elements within the setup and pull with a defined force. The resulting force-extension curves provide quantitative information about unfolding and refolding behavior of a protein and allow characterization of protein domains that unfold at a certain force regime[140].

1.3.1.2 Cells exert traction forces upon their extracellular environment

Forces generated by the cell – e.g. during cell adhesion or cell migration – can be measured by a light microscopy approach called 'traction force microscopy' (TFM). The term TFM is commonly used for two types of experimental setups. In the micropost-array technique, cells are seeded on small polydimethylsiloxane (PDMS) pillars. Cellular traction forces correlate with the displacements of the microposts which can be microscopically determined. The displacement of the posts depends on stiffness that can be controlled by the pillar radius and height. The resulting data are rather easy to interpret[141], however, the surface microstructure of pillars can influence cell behavior and adhesion.

In the second approach, fluorescent beads are embedded into polyacrylamide matrices. Adhesion of cells on the matrices and generation of traction forces lead to lateral bead displacement that can be microscopically quantified. In this method, however, forces need to be extracted by an inverse stress-strain formula as all beads are interconnected through the gel matrix[142]. This strategy of force extrapolation assumes ideal conditions in the polymer and requires complex computational analysis. Recent studies, however, could even resolve forces generated by nascent adhesions by optimization of the tracking algorithm to show that maturation of nascent adhesions into FAs is stress-dependent[71].

1.3.1.3 Molecular probes allow intracellular force measurements

Even though cellular as well as molecular and subcellular forces have become of close interest within the last years, adequate techniques to quantitatively measure forces across individual

proteins in cells were still missing. However, with the growing interest in biological function of force, several approaches to identify force related protein functions *in vivo* have emerged.

The most common ways to analyze forces across individual molecules are based on the radiation-free Förster resonance energy transfer (FRET) between an acceptor and a donor fluorophore with overlapping emission and excitation spectra (FRET pair). FRET is highly distance dependent and therefore commonly used to study protein-protein interactions, although it is also subjected to other factors such as changes in local pH and fluorophore orientation[143]. In a first approach to measure force on the molecular level, a donor and acceptor dyes were conjugated to fibrillar FN to examine load dependent changes in ECM organization[144].

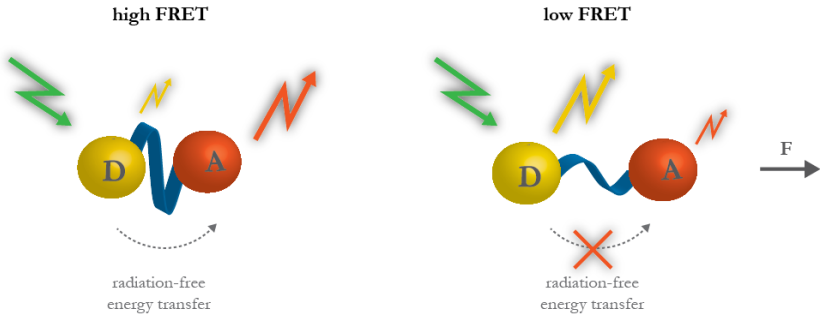

Figure 1.8: Schematic model of tension sensor principle. Under low force conditions, the linker peptide of the sensor is in a relaxed state and both fluorophores are in close proximity. Exiting the donor fluorophore therefore leads to high radiation free energy transfer (FRET) and excitation of the donor molecule (indicated by red arrow). Application of forces across the sensor module enhances the distance between both fluorophores and thus decreases FRET. Therefore excitation of the donor no longer leads to emission of acceptor but only donor signal.

Another strategy to measure subcellular forces is the introduction of a force-sensitive linker element in between the FRET pair. Application of loads in corresponding force regime of the sensor peptide leads to elongation of the linker, a separation of the fluorophores and decrease in FRET (Figure 1.8). Previous studies have analyzed various linker peptides such as α-helices used to probe the mechanical load on α-actinin[145], an AS(GGS)9 repeat linking a GFP-cpGFP-dimer to analyze mechanics of myosin II[146], and a spider silk protein derived flagelliform linker (F40) to investigate forces and dynamics of cell adhesion and cell junction proteins[12,147]. Other studies introduced the F40 tension sensor in extracellular approaches to analyze forces exerted by cells onto ECM components[148]. Calibration of molecular tension sensor linker peptides, for example via single molecule force spectroscopy, is essential to reliably evaluate forces transmitted across the selected proteins. Whereas the F40 sensor was analyzed – it is sensitive to mechanical forces of 1-6 pN – single-molecule calibration data from other sensors are missing.

1.4 Aim of the PhD Thesis

Intramolecular force measurements provide closer insights into various processes including migration and cellular rigidity sensing. Though all sensors have individual limitations, those techniques provide closer insights into mechanical properties of individual proteins in living cells. In this study analysis of tension across the central FA protein talin-1 was of central interest. As a direct link between integrins and the f-actin cytoskeleton, the FA resident protein talin-1 became of great interest as a force transducing molecule. Previous studies on talin-1 suggested forces in the low pN range, but discrete force measurements in living cells was still missing. However, not only force measurements across talin-1 but also the development of a suitable tension sensor probe to measure talin-1 tension in living cells was included in the project. Additionally, an appropriate cellular system for the biosensor analysis had to be generated in order to exclude confounding effects of endogenous protein expression. Therefore, talin-1 knockout cells were generated and characterized. Finally, analysis of different factors that potentially regulate talin-1 tension, such as f-actin and integrin binding, talin-1 homodimerization and vinculin recruitment, was of closer interest in this study.

2 Results

2.1 Cell lines

For the evaluation of tension sensors and the subsequent analysis of force transduction, talin-1 deficient cells were generated allowing the tension sensor evaluation in the absence of endogenous protein.

2.1.1 Generation of talin-1 deficient cells (Talin-1 (-/-))

To generate talin-1 deficient cells, fibroblasts from adult mice in which the talin-1 gene was marked with loxP sites were isolated (compare Figure 4.2), and subsequently immortalized by the expression of SV40 large antigen; a GFP-tagged Cre-recombinase was introduced via adenoviral infection to delete both talin-1 alleles. The cells were FACS sorted for GFP-Cre expression to enrich the population for infected cells and clonal cell lines were generated (chapter 4.2.5).

Before reconstitution of the knockout cell line with talin-1 constructs, *talin-1$^{(f/f)}$* (further called (f/f)) parental line and *talin-1$^{(-/-)}$* knockout cells (further called (-/-)) cell lines were tested for efficient knockout of talin-1, as well as basic cellular functions such as cell spreading on ECM-coated glass surfaces, expression levels of other FA core components and integrin surface expression.

To confirm efficient knockout of talin-1, genomic DNA was isolated from (f/f) and (-/-) cell lines and genotyping PCRs were performed (chapter 4.1.2.2.1). PCRs revealed efficient deletion of talin-1 exons 1-4, as primers binding only in exon 1 of talin-1 region did not lead to products in the (-/-) cells but in (f/f) cells (expected band size 779 bp). A second primer pair, designed specifically for knockout verification, led to amplification of specific product only in the (-/-) cell line (expected band size 707 bp) (Figure 2.1).

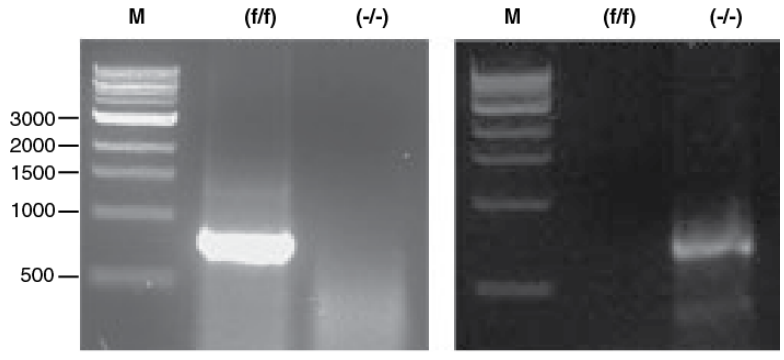

Figure 2.1: Genotyping PCR products show efficient talin-1 knockout. The left image shows the band positive for Cre recognition element. The right image is showing the product for the deleted allele.

Loss of talin-1 protein was subsequently confirmed by western blot (chapter 4.4.4). Analysis of both cell lines revealed knockout of talin-1 and slight reduction in expression levels of other FA molecules like paxillin, vinculin and FAK; these experiments also showed reduced FAK Y397 phosphorylation as described in earlier knockdown experiments of talin-1[92] (Figure 2.2).

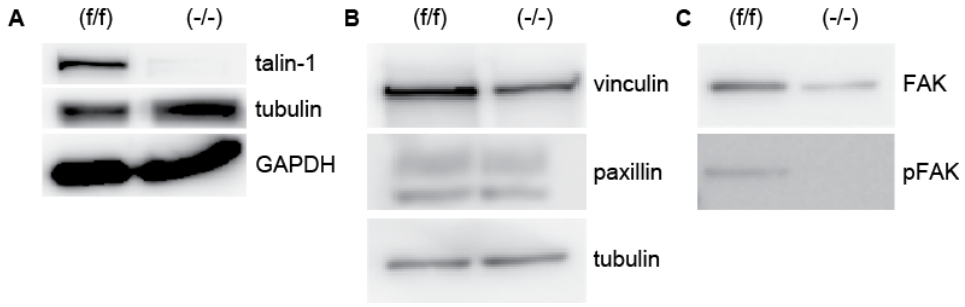

Figure 2.2: Western blots showing protein expression levels in talin (f/f) and talin (-/-) cell lines. (**A**) Whereas mouse embryonic fibroblasts (MEF) and talin (f/f) cells express comparable amounts of talin-1, no talin-1 can be detected in smooth muscle cells and talin (-/-) cells. (**B**) Vinculin and paxillin levels are comparable in both cell lines. (**C**) FAK phosphorylation is reduced in talin (-/-) cells but not in (f/f) cells. Tubulin and GAPDH were used as loading controls.

As talin-2 was postulated to compensate for loss of talin-1 and integrin activation was only slightly impaired in the (-/-) cells, expression of talin-2 in this cell line was tested. Even though talin-2 expression was low as compared to heart tissue lysates, direct comparison of parental and knockout cell lines showed expression of talin-2 in both lines (Figure 2.3).

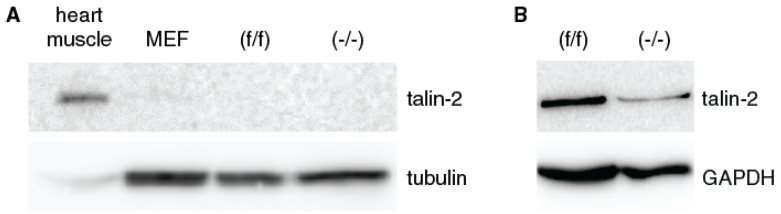

Figure 2.3: Talin-2 is still expressed in (-/-) cells. (**A**) talin-2 expression in heart muscle tissue, mouse embryonic fibroblasts (MEF), talin (f/f) and talin (-/-) cell lines. (**B**) Talin-2 expression in talin (f/f) and talin (-/-) cell lines only, Tubulin and GAPDH were used as loading controls.

Using immunostainings (chapter 4.3.3), subcellular localization of paxillin and pFAK as well as f-actin was tested and furthermore, cell spreading on FN coated glass surfaces was analyzed by evaluation of cell sizes. Compared to the (f/f) cells, (-/-) cells failed to enlarge their surface area over time (Figure 2.5) to FN and even though individual cells induced isotropic cell spreading, the majority of cells could not form proper FAs (Figure 2.4).

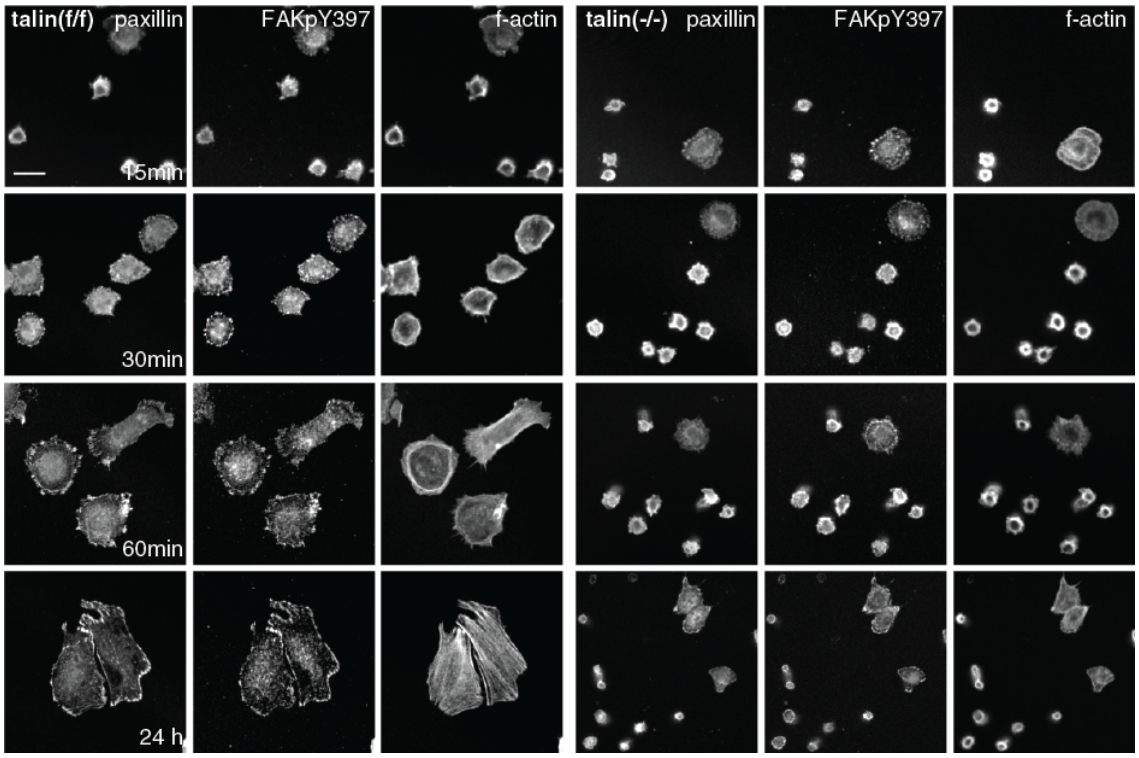

Figure 2.4: Compared to (f/f) cells, (-/-) cells fail to enlarge their cell area over time. Immunostainings of (f/f) and (-/-) cell lines with paxillin and pFAK antibodies and f-actin staining with phalloidin after 15, 30 and 60 min and 24 h. (f/f) cells are able to enlarge their surface area whereas talin(-/-) cells fail to spread on FN within 24 h. Scale bar 20 µm.

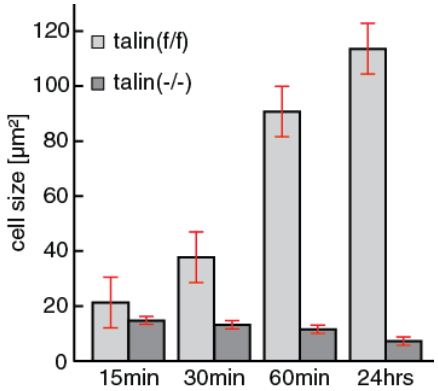

Figure 2.5: Compared to (f/f) cells, (-/-) cells fail to enlarge their cell area over time. Cell size quantification was performed with actin signal of immunostainings shown in Figure 2.4. Error bars represent s.e.m.

The observed spreading defect to FN was postulated to be due to impaired integrin functionality or activation. First tests on integrin function were performed using plate and wash assays, where cell adhesion to FN was tested (chapter 4.2.12). After seeding for 30 min at 37 °C, (-/-) cells demonstrated poor adhesion as compared to (f/f) cells (Figure 2.6), indicating impaired integrin function as a consequence of reduced integrin activation through talin-1.

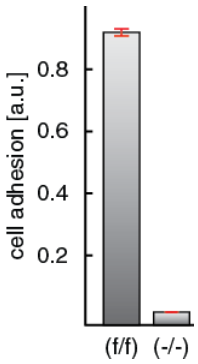

Figure 2.6: Cell adhesion to FN in talin (f/f) and talin (-/-) cell lines. In plate and wash assay, (-/-) cells are characterized by poor adhesion to FN compared to the (f/f) cells. Error bars (red) represent s.e.m.

In FACS analysis (chapter 4.3.4) surface expression of total and active β1 integrin was tested with specific antibodies. Active β1 was detected by a monoclonal antibody specific for the 9EG7 epitope that is only accessible in an unclasped conformation of the integrin (chapter 1.2.1.2). Interestingly, comparing both cell lines, no significant reduction of surface expression levels with both antibodies could be detected (Figure 2.7). It thus appears that the expression of talin-2 (Figure 2.3) (as well as kindlin-2 expression) compensates for the loss of talin-1 during integrin activation. The observation that cell spreading is affected suggests, however, that talin-2 expression is insufficient to fully rescue cell spreading.

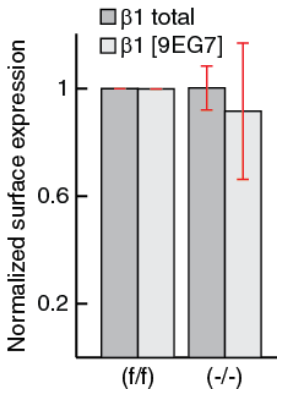

Figure 2.7: Integrin activation is not affected by loss of talin-1 in (-/-) cells. Evaluation of integrin surface expression levels in FACS experiments revealed no changes between (f/f) and (-/-) cell lines. Total β1 levels as well as 9EG7 expression was not significantly different between both cell lines. Error bars represent s.e.m.

2.1.2 Talin double knockout cells

Excluding effects of talin-2 expression in all experiments was required for the subsequent tension sensor analyses; therefore a different knockout cell line derived from *talin-1$^{f/f}$/talin-2$^{-/-}$* cells (further called 'WT') was used, that do not express talin-2. Cre-recombinase was transiently expressed in WT cells by adenoviral transduction to delete exons 1-4 out of the talin-1 allele and a clonal cell line was generated. Both cell lines were generated and provided by Roy Zent and Moritz Widmaier (Chapter 4.2.5).

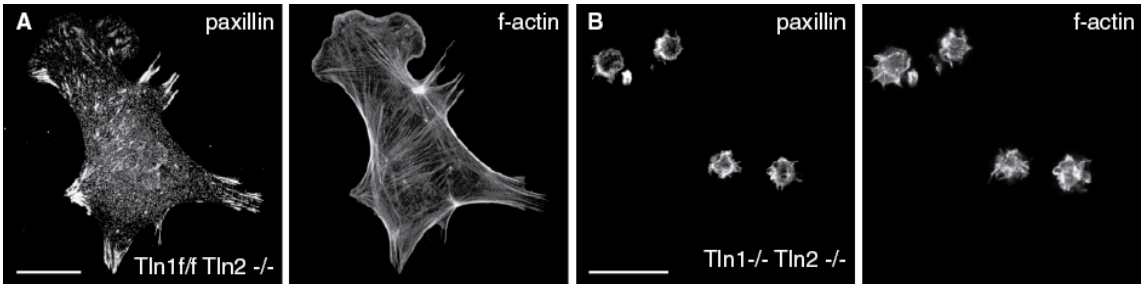

Figure 2.8: Immunostainings of talin WT (*Tln1$^{f/f}$ Tln2$^{-/-}$*) and KO (*Tln1 $^{-/-}$ Tln2$^{-/-}$*) cells. (**A**)WT cells form paxillin positive FAs and stress fibers, when stained with anti-paxillin antibody and f-actin labeled with phalloidin but (**B**) KO cells fail both. Scale bars 20 μm.

The *talin-1$^{-/-}$/talin-2$^{-/-}$* double knockout cell line (further called 'KO') showed no FA formation in immunostainings and only poor adhesion to FN in plate and wash assays, as compared to the talin-1 expressing WT cells (Figure 2.8). Moritz Widmaier performed experiments testing efficient talin-1 knockout in western blot, cell size and cell adhesion to various ECM compliances[27]. He could show that both talin isoforms are deleted in the KO cell line and that the cell line is characterized by a spreading defect as well as poor adhesion to FN.

2.2 Tension sensor insertion into talin-1

2.2.1 Talin-1 linker region serves as appropriate

As the insertion of the 508 aa sized tension sensor module might interfere with protein function, selection of an adequate insertion site in talin-1 was a critical step in generating a functional biosensor. The talin-1 head comprises a FERM domain with many interaction domains in particular interaction site for β integrin tails. The talin-1 rod comprises several helix bundles carrying several interaction sites e. g. for vinculin and RIAM (chapter 1.2.3.1). Integration of the tension sensor in one of these domains could alter binding properties to talin-1 interaction partners but also could lead to alterations in the protein structure. Therefore, both major domains of the talin-1 were not chosen for integration site. The linker region between head and rod domain, however, is a supposedly unstructured region with few interactions described so far. Talin-1 cleavage by the protease calpain-2 was shown to occur between residues Q433 and Q434 in the unstructured linker region[96] leading to changes in cellular contractility[149], so an insertion site between V447 and A448 was selected. By choosing an insertion site N-terminal to the calpain-2 cleavage site, also the interference with integrin binding of the FERM domain and therefore integrin activation was minimized.

2.2.2 Generation of biosensor constructs

Tension measurements in living cells not only require the actual tension sensor module integrated in the protein of interest, but also a set of control constructs. First, a donor-only control is essential in order to evaluate FRET efficiencies; in this study, talin-1 was C-terminally tagged with the donor fluorophore YPet (Tln1Y). Second, a reference value for FRET in the absence of force is required to distinguish tension-dependent and potential tension-independent effects on FRET. Therefore, the tension sensor module was C-terminally fused to talin-1 (Tln1cTS). For the actual talin-1 tension sensor (Tln1iTS), the sensor module was integrated in the unstructured linker region between talin-1 head and rod (Figure 2.9, chapter 2.2.1) at the chosen insertion site between V447 and A448.

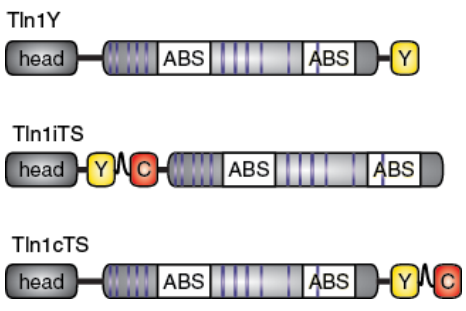

Figure 2.9: Schematic representation of talin-1 constructs. The upper images shows talin-1 C-terminally tagged with a YPet fluorophore (Y). In the middle scheme, the tension senor module is integrated in the talin-1 linker region and the buttom image indicates a C-terminal tagging of talin-1 with the tension sensor module. ABSs in the talin-1 rod are indicated with white boxes, purple lines represent vinculin binding sites.

2.3 Calibration of FRET based tension sensors

Molecular sensors, sensitive to low force ranges are essential for the analysis of forces across single molecules. Previously, forces across vinculin could be analyzed by a FRET based tension sensor probe, sensitive in the range of 1 – 6 pN[12]. As in vitro experiments had indicated that talin-1 is subject to significantly higher forces (del Rio reference), however, new tension sensor modules with adjusted force sensitivities were generated (chapter 1.2.4).

2.3.1 Force sensitive linker elements are the central unit of tension sensors

The central element of the tension senor probe is the force sensitive linker peptide, integrated between donor and acceptor fluorophore (1.3.1.3). The peptide should not bind to other intracellular components and do not disturb functionality of the protein of interest. It needs to be small (i.e. less than 10 nm) to ensure efficient FRET and elongate/unfold in response to piconewton forces. Importantly, the peptide should be reversible and return without hysteresis to its native conformation once forces dissipate. Ideally, a force sensitive peptide is also independent of the velocity at which forces are applied and undergoes the conformation changes quickly. Thus, the generation of such a sensor module requires a detailed evaluation to allow a reliable interpretation of FRET data.

2.3.1.1 Flagelliform peptide

The flagelliform (F40) linker is a previously used 40-amino-acid long peptide, derived from the spider silk protein flagelliform. The required flexibility is given by a repetitive motive, forming entropic nanosprings that unfold on forces of 1-6 pN (Figure 2.10, for detailed information see[12]). The F40 peptide was calibrated by fluorescence force spectroscopy (Figure 2.11) and has been applied to various intra- and extracellular proteins for example to determine low pN forces during cell-matrix and cell-cell adhesion.

Figure 2.10: Flagelliform peptide forms a force sensitive nano spring. Model structure of the flagelliform peptide. Adapted from [150].

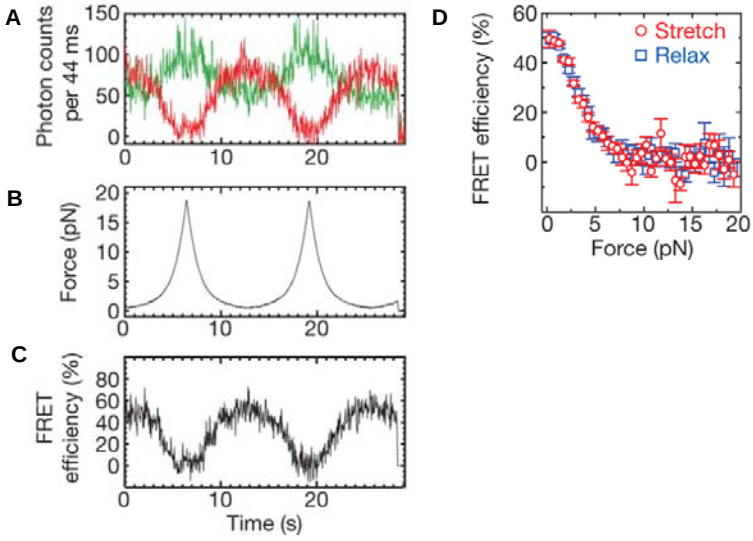

Figure 2.11: Calibration data of the F40 peptide from Grashoff et. al [12]. **A–C**, Multiple stretch/relax cycles of a single F40 peptide using fluorescence force spectroscopy. **A**, Fluorescence intensity time traces for donor (green) and acceptor (red). **B**, Applied force versus time. **C**, FRET efficiency versus time. **D** Averaged FRET–force curves show reversible stretching and relaxing of F40 between 0.25 and 19 pN. All error bars represent s.e.m.

In previous publications, however, it was suggested that forces across talin-1 exceed forces of 6 pN[129,135]. Thus it seemed likely that the talin-1 F40 would not show minor differences in FRET efficiencies, as when talin-1 is integrated into FAs, the sensor would be under constant force and therefore permanently entirely extended. Small differences in FRET should not be detectable with this specific sensor peptide. Consequently, the generation of new sensors with linkers sensitive to higher force regimes was one aim of this study.

Testing the hypothesis that the F40 peptide is constantly elongated in FAs, the talin-1 F40 tension sensor construct and the C-terminally tagged control were expressed in KO cells. Both constructs rescued the KO phenotype (chapter 2.1.2) and showed proper localization to paxillin positive FAs (Figure 2.12).

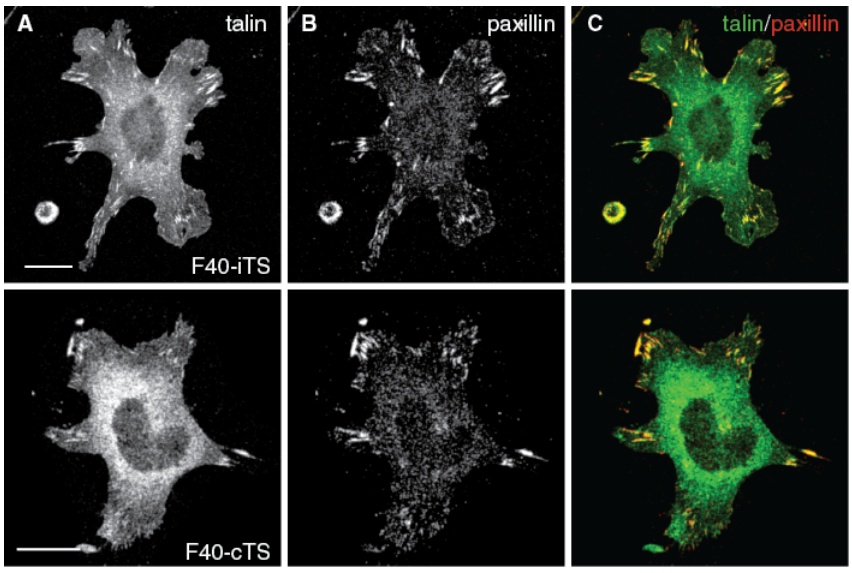

Figure 2.12: F40 sensor constructs localize to paxillin positve adhesion sites. Rescued KO cells, re-expressing (**A**) talin-1 F40 tension sensor constructs, (**B**)stained with anti-paxillin antibody. (**C**)All constructs efficiently localize in paxillin-positive FAs (indicated by yellow areas in the merged image. Scale bars 20 µm.

2.3.1.2 Leucine zipper motive

Figure 2.13: Model of leucine zipper structure from [155]. Two helices form a heterodimeric coiled coil with a hydrophobic core that promotes refolding after application of force.

Leucine zipper motives (LZ) occur naturally in many protein-protein interaction domains, as they are, for example, essential motives in many transcription factors. The appearance of leucine residues at every seventh position in the aa sequence leads to the formation of an α-helix and facilitates the parallel or antiparallel orientation of two adjacent helices by the formation of an interhelical hydrophobic core[151,152]. Previous publications on LZ-like, parallel homodimeric coiled-coil helices found force responses of the peptide at about 14 pN[153], thus LZ peptides were tested as candidates for tension sensors in this force regime. Those helices, however, were not interconnected but dimerizing upon expression and cross-linked by cysteine interactions at the C-terminus to avoid dissociation upon complete unfolding. Therefore, two antiparallel heterodimeric helices were fused by a flexible aa linker to obtain an single chain antiparallel LZ peptide. Force applied on the zipper region should lead to a separation of the coiled-coil structure that quickly refolds in the absence of tension, due to the hydrophobicity of the leucine side-chains[153]. Single molecule force measurements with optical tweezers[154], revealed adequate and fast refolding behavior around 8 pN and not within the expected range of about 14 pN of the artificial LZ motive (data not shown, personal communication with Alexander Mehlich).

Expression of the constructs (iTS and cTS) in cells rescued the KO spreading defect (data not shown) and both constructs were colocalizing with paxillin in FAs (Figure 2.14).

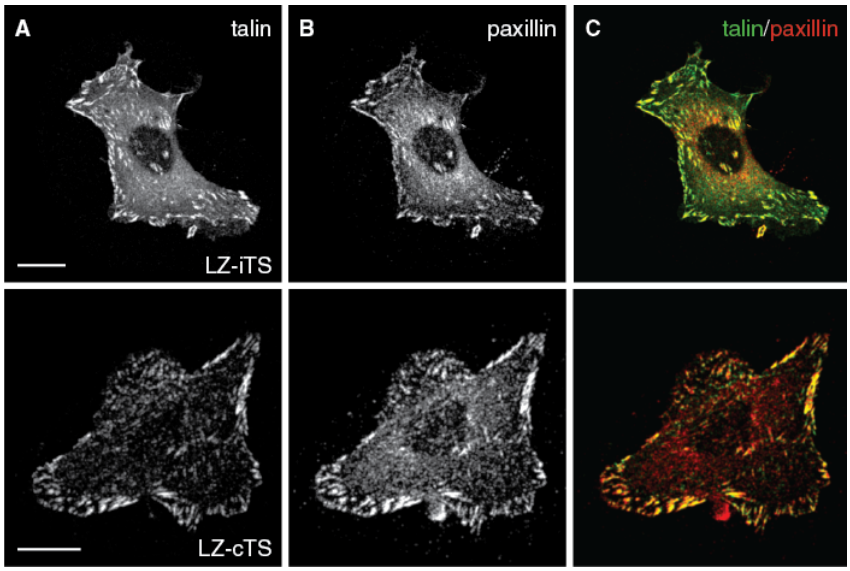

Figure 2.14: LZ-based tension sensor constructs localize in FAs. Rescued KO cells, re-expressing (**A**) talin-1 LZ-tension sensor constructs stained with (**B**) anti-paxillin antibody. (**C**) All constructs efficiently localize in paxillin-positive FAs (indicated by yellow areas in the merged image. Scale bars 20 μm.

2.3.1.3 Villin headpiece

The villin headpiece (VH) peptide is a well- studied ultrafast folding peptide. Using single-molecule force spectroscopy, unfolding and refolding behavior of the isolated peptide, fused to two ubiquitins, have been extensively studied[156]. These studies revealed that VH adopts an folded conformation under zero force conditions, which can be induced to elongated by the application of about 6-8 pN. Once mechanical tension is released VH quickly folds back to its original state in less than 1 µs.

Figure 2.15: schematic model of villin-head peptide, modified from [157].

To test whether the remarkable properties of VH are retained after insertion between two fluorophores, a VH-based tension sensor was generated, expressed in cells, purified and subjected to single-molecule force spectroscopy-based calibration. As a result, not only the folding/unfolding properties of the VH but also fluorophore behavior upon force application

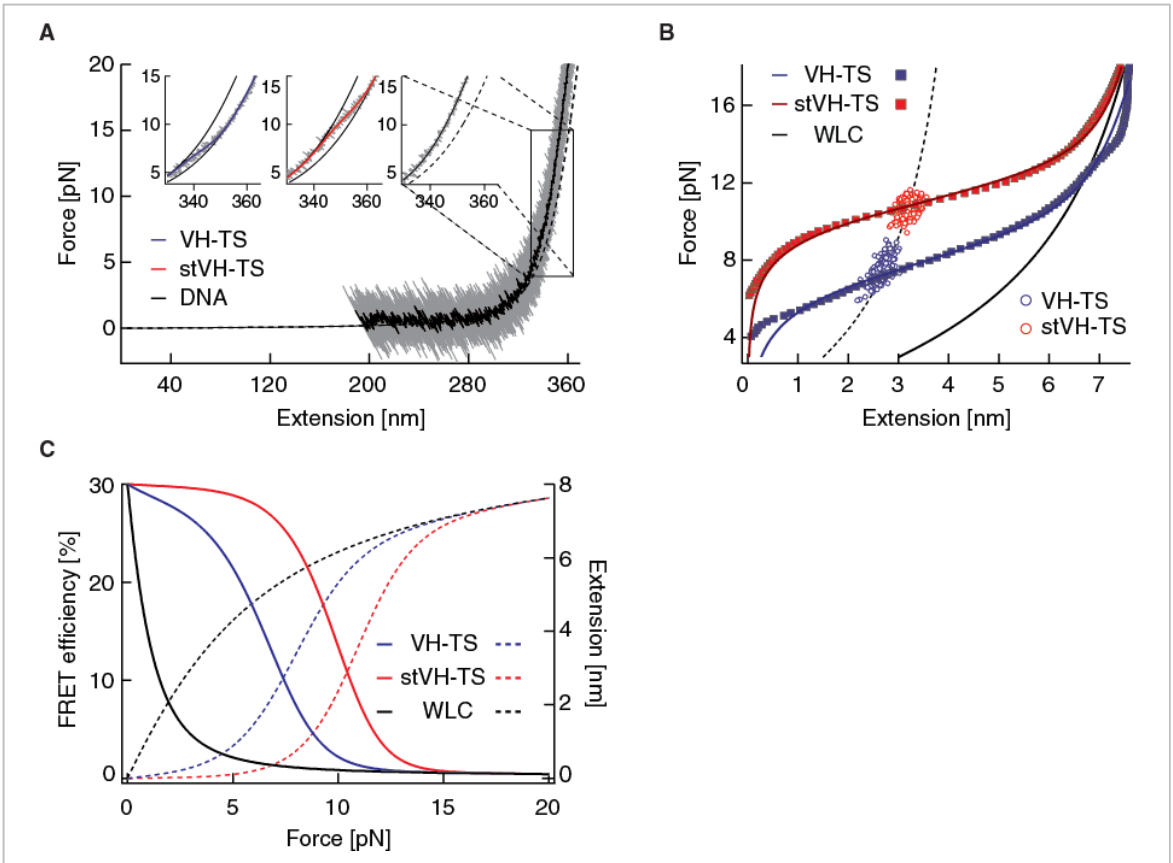

Figure 2.16: Single-molecule force spectroscopy calibration data for villin headpiece based tension sensor. (**A**) 200 kHz resolution force–extension trace (grey) fitted with an extensible worm-like chain model (black). Inset: zoom into representative force–extension traces of individual (st)VH-TS molecules as compared to DNA; the fit to VH-TS data is shown in blue, stVH-TS in red and DNA in black. (**B**) Average force–extension traces of individual VH-TS (blue) and stVH-TS (red) molecules. Experimental data are shown as filled squares; solid lines are fits to the data; open circles represent transition midpoints. (**C**) Modelled FRET–force (solid lines) and extension–force (dashed lines) correlations of (st)VH-TS.

could be analyzed. As expected, the VH-based tension sensors unfolds between 6-8 pN and quickly return to its folded state once forces are relieved. As the peptide properties did not seem to be affected by the insertion between two fluorophores, a second tension sensor module was constructed using a mutant VH peptide that was expected to unfold between 9-11 pN. Single-molecule calibration of this constructs revealed that the properties of this linker peptide are also unaffected.

Single molecule measurements as well as computational analysis were done by Alexander Mehlich (Technical University of Munich, Physics Department E22).)[156]. The experiment revealed a three state opening and closing behavior for both linker peptides (closed, half-closed/half-opened and opened state). The modeling results were further used to calculate the force-FRET response of the VH and stVH tension sensors (Figure 2.16). Calibration revealed that the VH based tension sensors are not only fast responding and correctly folded but also in the suitable force regime for talin-1 force analysis with transition midpoints at 7 pN and 10 pN.

The VH based sensor constructs expressed in KO cells localized in paxillin positive FAs that terminated f-actin bundles, as shown in immunostainings (Figure 2.17).

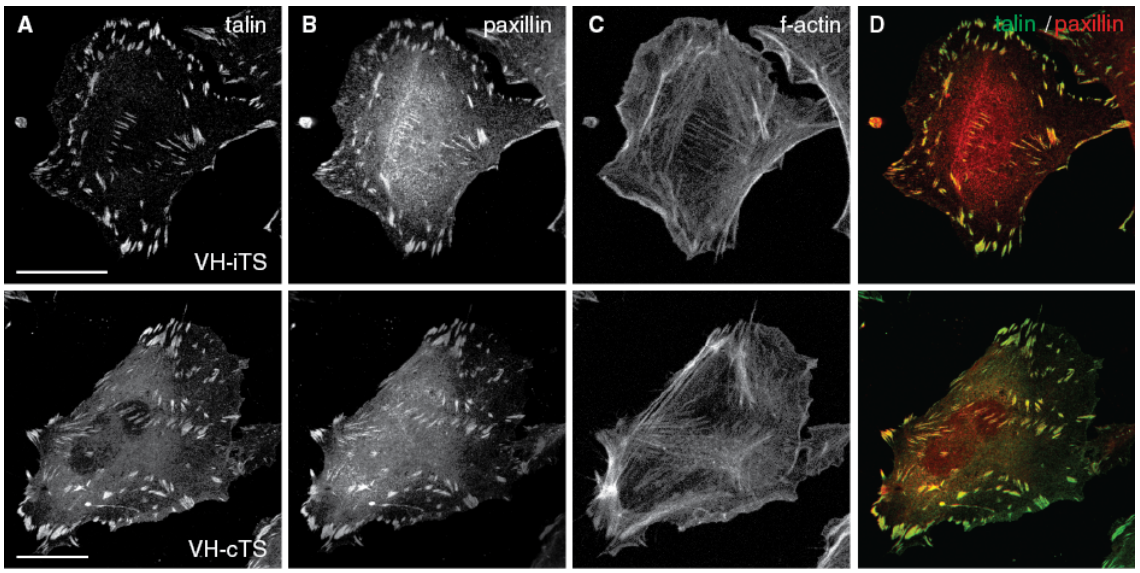

Figure 2.17: Immunostainings of rescued KO cells, re-expressing talin-1 VH based tension sensor constructs. (**A)** talin-1 internal VH based tension sensor (VH-iTS) and talin-1 C-terminally tagged with the tension sensor module (VH-cTS)) constructs stained with (**B**) anti-paxillin antibody and (**C**) phalloidin. (**D**) Talin-1 and paxillin co-localization is indicated by yellow color in merged images. Scale bars 20 µm.

2.3.1.4 VH peptide is the most promising linker candidate for force measurements across talin-1

All three tested variants of the talin-1 tension sensor construct efficiently localized to paxillin positive FAs and rescued the severe adhesion and spreading defect of talin-deficient cells. TSCPC-FLIM measurements of the F40 peptide sensor revealed that the F40 peptide can monitor forces across talin-1, as the internal sensor showed lower FRET efficiencies than the C-terminal control but the dynamic range of the sensor was lower than for the VH based tension sensor. Small differences in talin-1 forces could not be detected by the F40 sensor, leading to the conclusion that the VH based sensors monitor talin-1 tension more efficiently than a biosensor using F40 peptide[154].

Single molecule force calibration of the LZ motive showed that the peptide was able to withstand forces in the relevant range of about 8 pN, not the expected higher force range of about 14 pN. However, fitting of the force-extension data showed multi-state folding reaction of the LZ peptide, making assumptions on force-FRET correlations difficult. In contrast, the VH peptide was sensitive to a comparable force regime but could be fitted in a more simple three-state model[154].

Altogether, the VH based tension sensors were the most appropriate candidate to measure forces across talin-1 and was therefore evaluated in more detail concerning protein functionality.

2.3.2 Talin-1 constructs rescue KO phenotype

2.3.2.1 Talin-1 constructs localize to paxillin positive FAs

Integrity of protein function by the insertion of a large protein construct as the tension sensor probe was critical for all further analysis. Hence, not only the integrity of the inserted fluorophores but also talin-1 functionality was tested by various approaches, such as subcellular localization in immunostainings, integrin surface expression and -activation by FACS and protein expression levels by western blot analysis. In all experiments, KO cells re-expressing C-terminally YPet-tagged talin-1 were used as reference. The C-terminally tag did not interfere with protein localization to FAs and co-localized with paxillin (Figure 2.18).

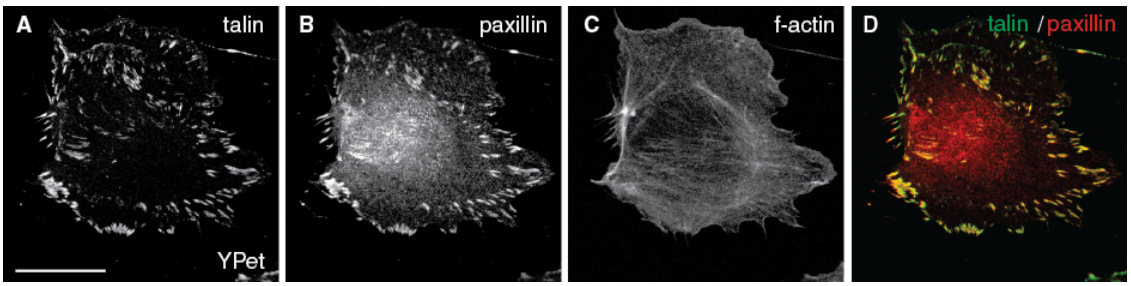

Figure 2.18: Immunostainings of rescued KO (*Tln1 -/- Tln2 -/-*) cells, re-expressing (A) talin-1 YPet constructs; stained with (**B**) anti-paxillin antibody and (**C**) phalloidin. (**D**) Talin-1 and paxillin co-localization is indicated by yellow color in merged images. Scale bar 20 μm.

2.3.2.2 Protein expression levels are comparable in western blot

Knockout of core components within a protein complex can sometimes lead to downregulation of other proteins within the complex. Furthermore, re-expression of proteins in knockout cells lines should match wildtype expression levels to exclude artefacts of overexpression. To examine expression levels of different FA related proteins in all used cell lines, western blot analysis was performed. The analysis showed comparable expression levels of all three reconstituted talin-1 cell lines and WT. Expression of other FA resident proteins such as vinculin and FAK was unchanged (Figure 2.19).

The reduction of FAK phosphorylation at Y397 in the talin-1 knockout cells, that has been described before[92], was rescued by re-expression of all constructs. Tubulin expression was used as loading control.[154]

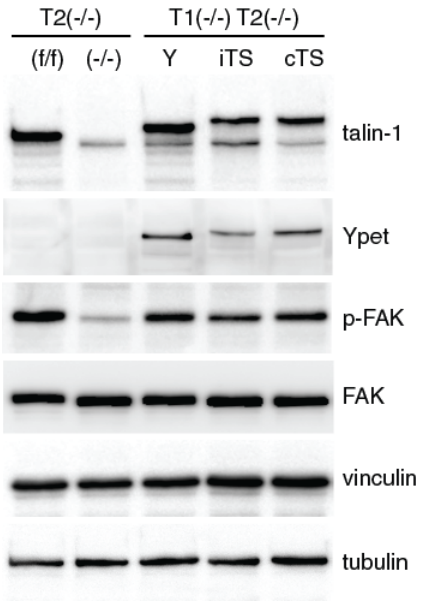

Figure 2.19: Western blots of talin-1 parental and stable cell lines. Tension sensor constructs (iTS and cTS) express lower protein levels than Tln1 f/f Tln2 -/- (WT) and Tln1Y (Y) cells. Talin-1 expression is abolished in Tln1 -/- Tln2 -/- (KO)cells. Western blots shown were performed by Carsten Grashoff and published in [154].

2.3.2.3 Integrin expression and function defects are rescued by re-expression of talin-1 constructs

As a first readout for cellular adhesion and thus integrin functionality, plate and wash assays were performed, where adhesion capacity to FN was tested (chapter 4.2.12). Compared to WT cells, KO cells failed to adhere to FN coated surfaces after 30 min seeding at 37 °C. This adhesion defect was rescued by the re-expression of all talin-1 constructs (Figure 2.20).

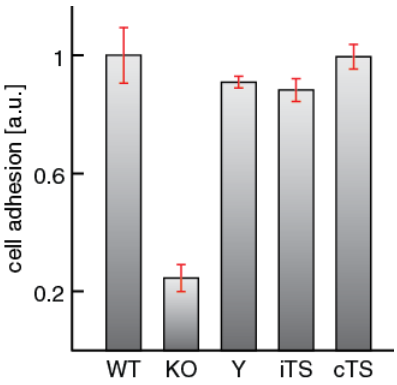

Figure 2.20: Adhesion defect of KO cells is rescued by the re-expression of all talin-1 constructs. Adhesion was normalized to WT cells. KO cells showed poor adhesion to FN after 30 min seeding that could be rescued to by the re-expression with all talin-1 constructs: eighter YPet tagged, integraded (iTS) or C-terminally tagged (cTS) tension sensor. Error bars indicate s.e.m..

Molecular basis for the observed adhesion defect was found by FACS analysis that showed a reduction of total as well as activated β1 surface expression and thus integrin activation in the KO cells. As a control for unspecific labeling of the antibodies, cells deficient of integrin surface expression were used (control)[158].

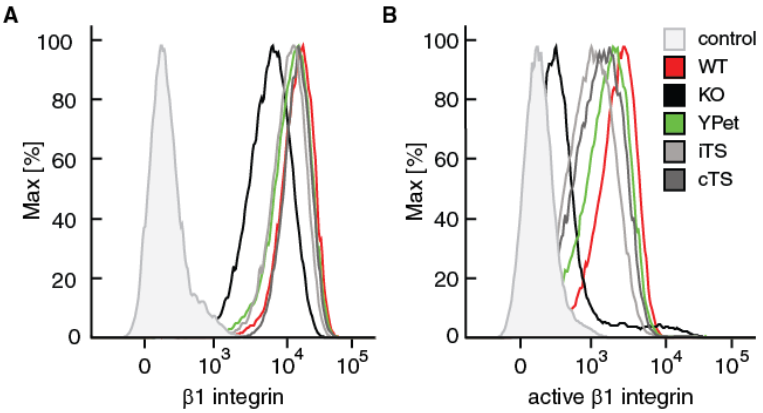

Figure 2.21: Integrin β1 surface expression levels in FACS. Representative intensity blots of WT, KO, Tln1YPet , Tln1iTS and Tln1cTS cell lines showing (**A**) total β1 or (**B**) active β1 (9EG7) integrin surface expression levels. Both levels are reduced in KO cell lines and rescued upon talin-1 re-expression. Pan-integrin knockout cells served as negative control.

Re-expression of all three talin-1 constructs efficiently rescued the reduced β1 surface expression (Figure 2.21, Figure 2.22) and activation. Interestingly, rescue capacity in FACS correlated with talin-1 expression levels in western blots (Figure 2.19).

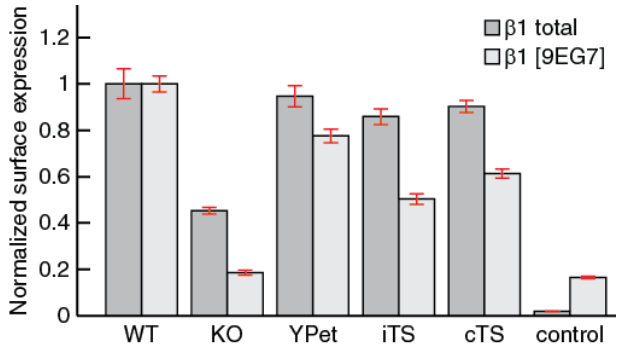

Figure 2.22: Evaluation of FACS data shown in Figure 2.21. Total β1 (dark gray) and active β1[9EG7] (light gray) surface expression levels in talin-1 cell lines. Expression levels were normalized to expression levels of WT cells. Pan-integrin knockout levels are indicated by 'control'. Data were pooled from 3 independent experiments. Error bars indicate s.e.m..

2.3.2.4 Protein turnover in FRAP of Tln1Y and Tln1iTS cells is comparable

Protein turnover analyzed by FRAP in living cells was used as indicator for protein functionality in living cells (chapter 4.5.3). To evaluate protein turnover in FAs, Tln1YPet and Tln1iTS cells were seeded on FN coated, micropatterned substrates on which they adopted a very regular shape and similarly sized FAs. A critical point in FRAP experiments of FAs is the difference in migratory state of the cells and the varying size of bleached FAs. When cells were seeded on pattern, both factors that complicate data evaluation could be overcome. In all experiments, the fluorescence of both talin-1 constructs (Tln1Y and Tln1iTS) recovered equally fast and both cells lines showed comparable mobile and immobile fractions (Figure 2.23). Hence, talin-1 turnover in FAs is unchanged by the introduction of the tension sensor module in the unstructured linker region.

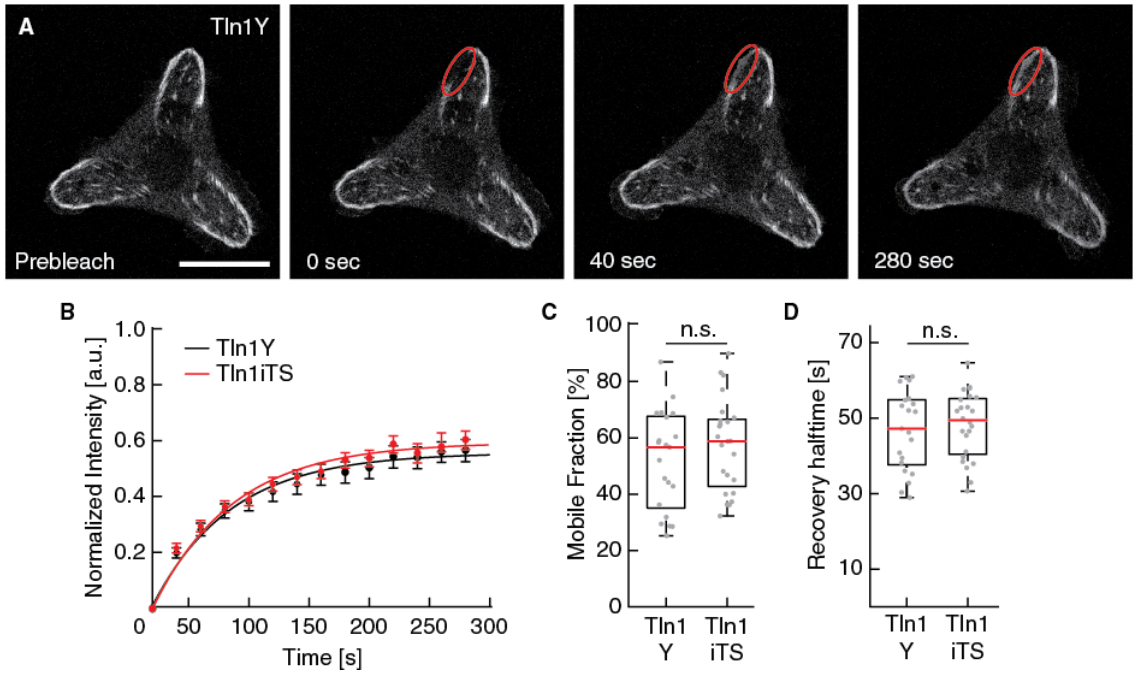

Figure 2.23: Results from FRAP experiments reveal no significant difference between Tln1Y and Tln1iTS. (**A**) Representative confocal images of FRAP experiments at indicated time points. Red oval highlights bleaching area. Scale bar 20 µm. (**B**) Normalized intensity blot, (**C**) mobile fraction and (**D**) recovery halftime of talin-1 YPet (Tln1Y) and talin-1 tension sensor (Tln1iTS) cells. No differences in protein recovery could be detected. Error bars indicate s.e.m..

2.3.2.5 Talin-1 function is not impeded by tension sensor insertion

Taken together, all talin-1 constructs localized efficiently to paxillin positive adhesions and showed comparable integrin surface expression and activation levels. Furthermore, talin-1 expression levels in the reconstituted cell lines were approximately the same as WT levels in western blot. In FRAP experiments, protein turnover in FAs of Tln1iTS cells resembled turnover of Tln1Y.

All these results suggested that protein function of talin-1 is unchanged by either insertion or C-terminally tagging with single fluorophores or the tension sensor probe.

Notably the rescue capability of the construct correlated with protein expression levels, as the internal tension sensor that showed lowest expression levels in western blot also showed lowest β 1 surface expression and least adhesion to FN.

2.3.3 Fluorophore stability is unchanged by the insertion into talin-1

Insertion of fluorophores into a potentially force bearing protein might lead to (partial) unfolding of the fluorophore under force and therefore changes in lifetime and FRET. To test potential effects of the insertion into talin-1 on donor and acceptor fluorophores, constructs with single YPet and mCherry inserted at our chosen insertion site were generated and compared to constructs C-terminally tagged with either fluorophore, but no property changes for both fluorophores could be detected. Both live cell emission spectra and fluorescent lifetimes were not significantly changed between C-terminally tagged or integrated fluorophore versions of talin-1, indicating that the insertion of the fluorophores into talin-1, does not affect fluorophore properties due to inefficient folding or partial unfolding (Figure 2.24). (The experiments were performed by Pia Ringer (MPI of biochemistry) and published in[154])

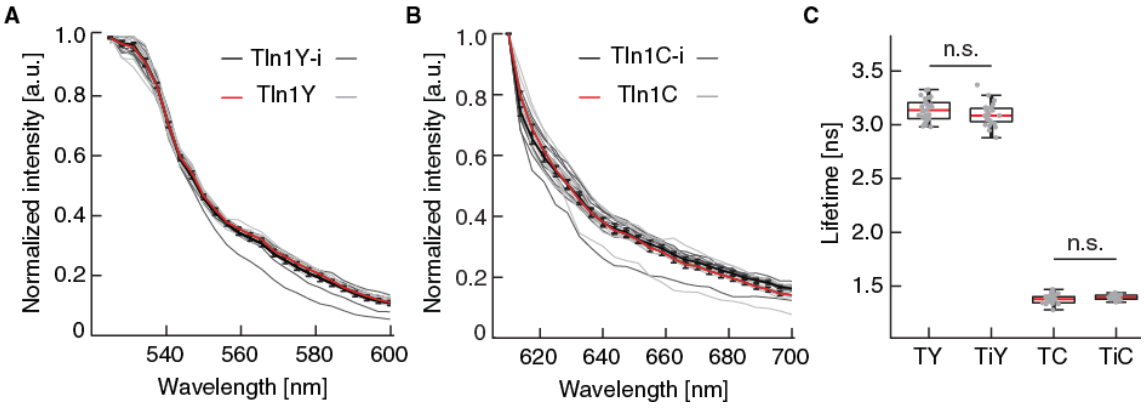

Figure 2.24: Test experiments for fluorophore stability after integration in talin-1. (**A+B**) Live cell emission spectra are comparable when fluorophores ((**A**) YPet, (**B**) mCherry) are integrated at the tension sensor insertion site or C-terminally tagged. (**C**) Live cell fluorescence lifetimes of internally and C-terminally tagged talin-1constructs do not show changes depending on fluorophore position. Experiments were performed by Pia Ringer (MPI of biochemistry) and published in [154].

Additionally, experiments concerning fluorophore stability were performed during the calibration of the VH tension sensor by single molecule force spectroscopy. Stretching of the full tension senor probe - including both fluorophores - revealed no unfolding when forces of 24 pN were applied to the peptide and held for more than 5 minutes. Only at pulling forces above 35 pN (pulling velocity: 500 nms^{-1}) unfolding of fluorophores could be observed, a force regime not expected for talin-1 (Figure 2.25, experiments were performed by Alexander Mehlich and published in [154]).

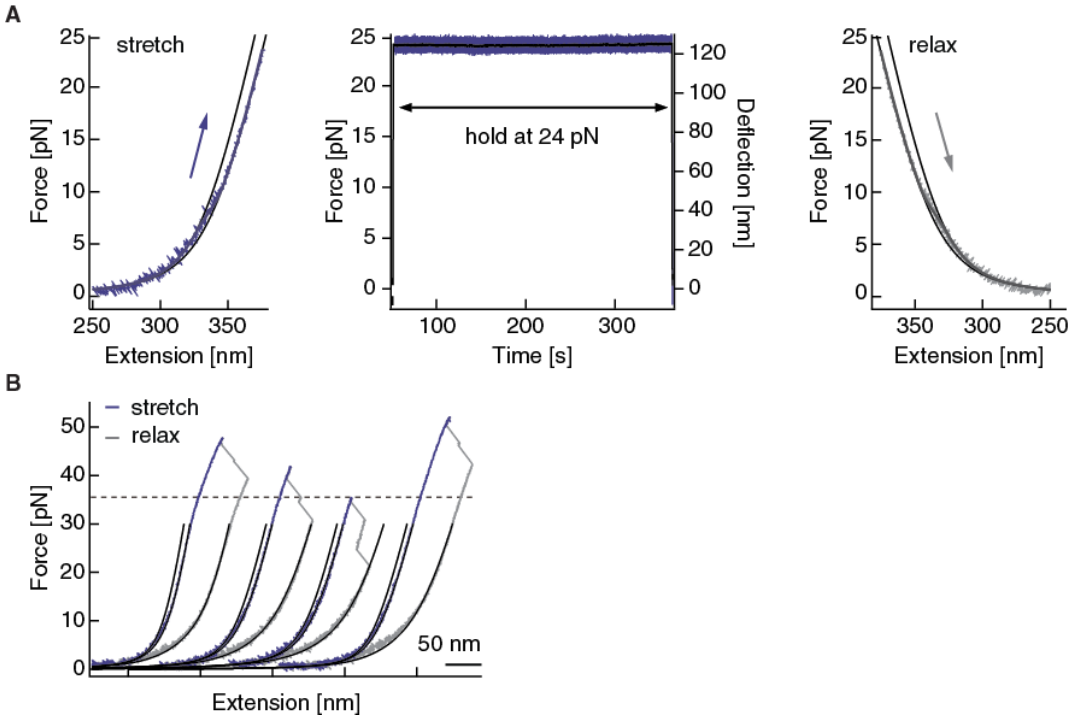

Figure 2.25: Analysis of fluorophore unfolding in VH tension sensor module perfomed by Alexander Mehlich. (**A**) After stretching to 24 pN, VH-TS was exposed to high force for more than five min before relaxation; no indications of fluorophore unfolding were observed. (**B**) Force–extension traces of four representative HP35-TS molecules showing fluorophore unfolding at high (35 pN) forces following stretching (pulling velocity: 500nm s^{-1}); traces were horizontally shifted for better representation.

2.3.4 Tension sensors monitor forces across talin-1

2.3.4.1 Talin-1 experiences mechanical forces in integrin engaged FAs

After probing of talin-1 functionality, forces were analyzed across the talin-1 tension sensor with TCSPC-FLIM and ratiometric FRET. In order to exclusively analyze signals from integrin engaged talin-1 molecules, a thresholding algorithm was applied to the images to specifically isolate FRET-signals from FA but not the cytoplasmic background (chapter 4.5.8). Ratiometric FRET measurements were performed by Pia Ringer and published in Austen et al.[154]. In summary, both FRET-methods showed reduced transfer rates in iTS cells seeded on FN as compared to cTS, indicating separation of the fluorophores due to forces across talin-1 in the tension sensor construct.

Using TCSPC-FLIM (chapter 4.5.5), forces across talin-1 were analyzed in more detail. When seeded on poly-L-lysine (pL), cells were unable to spread and showed only cytoplasmic localization of all talin-1 constructs. Under this condition no integrin association of talin-1 and thus no force propagation was expected.

Indeed, transfer rates in cells on pL were significantly raised for Tln1iTS, compared to cells seeded on FN, but no significant effect could be detected for the Tln1cTS cells (Figure 2.26 A). To analyze forces across talin-1 in more detail, the second variant of the VH based tension sensor was integrated into talin-1 (stiTS). Two point mutations in the VH aa sequence stabilize the peptide and raise the average equilibrium transition mid-forces from 7.4 pN to 10.6 pN (chapter 2.3.1.3). When analyzing the stiTS variant of the talin-1 tension sensor, the values for both sensors remained unchanged when seeded on pL, but elevated FRET values for the stable variant on FN suggested a larger proportion of talin-1 molecules were carrying forces of about 7 pN (Figure 2.26 B).

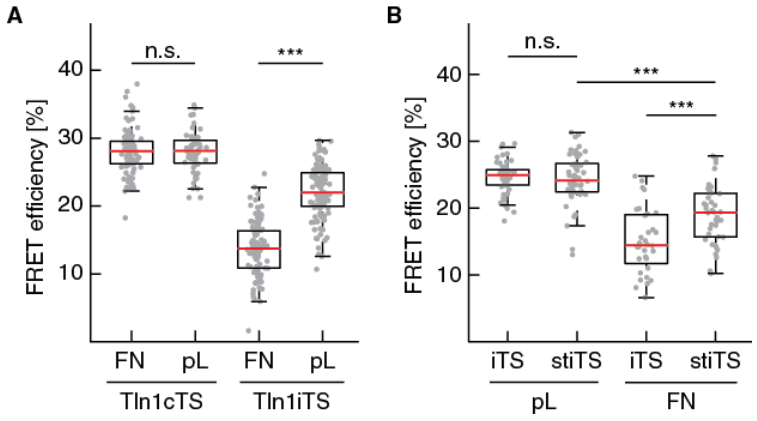

Figure 2.26: Talin-1 tension sensor montiors forces of 7-10 pN in integrin engaged FAs. (**A**) FRET values are highest in control cells (Tln1cTS) where the tension sensor module is persumably not under force. Tln1iTS cells seeded on pL, where talin-1 is not engaged in FAs, transfer rates are elevated compared to cells seeded on FN. (**B**) Cells seeded on pL show elevated transfer rates, independent of the linker force regime. In cells expressing the 7 pN linker, FRET is significantly lower than in the 10 pN sensor cells.

2.3.4.2 Influence of fluorescence intensity and intermolecular FRET are negligible in tension sensor experiments

Considering the intensity dependence of FRET measurements, correlation between FRET efficiencies and mean FA intensity was calculated to exclude expression level dependent changes in talin-1 forces. For cells seeded on FN, no correlation between both values could be measured in the tension sensor (Tln1iTS, Pearson correlation coefficient 0.3216) or the control (Tln1cTS, Pearson correlation coefficient 0.1609) cell lines (Figure 2.27) in TCSPC-FLIM experiments.

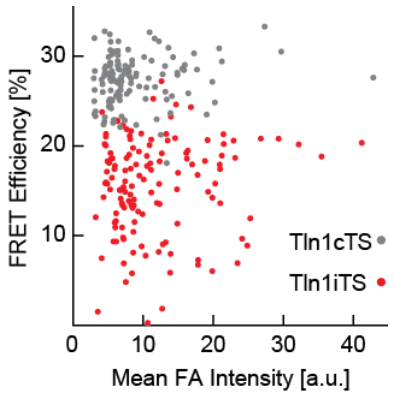

Figure 2.27: FRET efficiencies are independent of fluorescent intensitys. When plotting FRET efficiencies for the Tln1iTS and Tln1cTS against the mean intensity in FAs, no correlation between both values could be found. Pearson-correlation coefficient (FRET vs. intensity) Tln1iTS: 0.3216, Tln1cTS: 0.1609.

Intermolecular FRET is the energy transfer between fluorophores of neighboring molecules. To evaluate this potential side effect, constructs with single fluorophore insertions of Ypet and mCherry (see Figure 2.28) were co-expressed in KO cells. Co-transfected cells were seeded on FN and pL to measure intermolecular FRET values by TCSPC-FLIM in FAs as well as the cytoplasm.

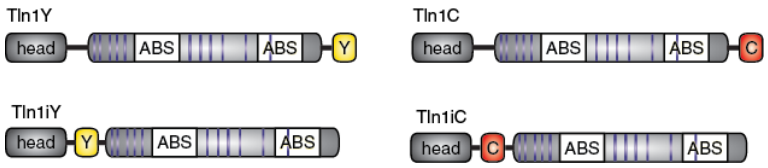

Figure 2.28: Schematic representation of control constructs for intermolecular FRET. Fluorophores used in the tension senor probes (YPet (Y) and mCherry (C)) were integrated in or C-terminally tagged to talin-1. Integration occurred at the same aa position as for the tension sensor probe.

FRET values in all experiments varied from 1-4 %, indicating that intermolecular FRET only plays a minor role in these experiments (Figure 2.29). Comparing internal and C-terminal constructs, a slight increase of intermolecular FRET was detected when the fluorophores were attached C-terminally, a result that might be explained by talin-1 dimerization at the C-terminus (chapter 1.2.3.5). In this case, the increased FRET efficiencies of Tln1cTS on FN compared to Tln1iTS on pL (Figure 2.26 A) could be a consequence of intermolecular FRET.

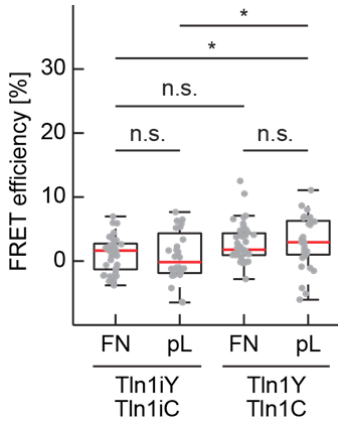

Figure 2.29: Intermolecular FRET is negligible in FRET measurements. Internal (Tln1iY and Tln1iC) and C-terminal control (Tln1Y and Tln1C) constructs were co-transfected in KO cells and seeded on FN and pL. In all cases, FRET efficiencies were considerably lower than with the tension sensor (see Figure 2.26).

2.3.5 Talin-1 tension sensor FRET measurements are insensitive to conformational changes

Talin-1 is believed to adopt an autoinhibited conformation in the cytoplasm via a head F3 and tail R9 domain interaction[109]. With mutations that inhibit the intramolecular association, effects of conformation in the tension sensor measurements were examined. We reasoned that the activation of talin should lead to altered FRET efficiencies in suspension if the FRET measurements were conformation sensitive. Several amino acids were shown to be important for inter-domain association in talin-1 as point mutations in these residues led to constitutive activation of talin-1 and therefore an increase in downstream effects, e. g. integrin activation[108]. Two mutants that were previously described (M319A[108] and K324D[159]) were introduced in the talin-1 tension sensor probe in order to control for effects of conformational changes in talin-1 in FRET experiments.

In immunostainings, both mutant proteins were recruited efficiently to FAs and co-localized with paxillin when re-expressed in KO cells (Figure 2.30).

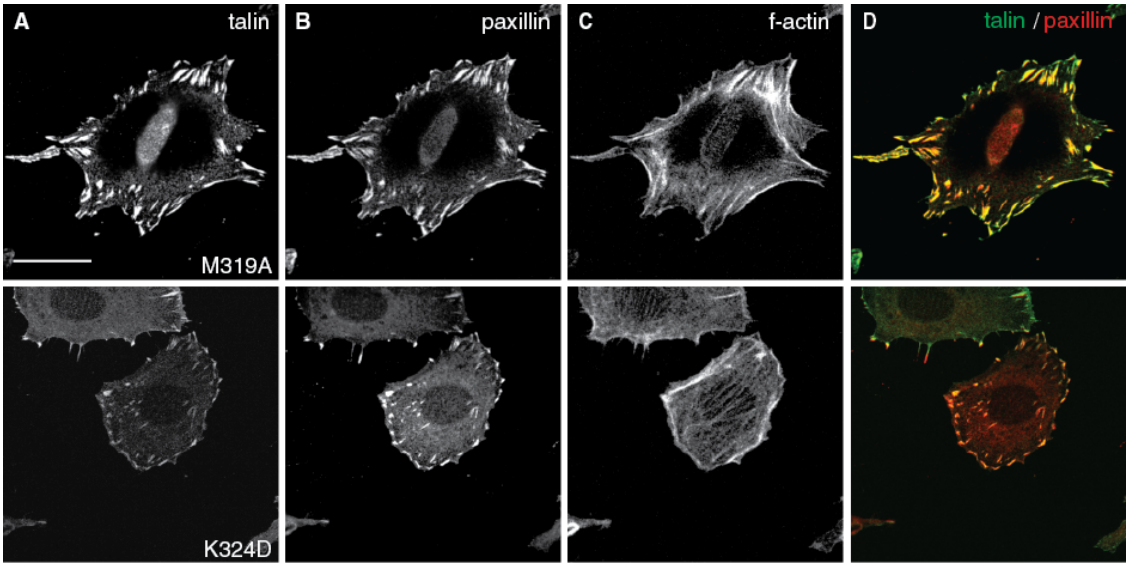

Figure 2.30: Immunostainings of KO cells, re-expressing activation mutant talin-1 constructs. (**A**) All constructs localize in (**B**) paxillin-positve FAs. (**C**) F-actin stress fiber formation was also not impared due to mutations in talin-1. (**D**) Talin-1 and paxillin colocalization is indicated in yellow areas in the merged image. Scale bar 20 μm.

In FACS analysis, total integrin β1 surface expression was not entirely recovering to WT levels after reconstitution with the mutant talin-1 proteins. In line with these observations, 9EG7 expression, was enhanced for M319A and K324D (Figure 2.31), indicating that the mutations in talin-1 enhance integrin activation due to inhibition of talin-1 auto-inactivation.

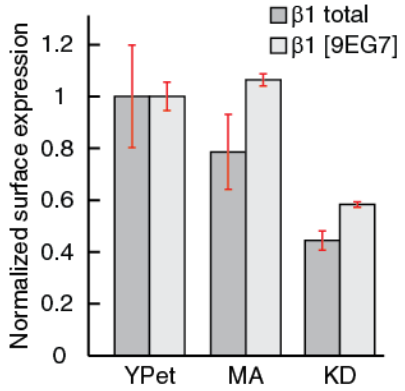

Figure 2.31: Active β1 surface expression in cells expressing active talin-1 mutants, measured by FACS. Values were normalized to wildtype talin-1 YPet (YPet) cells. Whereas 9EG7 levels are elevated in E1770A as well as M319A cells, they were significantly reduced in K324D. Error bars indicate s.e.m..

If insertion of the tension sensor would interfere with talin-1 function, e. g. by sterically inhibition of the head-tail interaction, cells expressing the mutant proteins seeded on pL should show altered transfer rates, but this was not the case for both analyzed mutants (Figure 2.32). These results indicate that inter-domain association of talin-1 has negligible effects in FRET measurements.

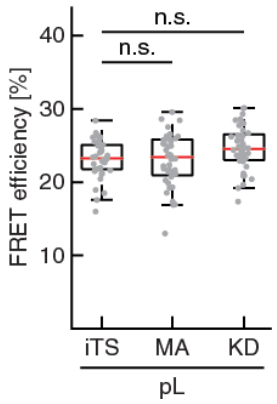

Figure 2.32: FRET efficiencies of activation mutant talin-1 tension sensors. When seeded on pL, the mutant proteins M319A (MA) and K324D (KD show no significant differences compared to the wildtype protein (iTS), suggesting that conformational changes are not the cause for changes in FRET in FAs.

2.3.6 Talin-1 tension is insensitive to changes in substrate rigidity

An important physical property of tissues is their rigidity. Cells respond to changes in tissue stiffness of their surrounding environment by reorganization of FAs as well as the cytoskeleton and thus surface area[160]. This suggests a force-dependent outside-in and inside-out signaling that might be dependent on central FA components such as talin-1. To test whether talin is subject to mechanical forces on substrates with physiologically relevant compliance, tension across talin-1 was analyzed by TCSPC-FLIM on substrates of varying stiffness indices (0.2 kPa, 0.5 kPa, 1 kPa, 2 kPa, 4 kPa, 12 kPa, 25 kPa and glass (~70 GPa)). Cells responded to different substrates in the expected rigidity dependent increase in cell area[154]. For example, when seeded on 1 kPa soft substrates, cells were able to form larger adhesion areas with actin fibers interconnecting the talin-1 positive adhesions. On 0.5 kPa in contrast, cells were not able to spread properly, although small adhesion sites enriched for talin-1 were still present (Figure 2.33).

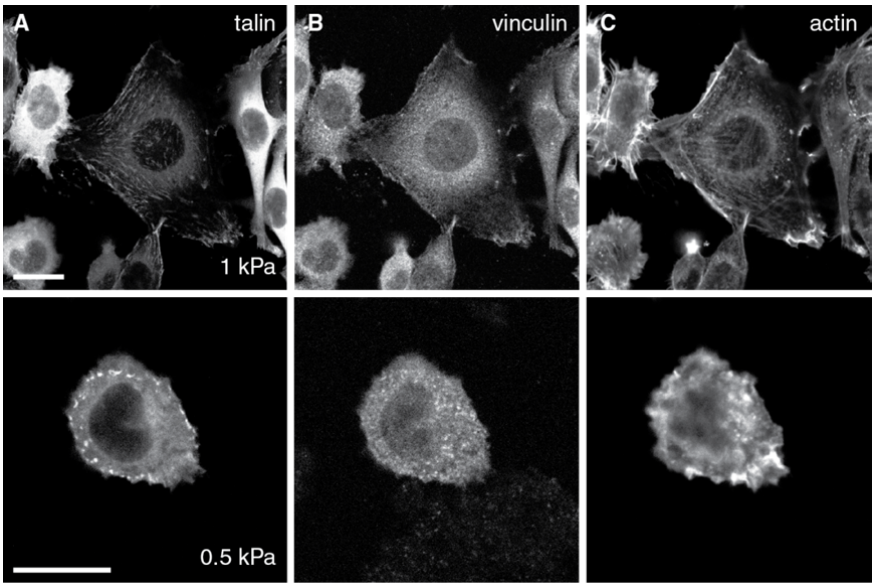

Figure 2.33: Representative images of Tln1iTS cells on soft substrates coated with FN. On both substrate rigiditys, Tln1iTS (**A**) positive adhesive areas are present. Cells were able to spread on 1 kPa but failed on 0.5 kPa, where only small talin-1 positve adhesion sites were formed. (**B**) Vinculin localized to adhesion sites on 1 kPa but with less efficiency compared to glass. (**C**) Acin filaments were formed on 1 kPa but not on 0.5 kPa. Scale bars 20 μm.

In TCSPC-FLIM measurements talin-1 forces stayed constant over a wide range of substrates and only increased below rigidities of 4 kPa (Figure 2.34). Missing actomyosin contractility, indicated by missing stress fiber formation, however, impeded force transduction across the talin-1 on softer substrates. Thus, talin-1 forces are mostly independent of external rigidity signals over a wide range of stiffness indices.

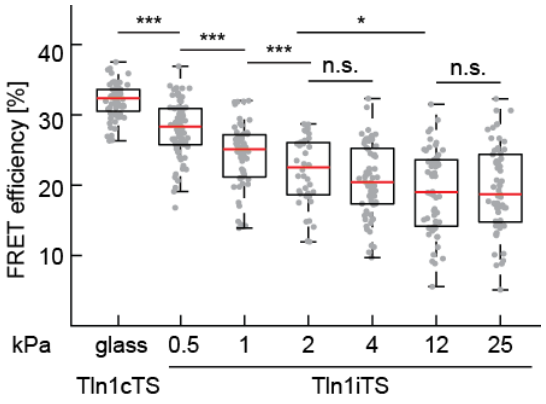

Figure 2.34: FRET efficiencies of the talin-1 tension sensor cells on different substrate rigidities. Compared to the C-terminal control (Tln1cTS) seeded on glass, talin-1 forces remain constant on a wide range of substrate stiffnesses but slightly rise at 2 kPa to 0.5 kPa, where almost control levels are obtained.

This observation seemed contradictory to the rigidity dependent increase in traction forces that has been reported before[161,162]. Hence, traction force experiments were performed in order to investigate forces exerted by the cell upon the extracellular environment (Chapter 4.5.4.4). In contrast to relatively stable forces across talin-1, traction forces exerted by the cells onto the underlying FN coated PAA substrates were increasing with substrate stiffness (Figure 2.35). This results match reports from earlier studies that found increased traction with rising substrate young's modulus[161]. Analysis of traction force data was performed by Benedikt Sabass (Princeton University).

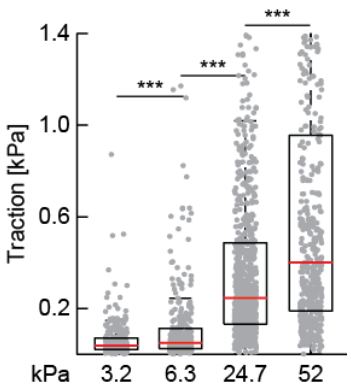

Figure 2.35: Traction forces generated by talin-1 tension sensor cells on PAA Gels of indicated stiffness. Mid forces rise with increasing rigidity defined by young's modulus [kPa].

Increasing cellular traction forces also correspond with increasing forces across talin-1 on low rigidities, but talin-1 forces reach a plateau above 4 kPa substrates, traction forces further increase in a rigidity dependent manner. As FAs increase their size on stiffer substrates it

appears that the increase in traction force rather correlates with increased talin recruitment rather than increased force propagation per molecule.

2.4 Regulation of talin-1 forces

If talin-1 forces are largely independent on external stimuli like substrate rigidity, other regulatory processes might be influencing talin-1 mechanotransduction. As integrin activation is a major function of talin-1, the integrin-talin-1 was analyzed in more detail.

2.4.1 Integrin binding is influencing talin-1 force transduction

The impact of integrin association on talin-1 forces was analyzed by reconstitution of KO cells with integrin binding deficient talin-1 constructs. Talin-1 carries two IBSs, one in the F3 site of the FERM domain in the talin-1 head (IBS1) and a second in the C-terminal end (residues 1984-2113) of the rod domain (IBS2). Whereas IBS1 was found to activate integrins through the association with the NPxY motive in integrin tails, the role of IBS2 is still unclear. It is thought to play a major role in establishing the linkage between integrins and the cytoskeleton through talin-1[163]. In Drosophila it was found that the IBS2 fulfills different functions than IBS1 during development and maintains the connection between integrins and other FA components[164]. As the concrete function of both IBSs has not been entirely solved yet, impact on force transduction of both sites was analyzed using the established talin-1 tension sensor. Point mutations in both sites were reported in earlier studies to impair FA localization (L2094A/I2095A[163]) or integrin binding (R358A[165]) of talin-1. By site specific mutagenesis PCR (chapter 4.1.2.2.4), these point mutations were introduced into Tln1iTS and expressed in KO cells. Surprisingly, constructs efficiently localized in paxillin positive FAs (Figure 2.36) suggesting that, in case of impaired functionality of one IBS, the other recognition site can compensate for the loss in binding capacity. Therefore, a mutant in which both sites were mutated (R358A/L2094A/I2095A, AAA) was generated but, also this constructs efficiently rescued the phenotype of KO cells and localized to paxillin-positive FAs.

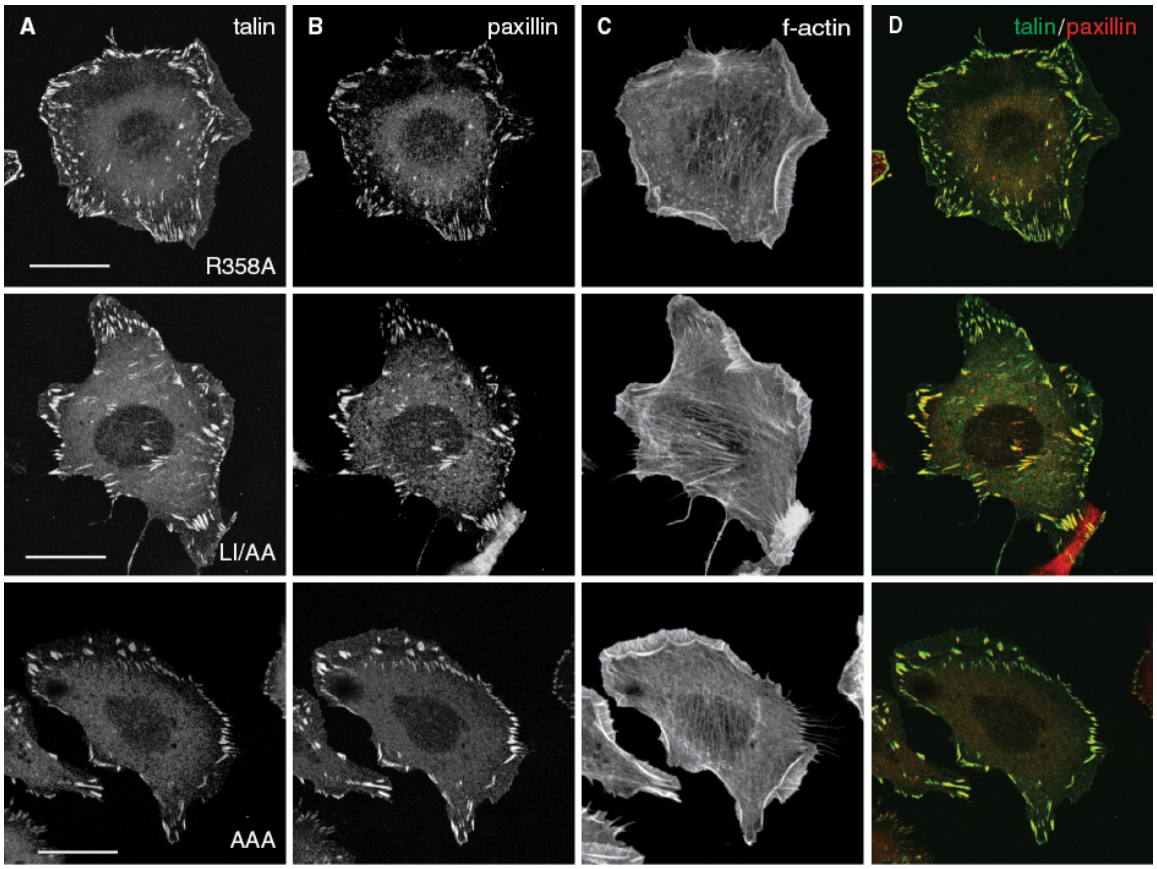

Figure 2.36: Representitve immunostainings of KO cells, expressing integrin binding deficient talin-1 variants (R358A (RA), L2094A/I2095A (LIAA) and R358A/L2094A/I2095A (AAA)). (**A**) Talin-1 constructs efficiently localize to adhesions, positive for (**B**) anti-paxillin antibody. (**C**) F-actin network stained by phalloidin. Stress fiber formation is not impared by the mutations. (**D**) Colocalization is indicated by yellow regions in the merge image. (third panel). Scale bars 20 μm.

Along with efficient localization to FAs, integrin β1 seemed not significantly impaired. Total β1 surface expression was not fully recovered after talin-1 re-expression, but activation measured by 9EG7 levels was not reduced when cells expressed integrin binding deficient talin-1 mutants. (Figure 2.37).

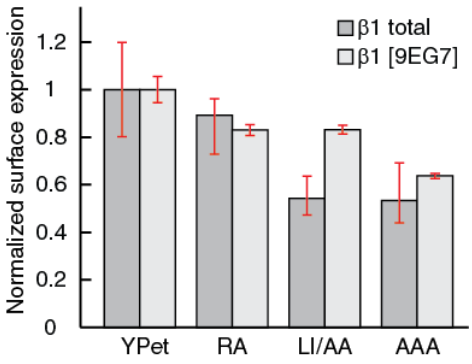

Figure 2.37: Integin β1 surface expression levels in KO cell lines expressing integrin binding deficient talin-1 mutants. In all three point mutations (R358A (RA), L2094A/I2095A (LIAA) and R358A/L2094A/I2095A (AAA)) total β1 (dark gray bars) and active integrin levels (9EG7, light gray) were lower compared to wildtype talin-1 (YPet). Error bars indicate s.e.m..

These experiments suggested that the mutations did not fully abolish talin-integrin interaction in our cell system. However, binding affinity of talin-1 to integrin tails could be lower compared to wildtype protein and thus minimize load bearing capacity of the interaction.
Analysis of FRET by TCSPC-FLIM in all three mutants revealed slightly reduced forces across the mutated proteins (Figure 2.38), indicating an impact of the point-mutations in force transduction probably due to shorter lifespan of the integrin-talin-1 connection. The localization of the three mutant proteins to FAs, however, suggests that single residue mutations are insufficient to study the impact of the IBS in talin-1 force transduction.

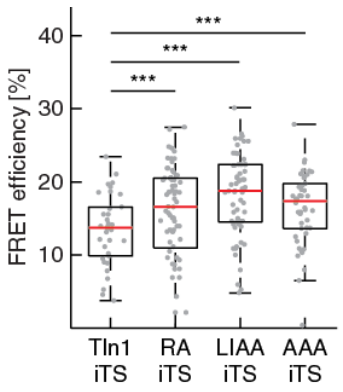

Figure 2.38: FRET efficiencies in cells expressing integrin binding deficient talin-1 variants. Compared to the 'wildtype' talin-1 tension sensor (Tln1iTS), all three integrin binding mutant proteins ((R358A (RA), L2094A/I2095A (LIAA) and R358A/L2094A/I2095A (AAA)) showed an increase in FRET efficiencies in TCSPC-FLIM experiments.

Nevertheless, these data demonstrate that the strength of the talin-1-integrin interaction is a critical determinant of force transduction across talin-1. They also indicate that both IBSs play a role in force transduction and integrin activation through talin-1. The minor effects of the mutations on FRET efficiencies, however, give reason to doubt the regulatory role of integrin association on talin-1 forces. Thus, other talin-1 interaction partners were analyzed concerning their regulatory role in talin-1 force regulation.

2.4.2 Talin-1 dimerization plays an important role in talin-1 function

Talin-1 is not only associated with various other FA components but also thought to form homodimers. Furthermore, homodimerization was suggested to play an important role in protein function and f-actin binding, thus force propagation[85]. In order to test this hypothesis, cell lines from KO cells were created, expressing talin-1 mutant proteins with either a point mutation (R2526G) in the C-terminal helix or full deletion of the DD (Δ2496). Hereby, the full deletion mutant was used as a control for the R2526G point mutation to exclude dominant negative effects of the point mutation and serve as positive control in FRET experiments for complete elimination of talin-1 homodimerization.

In contrast to earlier publications that reported a localization defect for the R2526G mutant protein[166], co-localization of the mutant talin-1 with paxillin in small adhesion sites was detected in immunostainings (Figure 2.39). Similar to the R2526G point mutation also the Δ2496 mutant localized in FAs. Compared to cells expressing wildtype talin-1, however, both cell lines appeared smaller and formed smaller adhesions. Due to the small size of the adhesions, the algorithm for FA size detection was not efficiently working, so an automated, quantitative evaluation was not possible in this case.

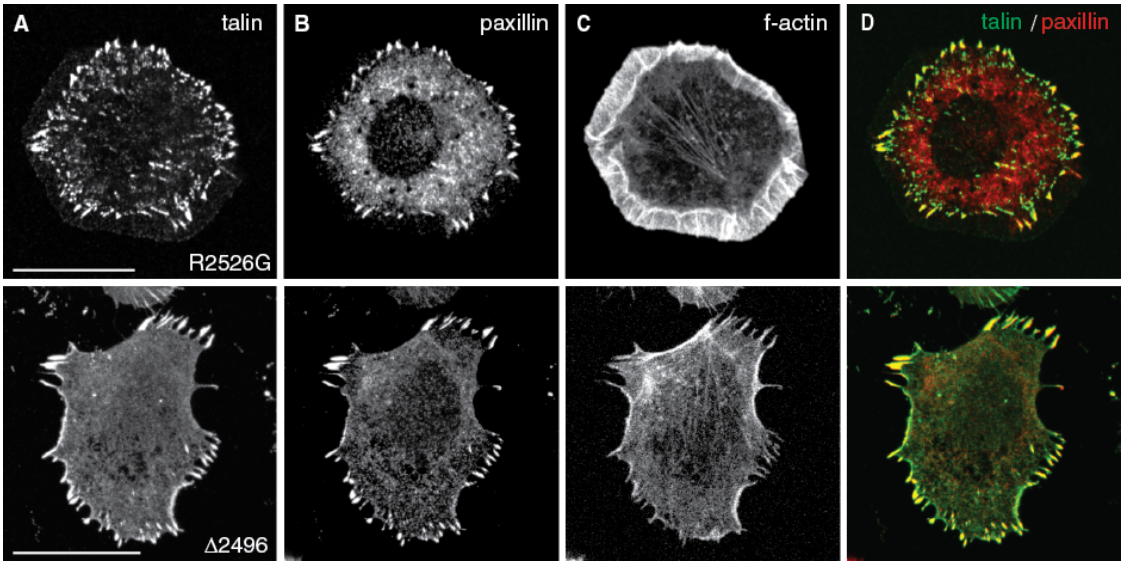

Figure 2.39: Talin-1 dimerization mutants localize in FAs in immunostainings (**A**) KO cells re-expressing talin-1 dimerization mutants stained (**B**) with anti-paxillin antibody to label FAs and (**C**) phalloidin to visualize f-actin fibers. (**D**) Areas of co- localization are indicated by yellow color in the merged image. Scale bars 20 μm.

To exclude implications of talin-1 function due to mutations in the dimerization helix, FACS analysis of active β1 surface expression was also performed in these cell lines. Lack of talin-1 dimerization, however, caused by point mutation or full deletion, reduced total β1 levels and slightly decreased 9EG7 binding (Figure 2.40).

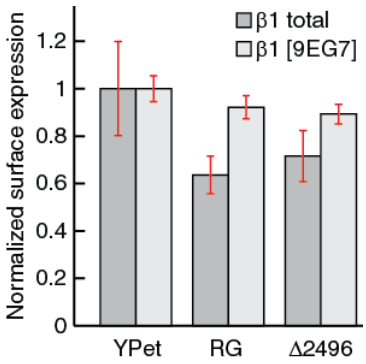

Figure 2.40: Active integrin β1 surface expression of cells expressing talin-1 dimerization mutants measured by 9EG7 expression levels in FACS. Both, point mutant (R2526G) and full deletion mutant (Δ2496) show only slightly reduced integrin activation in FACS. Error bars indicated s.e.m..

Subsequently to functionality tests, force propagation across talin-1 was analyzed by FLIM microscopy. Both talin-1 mutants showed reduced tension across talin-1 in FAs, as cells expressing both mutants are indicated by enhanced FRET efficiencies compared to wild type talin-1 (Figure 2.41).

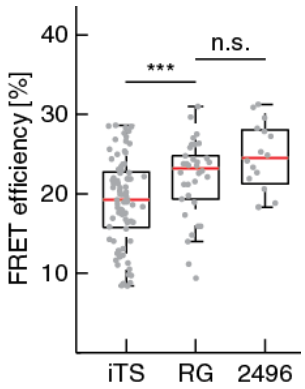

Figure 2.41: FLIM measurement of dimerization mutants. Transfer rates are elevated in dimerization mutant (point mutation R2526G and full deletion Δ2496) expressing cell lines, compared to wildtype protein.

Altogether, mutations that inhibit talin-1 seem to impair protein function, as cells show defects in spreading and FA maturation but similar to mutations in the IBSs, however, the role of talin-1 homodimerization role in talin-1 force regulation should be analyzed in more detail in the future.

If neither integrin association nor talin-1 dimerization is an essential factor for the force transmission across talin-1, engagement with the f-actin cytoskeleton is presumably a major determinant of talin-1 mechanotransduction. Talin-1 directly binds f-actin in 3 ABSs but is also indirectly linked through association with vinculin (Chapter 1.2.3.7). Thus, the influence of both binding partners was analyzed in more detail.

2.4.3 Talin-1 tension depends on f-actin and vinculin binding

2.4.3.1 Talin-1 forces are sensitive to changes in actomyosin contractility

Talin-1 binding to f-actin is thought to be a critical step in FA force transduction and thus mechanosensing. If this was the case, inhibition of actomyosin contractility should negatively influence talin-1 forces. Indeed, a significant increase in FRET efficiencies was detected when Tln1iTS cells were seeded on FN and treated with Y-27362 - a ROCK inhibitor blocking myosin light chain phosphorylation - controls (Tln1cTS) remained unaffected (Figure 2.42).

2.4.3.2 Mechanically engaged vinculin is important for high forces across talin-1

The connection between talin-1 and f-actin is not only established by direct interaction but indirectly enhanced through vinculin association at 11 VBS to the talin-1 rod (chapter 1.2.3.7). Thus, the correlation between f-actin binding and talin-1 forces was further analyzed by investigating the influence of vinculin in talin-1 force transduction. Therefore, vinculin expressing (*vin*$^{f/f}$) and vinculin null (*vin*$^{-/-}$) cells were transiently transfected with the talin-1 tension sensor (Tln1iTS) and tension was determined by TCSPC-FLIM measurements. These experiments revealed reduction in talin-1 forces upon loss of vinculin. This effect was reversible by the stable re-expression of vinculin-BFP (V-wt); a vinculin-head-BFP (V-mut) construct missing the f-actin binding tail in contrast was unable to rescue FRET levels in the vinculin null background, underlining the importance of f-actin association to talin-1 in force transduction (Figure 2.43).

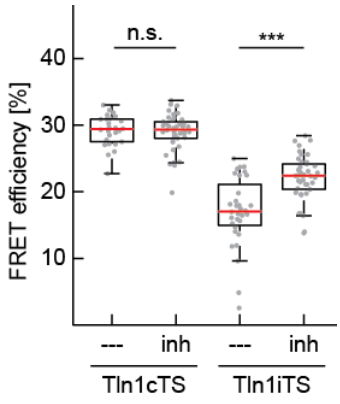

Figure 2.42: FRET efficiencies of cells treated with ROCK inhibitor. FRET efficiencies in tension sensor (Tln1iTS) and control (Tln1cTS) cell lines treated with ROCK inhibitor Y27362 (inh) or untreated control (---). Treatment has no effect on controls, but raises transfer rates in tension sensor cells, indicating reduced forces across talin upon reduced cell contractility.

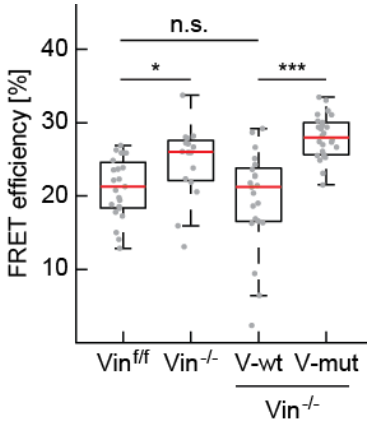

Figure 2.43: Vinculin expression regulates talin-1 forces. Compared to vinculin wildtype (*vin*$^{f/f}$) cells, vinculin deficient cells (*vin*$^{-/-}$) have increased FRET values when seeded on FN. This increase can be rescued by re-expression of full-length vinculin, tagged with BFP (V-wt) but not the vinculin head (V-mut).

In the absence of vinculin forces across talin-1 were reduced but not entirely absent. This was shown in Austen et al.[154] by treatment of *vin*$^{f/f}$ and *vin*$^{-/-}$ cells, stably expressing Tln1iTS with the ROCK inhibitor Y-27632 (Figure 2.44). Loss of actomyosin contractility in *vin*$^{-/-}$ cells increased FRET efficiencies significantly compared to untreated cells, indicating remaining forces of talin-1 in the absence of vinculin (Data shown in Figure 2.44 were generated by Pia Ringer, MPI of Biochemistry).

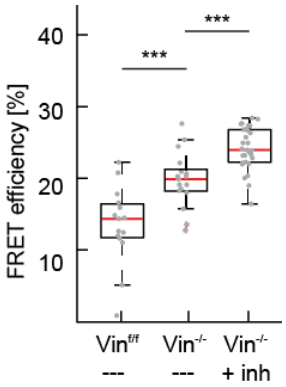

Figure 2.44: Inhibition of ROCK further increases FRET efficiencies in *vin*$^{-/-}$ cells. FRET efficiencies of *vin*$^{f/f}$ and *vin*$^{-/-}$ cells stably expressing Tln1iTS, untreated (---) or treated (+inh) with ROCK inhibitor Y-27632. FRET rates increase with reduction of actin association.

Taken together, these experiments indicate that f-actin and vinculin association are critical for force propagation across talin-1. Initial f-actin binding establishes low force bearing linkages whereas vinculin association further stabilizes the connection to withstand higher forces.

2.4.4 The role of ABSs and VBSs for talin-1 force transduction

To further analyze the role of the two ABSs and the 11 VBS in the talin-1 rod domain, three different deletion mutants were generated:

In the talin-1Δ2300 (Tln1-2300) construct, the C-terminal ABS as well as the DD was deleted. The shorter Tln1-1330 variant still carried the N-terminal ABS2 of the talin-1 rod but VBS 6-11 (R4- R13) were not expressed. Deletion of the ABS2 in addition to the six VBS (R7-R13) resulted in the short Tln1-950 mutant (Figure 2.45).

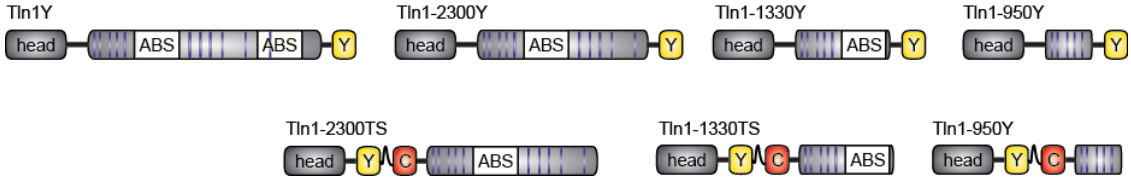

Figure 2.45: Schematic illustration of talin truncation constructs. In the upper row, all YPet tagged constructs are illustrated. Compared to full length talin-1, all truncation mutants are shortened from the C-terminus to varying degrees. In tension sensor constructs, the sensor module is integrated in the linker region between talin head and rod.

2.4.4.1 Truncated talin-1 mutants show characteristic phenotypes in immunostainings

Expression Tln1-2300Y in KO cells partially rescued the spreading defect of the knockout cells, even though cells were smaller than those reconstituted with Tln1Y. However, cells formed β1-9EG7 and vinculin positive FAs and displayed normal f-actin stress fibers.

Tln1-1330 and Tln1-950 showed almost identical phenotypes in immunostainings. Even though Tln1-1330 still carried ABS2, f-actin stress fibers could not be observed. These results match with a recent publication demonstrated that the R7 and R8 domains in the talin-1 rod are important for efficient f-actin binding[167]. In line with this observation, cells displayed a characteristic, round morphology and were only able to form small adhesion sites but no mature FAs. The adhesion structures were positive for the talin-1 constructs as well as active β1 integrin (9EG7) but vinculin colocalization could not be observed (Figure 2.46, Figure 2.47). For the quantification of talin-1 and vinculin co-localization, fluorescent intensity of talin-1 and vinculin in a FA was measured in a line horizontal to the FA principal axis and blotted in a histogram (Chapter 4.5.7). For Tln1Y and Tln1-2300Y higher Pearson-correlation-coefficients (Pearson correlation coefficient: Tln1Y=0.8011, Tln1-2300Y=0.6043) indicated co-localization of talin-1 and vinculin, whereas in Tln1-950Y and Tln1-1330Y low coefficients (Pearson correlation coefficient: Tln1-1330Y=0.2090, Tln1-950Y=0.2424) showed no vinculin association in talin-1 positive adhesion sites (Figure 2.47).

The shorter Tln1-950 mutant was used for further analyses, as the ABS2 was deleted in this mutant, so f-actin binding by the talin-1 rod was abolished. In this case it was hypothesized

that talin-1 f-actin association, either direct through the proximal ABS or indirect through opening of the N-terminal VBSs, was achieved. Hence, a more severe phenotype was expected in the Tln1-950 cell lines.

Recruitment of various other FA resident and talin-1 associated proteins was analyzed in immunostainings. Tln1-950 positive adhesion sites, though they were positive for active β1 integrin (9EG7), were devoid of FAK (Figure 2.48) and paxillin (Figure 2.49). Furthermore, α-actinin association with the f-actin cytoskeleton failed in the mutant cell line (Figure 2.48). Still, the structures were positive for kindlin-2 in stainings (Figure 2.50).

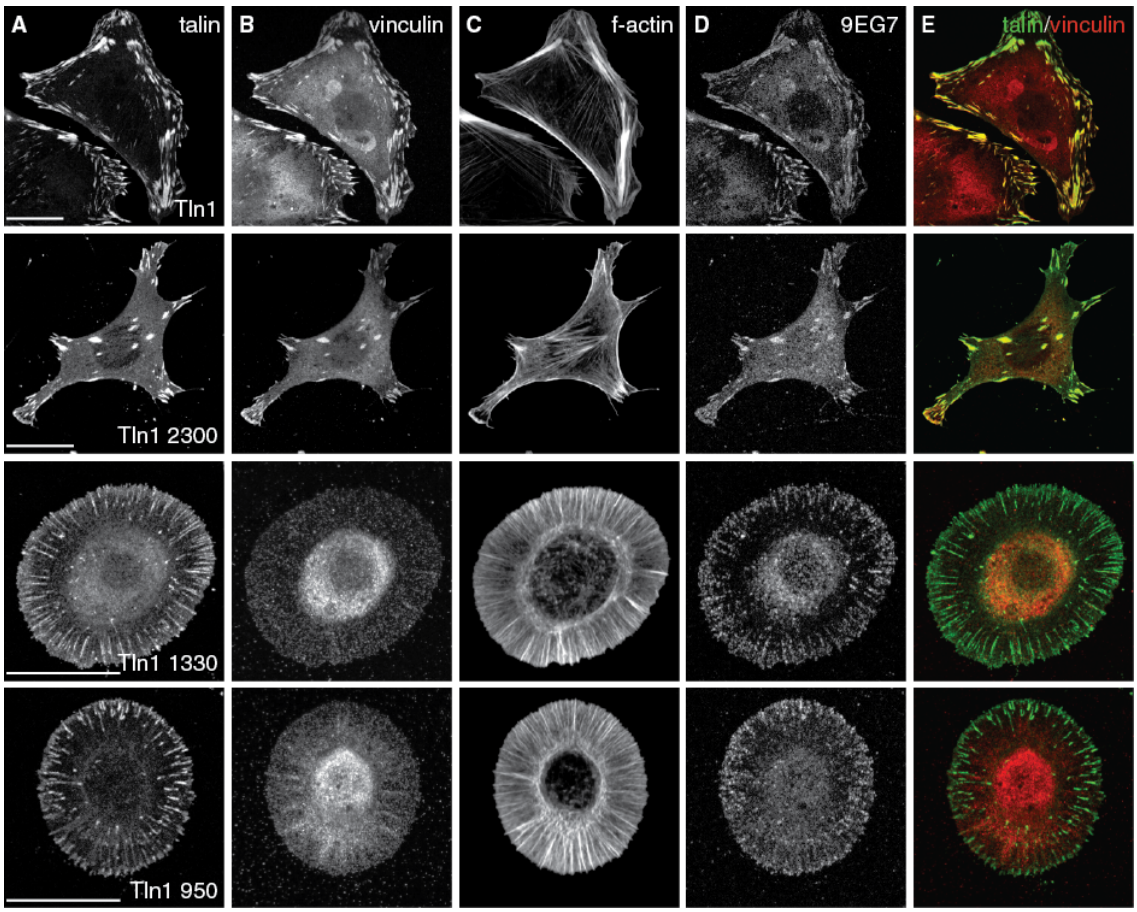

Figure 2.46: Representative immunostainings of cells expressing YPet constructs shown in Figure 2.45. (**A**) Talin-1 constructs are recruited to (**D**) active integrin β1 (9EG7) positive adhesion sites but only colocalizing with (**B**) vinculin in full length talin-1 (Tln1Y) and Tln1-2300, but not Tln1-950Y and Tln1-1330Y, (**E**) indicated by yellow areas in merged images. (**C**) F-actin network is built in all cell lines but stress fiber formation is associated with vinculin recruitment to FAs. Scale bars 20 μm.

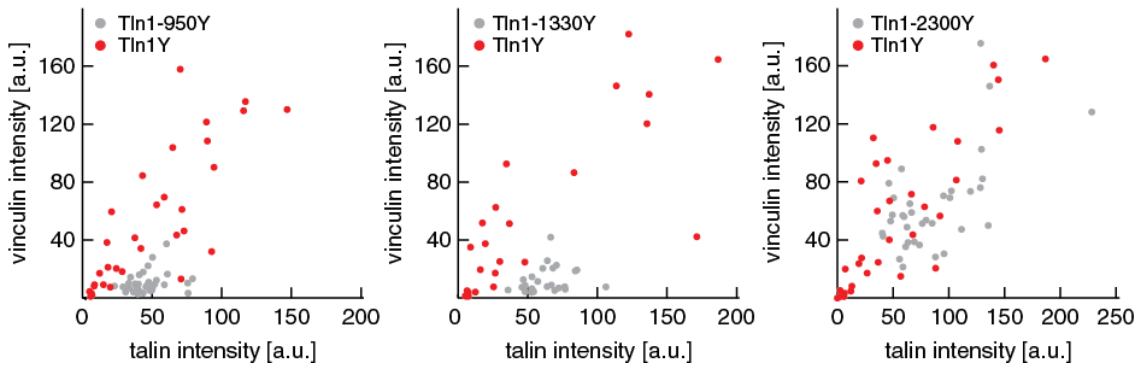

Figure 2.47: Vinculin is recruited to Tln1Y and Tnl1-2300Y positive FAs but not Tln1-1330Y and Tln1-950Y FAs. Analysis of fluorescence intensity in FAs of talin and vinculin of talin deficient cells, re-expressing talin-1 YPet constructs, shown in Figure 2.45. Tln1-950Y and Tln1-1330Y fail to recruit vinculin to FAs.

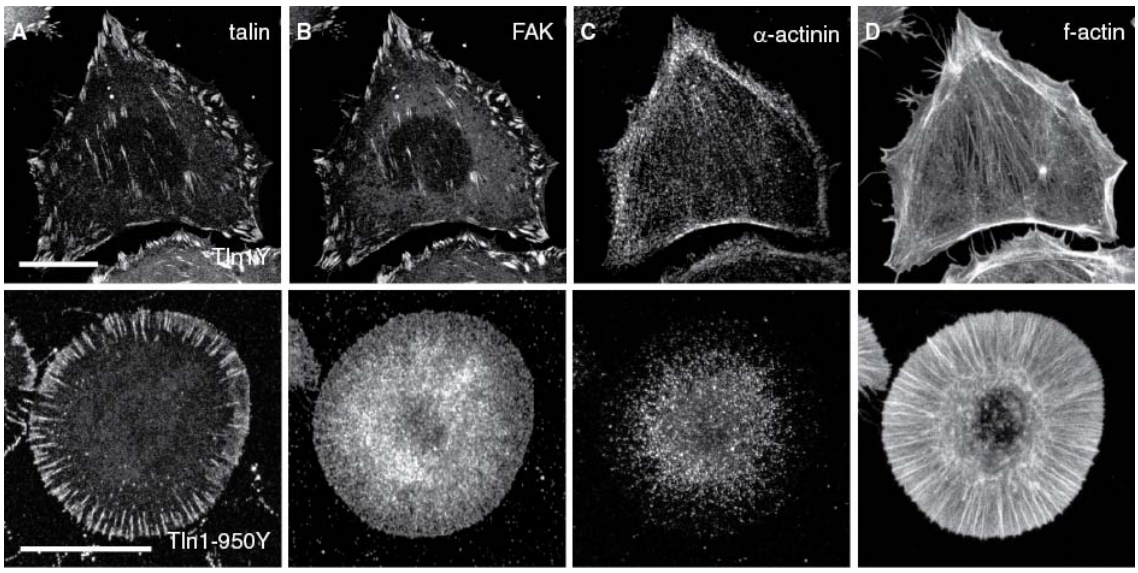

Figure 2.48: FAK and α-actinin are not properly localized in Tln1-950Y cells. (**A**) Tln1Y and Tln1-950Y cells stained with (**B**) FAK and (**C**) α-actinin antibodies. (**D**) F-actin was visualized by phalloidin. Scale bars 20 μm.

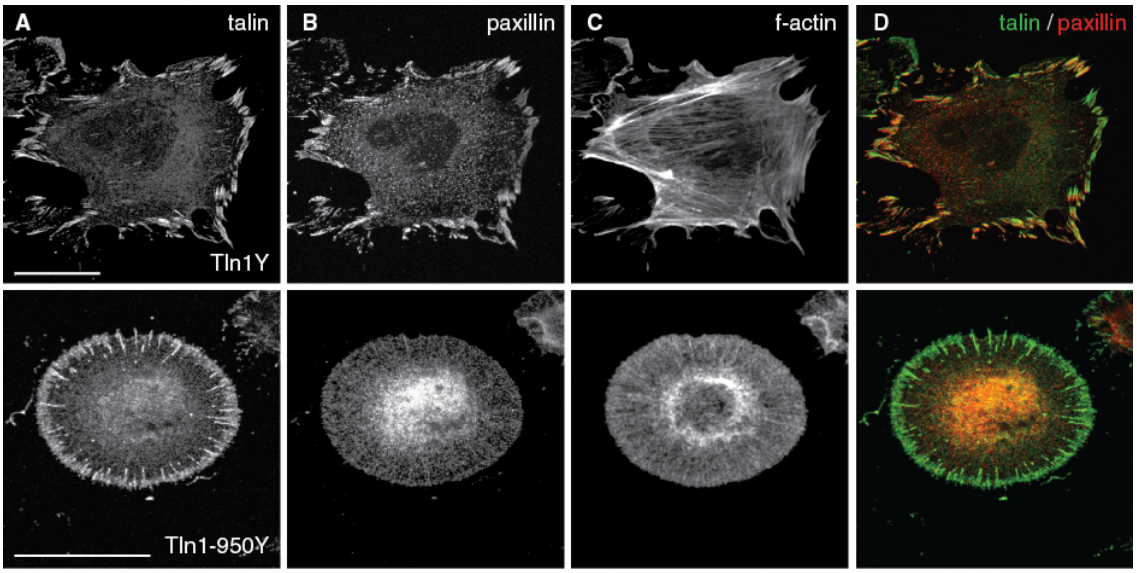

Figure 2.49: Paxillin is not efficiently localized to adhesion sites in Tln1-950Y cells. Immunostainings of (**A**) Tln1Y and Tln1-950Y cells (**B**) stained with anti-paxillin antibody; (**C**) f-actin was visualized with phalloidin. (**D**) Areas of colocalization are indicated by yellow areas in merged image. Scale bars 20 μm.

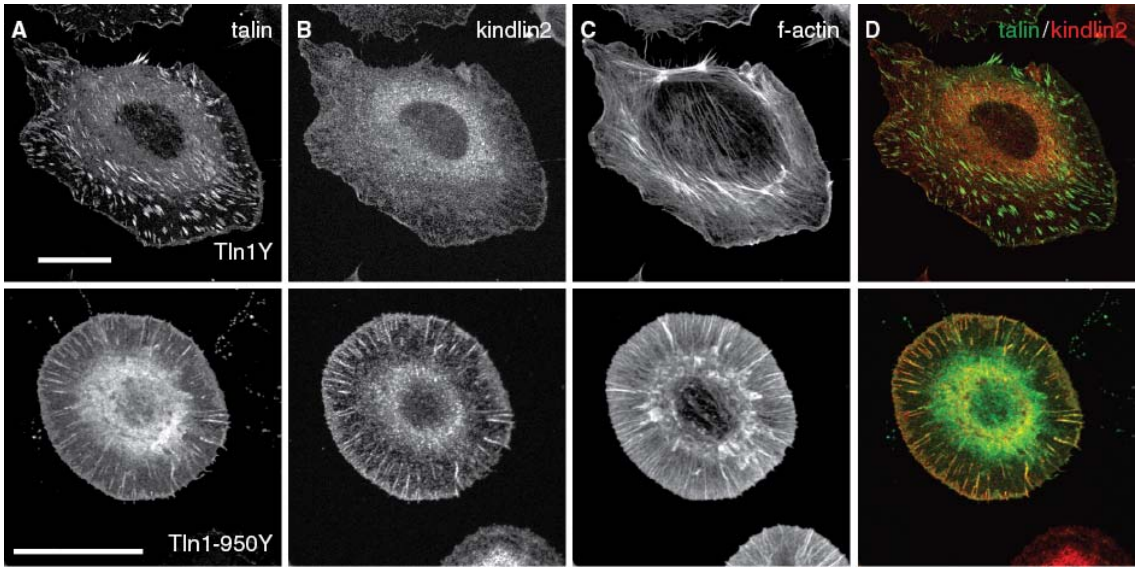

Figure 2.50: Kindlin-2 is localized in talin-positive adhesion sites in Tln1Y and Tln1-950Y expressing cells. (**A**)Tln1Y and Tln1-950Y cells (**B**) stained with anti-kindlin-2 antibody. (**C**) F-actin was visualized by phalloidin. (**D**) Areas of colocalization are indicated by yellow areas in merged image. Scale bars 20 μm.

2.4.4.2 Integrin β1 surface expression is unchanged in truncated talin-1 mutants

To test whether the observed phenotypes were caused by different levels of integrin expression or activation, integrin surface levels were determined by FACS analysis; comparable expression of total β1 and active β1 (9EG7 epitope) were detected in Tln1Y, Tln1-2300Y and Tln1-950Y (Figure 2.51). This observation concurs with previous studies that reported efficient integrin activation by the talin-1 head domain[168].

Furthermore, the integrin activating kindlin-2 still localized to integrin β1 positive adhesion sites (Figure 2.50) and could compensate for reduced talin-1 function.

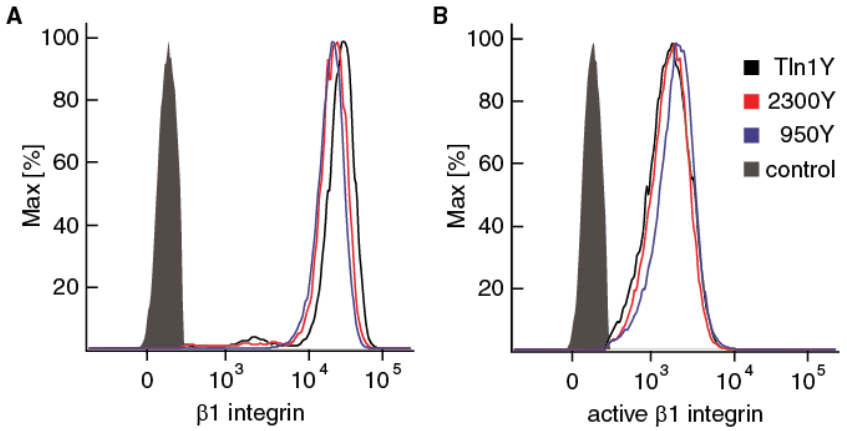

Figure 2.51: Beta1 surface expression levels are comparable to Tln1Y levels in cell lines expressing truncated talin versions measured in FACS experiments. . (**A**) Total beta1 levels as well as (**B**) active beta1 (9EG7) levels are comparable in all cell lines. Integrin deficient cell lines served as control.

2.4.4.3 Cell spreading and polarization are impaired in Tln1-950 cells

The spreading behavior in the Tln1-950 cells on FN was further evaluated. The results indicated showed that the missing f-actin association impedes cell area increase. Whereas cells expressing full length talin-1 (Tln1Y) enlarged their area over time, Tln1-950Y failed to spread (Figure 2.52).

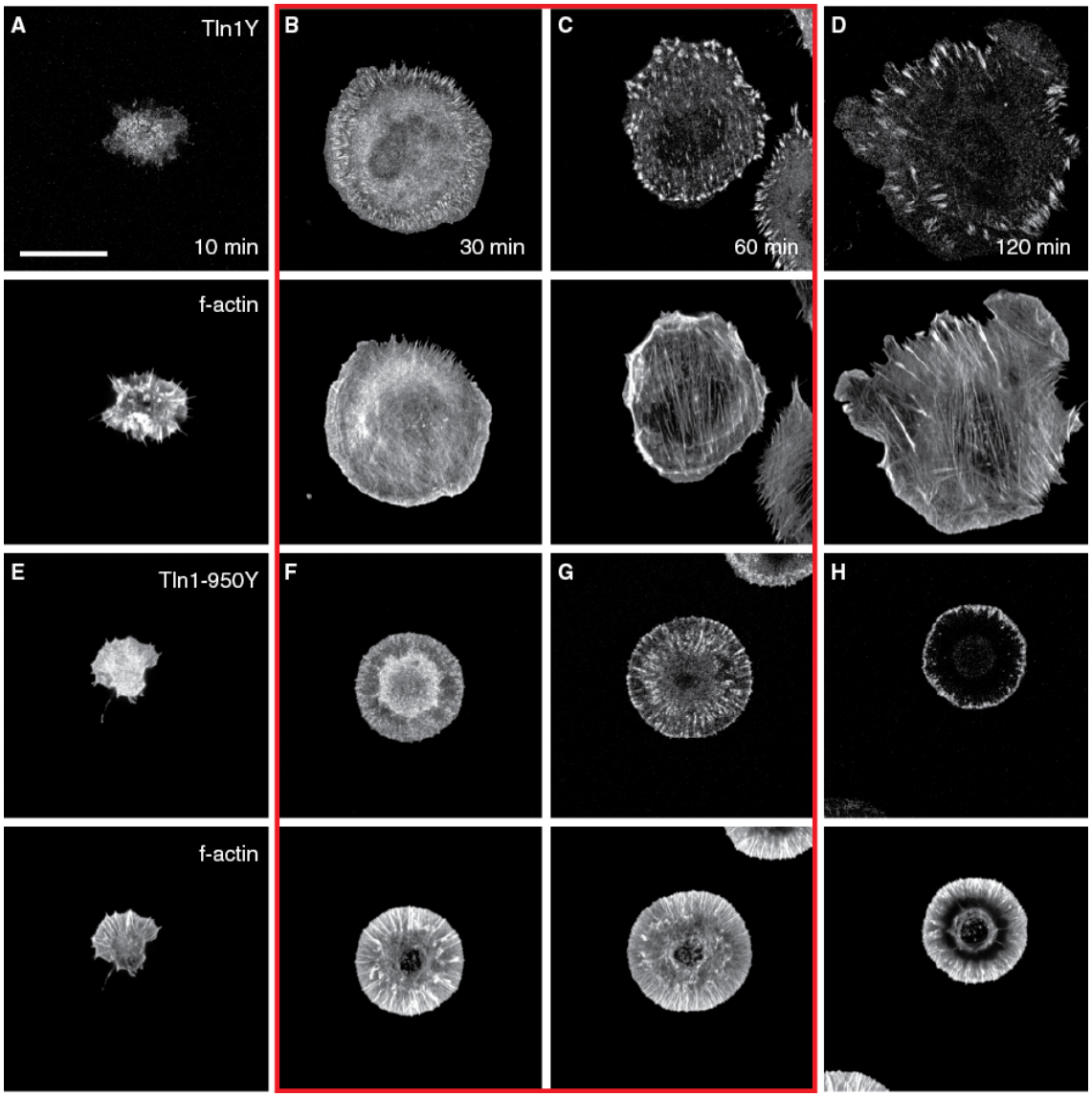

Figure 2.52: Tln1-950Y cells fail to enlarge their surface area over time. Confocal images of fixed Tln1Y (**A-D**) and Tln1-950 (**E-G**) cells after 10 (**A, E**), 30 (**B, F**), 60 (**C, G**) and 120 min (**D, H**) of seeding on FN, stained with phalloidin to label f-actin cytoskeleton. Conditions in red square were analyzed concerning cell size and FA characteristics (see Figure 2.53 and Figure 2.54). Scale bar 20 μm.

To quantify the defect, two time points (30 min and 120 min of spreading) were selected and cell spreading as well as cell morphology were quantified. After 120 min, Tln1-950 cells failed to spread on FN whereas Tln1Y cells were able to enlarge their cell area significantly (Figure 2.53 A). Additionally, the cells retained in a circular shape and were unable to polarize as shown by a low eccentricity (Figure 2.53 B) and the evenly relative angular distribution of FAs (Figure 2.54). In polarized Tln1Y cells (after 120 min seeding), FAs were oriented along the force field of the actin cytoskeleton, parallel to the major axis. In Tln1-950Y cells, polarization was abolished and FAs were evenly distributed at the cell borders.

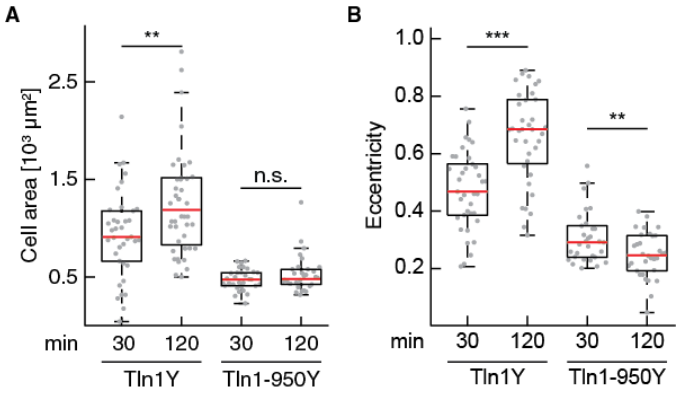

Figure 2.53: Quantification of cell area and eccentricity of full length talin-1 and talin-1 950 cells. (**A**) Tln1-950Y cells fail to enlarge their surface area after 30 and 120 min. (**B**) Cells expressing full length talin-1 polarize, indicated by higher eccentricity, but Tln1-950 cells remain their rounded shape.

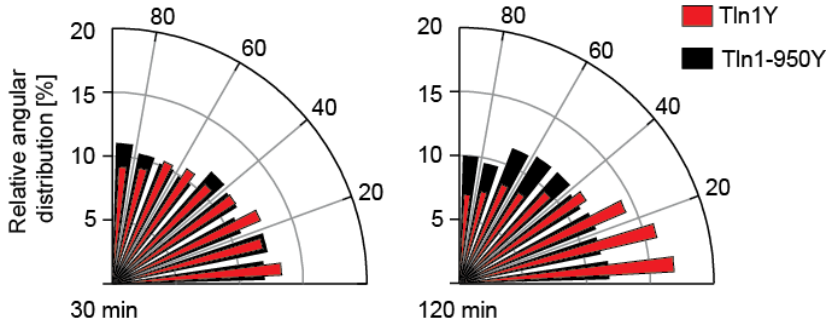

Figure 2.54: Relative angular distribution of FAs in Tln1Y and Tln1-950Y cells. After 30 min FAs are circularly distributed in both cell lines. Whereas Tln1-950Y cells remain the circular distribution after 120 min, Tln1Y cells polarize and reorganize the FA perpendicular to their major principal axis.

All these processes that are impaired in the Tln1-950 cells – cell spreading, FA enlargement and reorganization as well as stress fiber formation – require mechanical stabilization of the FA complex. Thus, mechanical anchorage of the FA complex might be limited due to the lack of mechanical engagement of talin-1 with the f-actin cytoskeleton and thus cells were expected to be less sensitive to changes in cell contractility.

Consequently to active RhoA (Q63L) expression, Tln1Y cells responded with the expected strengthening of FAs due to increased intracellular contractile forces, generated by enhanced myosin activity (chapter 1.2.1.5). In contrast, Tln1-950Y cells failed to stabilize the FA-f-actin connection and as a consequence lost the characteristic round phenotype (Figure 2.55).

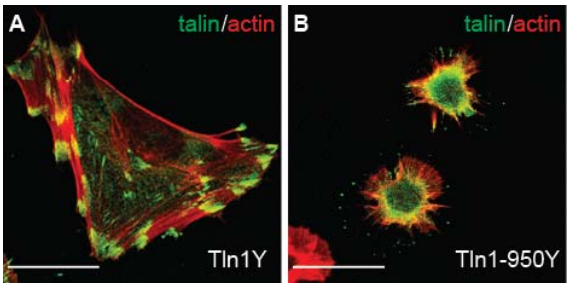

Figure 2.55: Expression of active RhoA in Tln1Y and Tln1-950Y cells. Representative images from (**A**) Tln1Y and (**B**) Tln1-950Y cells expressing active RhoA (Q63L), stained with phalloidin for f-actin (red). Talin constructs are shown in green. Scale bars 20 µm.

2.4.4.4 Tln1-950 cells fail in rigidity sensing

Besides response to intracellular force generation, FA stabilization is further required in ECM rigidity sensing[36]. Therefore, rigidity dependent increase in cell area was measured in Tln1Y and Tln1-950Y cells. As shown in Figure 2.56 and Figure 2.57, Tln1-950Y cells were unable to

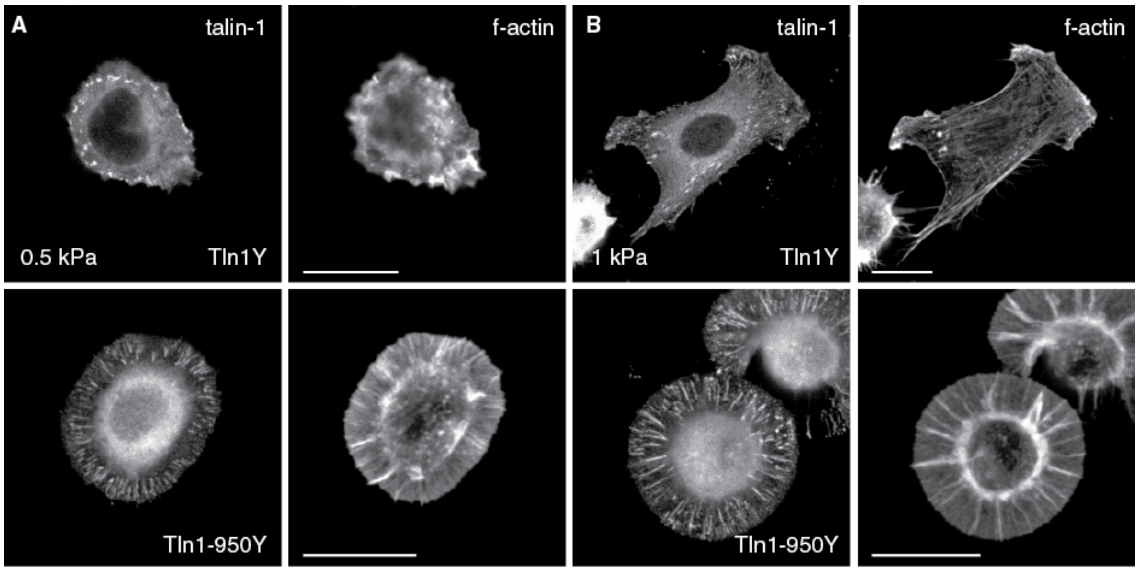

Figure 2.56: Representative confocal images of data shown in Figure 2.57. Tln1Y and Tln1-950Y cells seeded on (**A**) 0.5 kPa and (**B**) 1 kPa soft substrates stained for actin. Scale bars 20 µm.

respond to changes in matrix rigidity on soft substrates, whereas cells expressing Tln1Y responded with the expected increase in cell size that correlated with substrate stiffness.

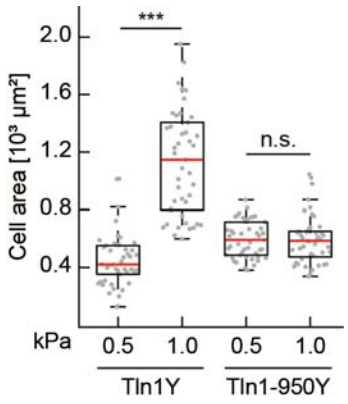

Figure 2.57: Rigidity dependent increase in cell area is monitored in cells expressing full length talin-1 (Tln1Y) but not in the truncated mutant (Tln1-950Y). Tln1Y cells significantly enlarge their surface area on 0.5 and 1 kPa soft substrates but Tln1-950Y cells do not.

As rigidity sensing seems to require mechanical resilient linkages within the FA complex through talin-1, we measured force propagation across all mutant cell lines. The cell lines are characterized by differential f-actin binding properties (direct or indirect through vinculin) and thus should transmit forces with varying efficiency. Even though deletion of the C-terminal ABS in Tln1-2300 had a slight effect on FRET efficiency, indicating a reduction of transduced forces, the effect was not as severe as for the shorter mutants (Figure 2.58). With decreasing f-actin association of the talin-1 mutants, FRET efficiencies increased, indicating that mechanical loads on talin-1 are tightly coupled with f-actin binding.

Interestingly, impaired force transduction was also correlated with a lack of vinculin co-localization in FAs, as shown in immunostainings (Figure 2.46) and intensity quantifications (Figure 2.47).

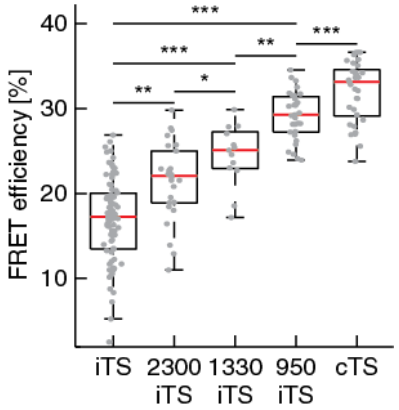

Figure 2.58: FRET efficiencies of cells expressing truncated talin-1 variants. Force propagation across talin-1 is abolished in Tln1-950 cells but increases with talin rod length.

Along with low intracellular forces and inefficient response to intracellular contraction, the Tln1-950 cells were unable to exert traction forces, even on very soft substrates of about 2 kPa. When full length talin-1 cells were able to deform their underlying substrates, Tln1-950 cells failed to cause bead deflection in traction force experiments (Figure 2.59).

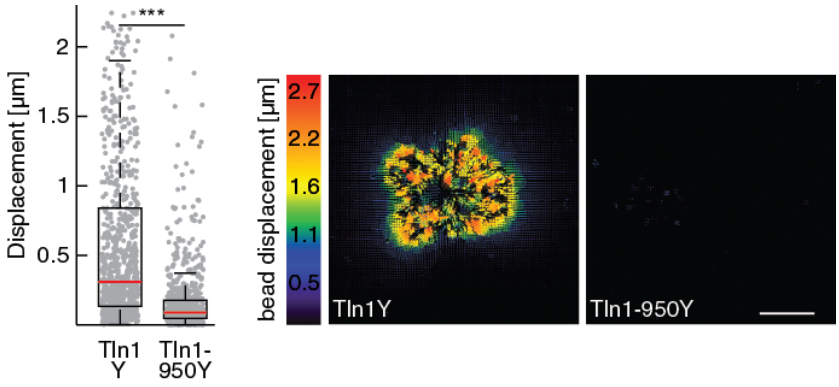

Figure 2.59: Bead displacement in 2 kPa PAA gels of talin-1 YPet (Tln1Y) and talin-1 950 YPet (Tln1-950Y) cell lines. Left: Traction forces, indicated by bead displacement, are significantly higher in Tln1Y cells. Right: Representative images of displacements of individual cells. Scale bar 20 µm.

2.5 Summary

Altogether, these findings provide strong evidence that integrin engaged talin-1 bears mechanical force in FAs. F-actin association, direct or indirect through vinculin recruitment, is modulating these forces, but other factors, such as dimerization or binding to IBS2 are of minor importance in force transmission processes.

Surprisingly, processes that require mechanical stabilization of FAs - such as cell spreading, polarization and traction force generation - are entirely abolished in cells that lack mechanical engaged talin-1. This is surprising because integrin activation is normal in these cells and other FA protein, such as α-actinin, paxillin or FAK are unable to compensate for the loss of the talin-mediated anchorage to the actin cytoskeleton. Thus, the mechanical engagement of talin-1 is indispensable for important cellular functions e. g. rigidity sensing. It is important to note that impaired vinculin recruitment is also coupled with impaired force transduction across talin-1. These findings confirm previous suggestions of a positive feedback regulation in FA strengthening, where talin tension positively regulates vinculin recruitment in an f-actin dependent manner[132].

In the future, the influence of integrin subunit association or other FA components will be of closer interest to better understand mechanical properties of those complex protein networks.

3 Discussion

Cellular systems are not only exposed to chemical but also many physical stimuli. Radiation, temperature as well as mechanical forces are epigenetic factors, critical for many cellular and developmental processes[169,170]. Malfunctions in mechanotransduction pathways are often resulting in impaired cell- or organ functionality or malignancy[171]. Therefore, understanding how forces are sensed, translated and further transmitted in cells has become a wide field of interest over the last years.

Integrin-positive adhesion sites, connecting the ECM with the intracellular f-actin cytoskeleton were proposed to play a key role in force sensing and force-response regulation[36]. Integrin mediated signaling triggers various cellular functions such as migration and cytoskeletal reorganization but is also involved in survival and proliferation processes[172,173]. Still, even though numerous FA components are known and single components, like vinculin[12], were shown to bear mechanical loads, actual force sensing mechanisms remain mainly illusive, owing to the enormous complexity of the system.

As a central component of FAs, talin-1 became of greater interest with respect to mechanotransduction as it not only serves as an integrin activator but also directly binds f-actin filaments[116]. Even though many *in vitro* studies previously suggested tension-related functions of talin-1, evidence from cell based studies was still missing.

In this study, two new tension sensor probes were developed and analyzed in order to measure physiologically relevant forces across talin-1. Additionally, we not only analyzed forces transmitted across talin-1 in cells but could also demonstrate, that tension across talin-1 is essential for downstream signaling events that trigger cell spreading and rigidity sensing.

3.1 VH tension sensor approach enables analysis of low pN forces

3.1.1 VH based tension sensors are sensitive in a physiologically relevant force regime

In previous studies, a FRET based tension sensor was used to analyze forces across the FA component vinculin in living cells[12]. The technique is characterized by a FRET pair of fluorescent proteins (in this case YPet as donor and mCherry as acceptor molecule) connected by a force sensitive linker peptide, derived from the spider silk protein F40. Force dependent separation of the fluorophores led to a significant decrease in FRET signal (Figure 1.8). Introduction of the F40-based tension sensor into talin-1, however, revealed that the force regime of 1-6 pN is unsuitable to evaluate talin-1 forces[154] (chapter 2.3.1.1).

In vitro experiments on talin-1 suggested that talin-1 bears forces of about 13 pN in cells, as cryptic (vinculin) binding sites could only be opened upon application of force[135]. The F40-peptide was therefore exchanged by a suitable force sensitive element. Peptides used as force sensitive linkers in the tension sensor approach need to fulfill distinct properties; fast and complete unfolding and refolding processes under force are required in line with a characteristic force regime. Furthermore, the peptide should not show hysteresis after stretching and be inert to protein-protein interactions. In addition to the initial F40 linker, three different peptides were tested as force sensitive linkers, namely the LZ element as well as two VH based peptides. Whereas the LZ motif, a heterodimeric helical structure that showed 'unzipping' upon applied force[174], was less appropriate due to multistep response after stretch (chapter 2.3.1.2), both VH based tension sensors showed promising results (chapter 2.3.1.3).

In single-molecule force measurements, the VH peptide was characterized as an ultrafast unfolding and refolding peptide[156] with an average equilibrium transition force of 7.4 pN (Figure 2.16). Furthermore, this transition force could be raised to 10.6 pN by the introduction of two point mutations[154]. Fitting of the force-extension data revealed that both sensors can adopt three different states: a folded, an unfolded and a half-folded/half-unfolded conformation. These characteristics put the assumption close that the VH is an adequate substitute for the previously published F40 linker in order to measure force transduction across talin-1.

For the analysis of other proteins that are exposed to higher forces, new linker peptides are needed to pinpoint the physiological relevant force regime. For the analysis of forces in proteins with an unknown force regime in the future, a combination of spring-like and switch-like sensors could be useful. Spring-like sensors as the F40 sensor could be useful to roughly

indicate the forces acting across a protein of interest, whereas switch-like behavior as the VH based tension sensor could help to define distinct force values for each protein.

Furthermore, using e. g. multi-color FLIM[175] could help to analyze forces acting across two independent proteins at the same time to gain more insight into spatial and temporal propagation of forces within a cell. Therefore, fluorophores would have to be changed to ensure no spectral overlap between different sensors, e. g. acceptor fluorophores could be changed to dark variants[176] to reduce intermolecular FRET between sensor variants.

Still, all tension sensors are restricted to a specific force regime and only allow rough estimations about the state of single molecules in a protein complex. In this study, mean FRET efficiencies of all FAs in one cell are averaged to determine the state of talin-1 forces. Information about individual proteins cannot be detected in this approach, meaning that a FRET ratio of e. g. 0.5 could either be the result of all molecules being in a half-folded/half-unfolded conformation or half of the molecules are in a folded and half of the molecules in an unfolded state. To overcome this experimental drawback, single-molecule FRET measurements using high resolution microscopy techniques could lead the way to new insights into spatial force distributions within a cell and how forces act on single proteins on a temporal scale.

3.1.2 Fluorophore properties are not affected by insertion into talin-1

Functional integrity of the fluorophores is mandatory for conclusive data evaluation in FRET measurements. Integration of fluorophores into a protein that is potentially exposed to forces can lead to conformational changes of the fluorophores as a consequence of force applied on the fusion protein. Although talin-1 was proposed to bear only low pN forces of 5-13 pN [130,135], fluorescence lifetime and emission spectra of donor and acceptor fluorophores were tested. When comparing talin-1 molecules with integrated or C-terminally tagged fluorophores, no significant changes in fluorophore properties could be detected (Figure 2.24).

Furthermore, analysis of the tension sensor probe including both, acceptor and donor fluorophore in single-molecule calibrations did not show unfolding of the fluorophores below 35 pN and did not occur when exposing the probe to 24 pN for more than five minutes (Figure 2.25). Hence, partial unfolding of the inserted fluorophores in tension sensor experiments within the force regime of the VH tension sensor (7-10 pN) is unlikely to be relevant for YPet and mCherry.

However, genetically inserted fluorophores also have drawbacks for life-imaging techniques like FRET. Imaging for several minutes or exposure to high laser intensities can lead to

bleaching of individual fluorophores. This bleaching is not necessarily linear and especially critical for long-term experiments with ratiometric FRET, as it can be different for donor and acceptor molecule and thus falsify FRET ratios. Consequently, alternative donor and acceptor molecules will be important for the tension senor approach. One possibility would be substitution of both fluorophores with recognition sites for organic dyes that can be covalently bound to the protein of interest[177]. These dyes have the advantage that labeling is not restricted to a specific wavelength but donor and acceptor molecules can be adapted for each experiment. Furthermore, they can be used for single-molecule applications and high resolution imaging techniques and provide insight into forces transmitted over single molecules.

3.2 Insertion or C-terminal tagging of the villin-head tension senor module does not alter protein function of talin-1

Wildtype talin-1 tagged with a fluorophore either N- or C-terminally was already reported to adequately localize to FAs and perform cellular functions similarly to the endogenous protein[41,93,166]. Talin-1 C-terminally tagged with the donor fluorophore YPet was therefore used as control in most experiments (Figure 2.18). An unstructured linker region connects talin-1 head and rod domains and is supposedly of minor importance for protein-protein interactions of talin-1 as it was only shown to carry a cleavage site for the protease calpain-2[96]. To not interfere with calpain-2 cleavage and integrin binding at the F3 subdomain of the talin-1 head, the insertion site between V447 and A448 was chosen for the tension senor module or single fluorophore tagging (chapter 2.2.1). The insertion of either single fluorophores or the tension sensor modules did not alter subcellular localization in immunostainings (Figure 2.17), protein turnover in FAs measured by FRAP (Figure 2.23) or integrin surface expression of total and activated β1 integrin in FACS (Figure 2.22) as compared to C-terminally tagged YPet controls. Also, C-terminal tagging with the tension sensor constructs did not alter FA localization of talin-1 or influenced other protein functions tested in the rescue experiments (chapter 2.3.2). Thus, talin-1 functionality seems not to be disturbed by the insertion or C-terminal fusion with one or two fluorophores. Insertion of the relatively large tension sensor module could potentially interfere with efficient folding of the protein or prevent efficient localization. Steric masking binding sites for interaction partners or signal sequences are potential reasons for disturbed localization. Hence, application of the tension sensor in other proteins of interest always requires investigations regarding proper protein functionality to ensure reliability of measured forces across the specific protein.

3.3 Cells depleted of both talin isoforms are required to study talin function

In vertebrates, two talin-1 isoforms are expressed but the existence of talin-2 is often neglected. Many previous studies on talin-1 function were performed without testing the influence of talin-2, though it was shown that talin-2 upregulation – at least partially – can compensate for the loss of talin-1 in knockdown experiments[92]. In addition, both, talin isoforms, seem to fulfill tissue specific functions; e. g. talin-2 was shown to be the predominant isoform in heart muscle tissue whereas both isoforms were expressed simultaneously during heart development[104]. Thus, it can be assumed that residual endogenous talin-2 can negatively influence measurements with an intramolecular tension sensor as the presence of untagged protein could block the full unfolding of the tension senor module, for instance. Thus, usage of the *talin-1*$^{-/-}$/*talin-2*$^{-/-}$double knockout cell line was important to efficiently study talin-1 forces (chapter 2.1.2). Using reconstituted knockout cell lines holds the advantage that competing effects of endogenous protein must not be considered, however other factors must be taken into account. Comparable expression levels between wildtype and the reconstituted protein are important to exclude effects of overexpression. Furthermore, influence of other splice isoforms, as in the case of talin-2, or alternative splicing variants need to be considered. If knockout cell lines are not available for a specific protein that would be an interesting target for the tension sensor approach, the recently emerging CRISPR/Cas9 approach could be used to target the endogenous gene locus with the sensor module[178]. This system holds the advantage that the protein of interest is expressed under the endogenous promotor and that cell type specific alternative splicing would not be affected. Though, not every cell type is suitable for this approach. Moreover, CRISPR/Cas9 can potentially lead to other side effects such as off-target effects due to unspecific binding of the guide RNA[179].

3.4 Talin-1 establishes the mechanical link between integrins and the cytoskeleton

3.4.1 Integrin engaged talin-1 is subject to forces about 7-10 pN

Talins bridge the connection between β integrin tails and the f-actin cytoskeleton and are central components of force bearing FAs. Force transmission capacity of talin-1 was already assumed before, as *in vitro* studies revealed a three-state unfolding of talin-1 in the physiologically relevant force regime of 5-30 pN[136] as well as force dependent accessibility of cryptic VBS in the talin-1 rod[129,159,180]. Furthermore, the association with vinculin at these cryptic binding sites was demonstrated to stabilize the intermediate, 'stretched' conformation of talin-1 *in vitro*[181]. As expected, FLIM measurements on the talin-1 tension sensor revealed that talin-1 tension is significantly increased in FAs as compared to cytoplasmic localization on pL (Figure 2.26 (A)). Moreover, FRET values were increased by the introduction of the stable 10 pN tension sensor variant (Figure 2.26 (B)), indicating that a smaller fraction of 10 pN sensor molecules are in an open conformation in FAs compared to the 7 pN sensor. If all forces across talin-1 would be below 10 pN, values for the stable tension sensor would be raised up to C-terminal control levels. Hence, talin-1 is subjected to low pN forces of 7-10 pN with a subpopulation of talin-1 molecules being subjected to forces higher than 10 pN, whereas other molecules bear forces lower than the 10 pN threshold.

However, deeper insights in talin-1 forces like the spatial-temporal resolution, for example during cell migration, are missing. Using the talin-1 tension sensors in ratiometric FRET measurements, force transduction during nascent adhesion formation and FA maturation could be analyzed to identify potential physiologically relevant differences in talin-1 tension in these processes. However, the always occurring problem of insensible measurements in TCSPC-FLIM and ratiometric FRET approaches can only be overcome by the super-resolution approach as discussed above (chapter 3.1).

Taken together, this study could show for the first time that integrin engaged talin-1, localized in FAs, experiences forces between 7 and 10 pN whereas cytoplasmic talin-1, uncoupled from integrin mediated adhesion, does not transmit forces within this range.

3.4.2 Talin-1 tension is independent of substrate rigidity over a wide range of stiffness

The observation that talin-1 bears mechanical tension during cell adhesion raised the question whether talin-1 might be also involved extracellular rigidity sensing[64]. The formation of stress fibers and network organization were proposed to be dependent on substrate stiffness[160,182], thus the mechanical information of the ECM needs to be transduced to the cytoskeleton. As a force-bearing, direct link between integrins and f-actin, talin-1 was an obvious candidate for tension related information transmission. Analyzing traction forces of Tln1iTS cells, the previously reported[161] substrate rigidity dependent increase in traction forces could be observed (Figure 2.35). Nevertheless, forces across talin‑1 remained constant above substrate stiffness of 4 kPa and only decreased on substrate of lower rigidities (Figure 2.34). Thus, talin−1 provides the actin-integrin connection independent of the elastic modulus of the substrate over a wide range of substrate stiffness. This suggests that talin-1 establishes mechanical resilient linkages but acts as a scaffolding protein required for FA stabilization and maturation rather than a direct force translator. However, the recruitment of talin-1 itself seems to trigger mechano-transmission processes as talin-1 localization to FA increased with substrate rigidity (Figure 2.33). It will be interesting to analyze which signaling pathways are driven by talin-1 forces and how downstream signals are propagated to be transduced into cellular responses. A set of kinases like FAK, Src and MLCK but also Rho-family GTPases act downstream of integrin mediated adhesion signaling and trigger FA maturation, stress fiber assembly and migration. Even if a correlation between signaling events and substrate rigidity could be shown[183], the force transmitting role of talin-1 is still not understood.

3.4.3 Tension sensor FRET efficiencies are unaffected by talin-1 conformation, fluorescence intensities and intermolecular FRET

Talin-1 adopts an autoinhibited conformation due to interactions between the F3 (head) and the R9 (rod) domains when localized in the cytoplasm[108,109]. Introduction of mutations that prevent or significantly render talin-1 autoinhibition lead to excessive FA formation in HUVEC cells[93,130]. Those mutations, blocking the talin-1 head-tail interactions, also lead to higher integrin activation. In this study, cells expressing the talin-1 tension sensor with mutations that prevent the autoinhibition were used to exclude that changes in talin-1 conformation are responsible for the changes in FRET between cells seeded on pL and FN. Experiments with mutations blocking the inter-domain association of talin-1 (K324D and M319A) in the talin-1 tension sensor, thereby mimicking the activated conformation within FAs, revealed that the changes in FRET between the pL controls and the integrin engaged cells were not caused by talin-1 inactivation in the cytoplasm, as the FRET ratios on pL for wt and mutant proteins did not change (Figure 2.32). Hence, it can be assumed that conformational changes during talin-1 activation do not cause the differences in FRET efficiencies when comparing talin-1 in FAs and the cytoplasm.

In tension senor experiments the effect of intermolecular FRET, meaning the energy transfer between fluorophores of different, neighboring molecules, always has to be taken into account. Intramolecular FRET between two talin-1 molecules could e. g. lead to increased FRET values in FAs as molecules immobilized in those structures are in close proximity compared to the cytoplasm. However, testing intramolecular FRET between talin-1 molecules, efficiencies of 1-4 % were detected in FAs and the cytoplasm (Figure 2.29). Furthermore, no intensity dependence of FRET measurements could be determined for Tln1iTS as well as Tln1cTS (Figure 2.27).

These experiments suggest that changes found in the talin-1 tension sensor experiments can be related to forces across talin-1, not secondary effects of the tension sensor insertion into the FA protein.

3.5 Modulations in talin-1 forces are achieved by talin-1-f-actin association

3.5.1 Mutations in the IBSs of talin-1 do not render talin-1 localization to FAs

Integrins are the most obvious modulators of talin-1 force transduction, as talin-1 is functionally coupled with the β-subunit of these transmembrane receptors[184]. Thus, reduction of the binding capacity of talin-1 to β integrin tails was expected to significantly reduce forces transmitted across talin-1. Previous studies on integrin activation reported reduced integrin binding and abolished talin-1 localization to integrin positive adhesion sites upon mutation of specific residues in talin-1's IBSs[163,165]. Expression of integrin binding deficient talin-1 mutants (R358A (RA), L2094A/I2095A (LIAA) and R358A/L2094A/I2095A (AAA)) in KO cells revealed that the point mutations in both integrin binding domains (IBS1 and IBS2) did not inhibit FA localization (Figure 2.36). Unexpectedly, energy transfer rates were only slightly increased in the mutant tension sensor probes (Figure 2.38), suggesting that mutant talin-1 molecules can still provide mechanically resilient linkages to the f-actin cytoskeleton. These findings indicate that single mutations in the talin-1 integrin interaction sites only decrease the binding affinity but do not completely abolish the interaction. Thus, a smaller number of talin-1 molecules are mechanically anchored in FAs, indicated by higher transfer rates in FRET experiments. However, these results need to be validated in further experiments. Loss of binding affinity of the talin-1 mutants to integrin should be confirmed using ligand binding assays or atomic force microscopy. Also FRAP experiments would give insight if turnover rates are enhanced for the integrin-binding mutants, indicating reduced immobilization of talin-1 in FAs as a result of low affinity to integrins. Additionally, talin-1 mutants with enhanced binding capacity to integrin β tails could be analyzed. Mutations enhancing the interaction should lead to lower talin-1 turnover in FAs and probably increase the amount of talin-1 molecules under force in FAs, thus increase FRET values in FLIM experiments.

Another obvious integrin-related question is whether forces across talin-1 vary in an integrin subunit dependent manner. Ligand specificity of integrins is determined by subclass composition and cellular functions[184]. Interestingly, talin-1 binds to intracellular tails of many β integrin tails and mediates integrin activation and connection to the f-actin cytoskeleton (see chapter 1.2.1.2). Expressing the talin-1 tension sensor in cell lines with specific integrin heterodimer surface expression, e. g. only β1 or β3 subtypes[158], could address the question if talin-1 forces are integrin subtype dependent. Moreover, it would be interesting to analyze if potential differences are coupled with different downstream signaling events.

3.5.2 Loss of talin-1 dimerization does not abolish talin-1 force transduction

The dimerization of talin-1 is controversially discussed in the field, as NMR data provided evidence for the existence of an auto-inhibited dimer in crystallization studies[109] and also molecular dynamics modeling were consistent with talin-1 dimerization[112]. Yet, quantitative experiments in cells or animals are missing. In this study it could be shown that mutations in the DD of talin-1, either point-mutations (R2526G) or full deletion of the domain (Δ2496) render protein functionality, as the phenotype of KO cells was only partially rescued after reconstitution with talin-1 dimerization mutants (Figure 2.39). The cell areas in dimerization mutant cells was reduced as compared to Tln1Y cells and full FA maturation was could not be observed in immunostainings, even though both constructs localized to FA. This finding was contradictory to previous results that reported a localization defect for the Tln1 R2526G mutant[166]. However, it is not clear whether impeded rescue capability of the mutant talin-1 proteins is directly related to abolished homodimerization or if mutations in the DD cause protein dysfunctions that are not related to homodimerization.

Furthermore, dimerization of talin-1 was suggested to play a role in mechanotransduction, as molecular dynamics modeling studies postulated an external stress dependent regulation of the dimer orientation[112]. The introduction of both mutations in the talin-1 tension sensor revealed increases in FRET efficiencies but force transmission across talin-1 seemed not entirely abolished (Figure 2.41). Structural analysis showed that the talin-1 DD is important for actin association with the C-terminal ABS (THATCH domain)[85], suggesting that not lack of talin-1 dimerization but interference with f-actin binding capacity of the THATCH domain could be responsible for the phenotype observed in the mutant cell lines. To test effects of dimerization of talin-1 on force transmission, direct evidence of dimerization of talin-1 in cells would be required first. So far, experiments using C-terminally tagged fluorophores did not show increase in FRET (Figure 2.29), however this could be due to other confounding factors like for example disadvantageous fluorophore orientation. The fluorophores in the C-terminally tagged constructs can rotate freely, so that the Förster radius is exceeded in most dimers. In order to confirm dimerization in cells using FRET, new constructs need to be designed. For example, insertion of the fluorophores before the dimerization helix would overcome the problem of free rotation but might also interfere with actin binding as discussed before. Nevertheless, confirmation of talin-1 dimerization *in vivo* will be essential for further studies on its role in talin-1 function.

3.5.3 Vinculin and f-actin association modulates forces across talin-1

As mechanosensitive element of the cell, the actomyosin network has long been suggested to modulate forces in adhesive complexes[185]. F-actin is coupled to talin-1 in FAs directly and indirectly via interaction with vinculin. Both connective routes are therefore likely to play a role in talin-1 dependent force transduction. Initial experiments with the ROCK-inhibitor Y-27632 revealed actomyosin contractility dependent reduction of forces transmitted by talin-1, as transfer rates were increased upon Y-27632 treatment when talin-1 was mechanically engaged in FAs but not in the cytoplasm (Figure 2.42).

3.5.3.1 High forces across talin-1 are enabled by vinculin association

Vinculin recruitment to FAs enhances the connection between talin-1 and f-actin and was shown to depend on myosin II activity[128]. Transient transfection of the talin-1 tension sensor in cells where vinculin expression was either depleted (*Vin*$^{-/-}$) or present (*Vin*$^{f/f}$), a reduction of talin-1 forces in the absence of vinculin was observed that could be restored upon the re-expression of full length vinculin-BFP. A vinculin head-BFP variant that is efficiently

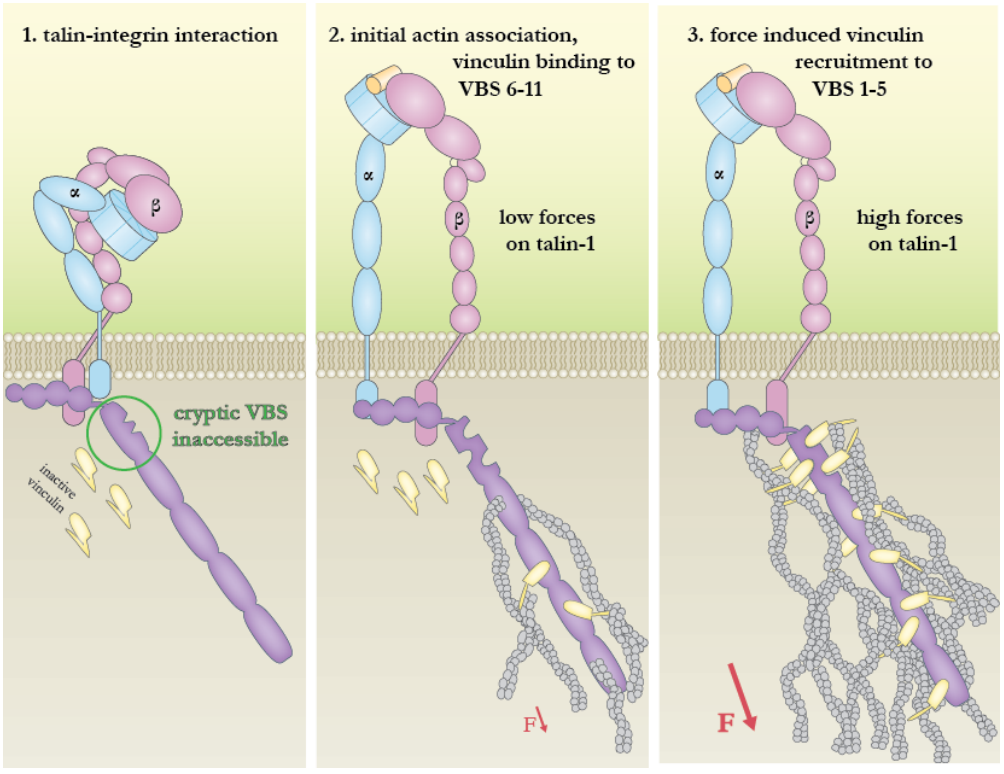

Figure 3.1: Model of force induced f-actin recruitment to talin-1. (**1**) Talin-1 binding to β integrin tails drives integrin activation, cryptic VBS in the R1-R3 domains are inaccessible. (**2**) Low forces on talin-1 are exerted by f-actin binding to ABS3 and vinculin association at VBS 6-11, resulting in exposure of VBS 1-5. (**3**) Enhanced vinculin association stabilizes unfolded conformation of talin-1 and leads to strengthening of the talin-1-actin connection. Thus, f-actin and vinculin binding to talin-1 lead increased forces across talin-1 and trigger FA maturation.

binding to talin-1 but unable to provide linkage to the f-actin cytoskeleton could not rescue reduction of forces across talin-1 (Figure 2.43). These experiments underline the importance of the direct talin-1-actin and indirect talin-1-vinculin-actin association. However, in the absence of vinculin, direct f-actin binding of talin-1 is still sufficient to establish mechanical engaged linkages in the low pN range, as treatment of *Vin*$^{-/-}$ cells with Y-27632 further decreased transfer rates across talin-1 (Figure 2.44)[154].

These data support the theory of a positive feedback loop in FA reinforcement[130] where initial f-actin binding to integrin engaged talin-1 promotes vinculin recruitment to talin-1 and thus leads to stabilization of the talin-1-f-actin connection (Figure 3.1).

3.5.3.2 Force transduction across talin-1 mutants is coupled to vinculin and f-actin binding

In vitro data previously suggested force dependent elongation of talin-1 upon f-actin association and a stabilization of the extended protein conformation through vinculin binding[127,129,130]. In this study, the importance of individual ABS in the talin-1 rod was analyzed using truncation mutants of talin-1 (Figure 2.45).

Previous publications found that mutations in the C-terminal ABS (ABS3) of talin-1 lead to higher FA stability, thus they conclude that this particular ABS has a key role in talin-1 function, even though two more ABSs are present within the molecule[93]. ABS3 as well as the DD domain have been proposed to play an important role in adhesion formation and cell cycle progression[166]. In contrast, this study demonstrated that a truncated mutant of talin-1 depleted of ABS3 (Tln1-2300) still showed localization to FAs and efficient vinculin recruitment to FAs (Figure 2.46). Furthermore, cells expressing Tln1-2300 showed only slightly enhanced transfer rates in FRET experiments. These data suggest that in the Tln1-2300 mutant talin-1 interactions with f-actin could nevertheless be established at ABS2 or by vinculin association to the talin-1 rod (Figure 2.58) to provide mechanical resilient linkages between talin-1 and f-actin. However, the connection seems to be less robust upon application of stress than in full-length talin-1, as fewer molecules seem to be under force in FLIM experiments.

In a shorter truncation variant of talin-1 (Tln1-1330) the connection is further weakened as only ABS2 but not VBS 7-11 are present in the talin-1 rod. These cells display a series of defects, including polarization, vinculin recruitment and FA maturation (chapter 2.4.4.1). Recently, single molecule manipulations using a high force vertical magnetic tweezers setup proposed accessibility of VBS3 and VBS4 only at pulling forces above 2 pN[130]. In Tln1-1330 cells, f-actin attachment to ABS2 is supposedly insufficient to overcome this threshold for R3

extension (Figure 3.2), thus vinculin recruitment to VBS 1-5 in R1-R3 domains is strongly impaired, resulting in significantly reduced force transduction across Tln1-1300 (Figure 2.58). Furthermore, recent studies on ABS2 suggest that the R7 and R8 helix bundles play an important role for talin-1 functionality as well as actin binding and are essential for FA stabilization. Thus the ABS2 in the Tln1-1330 mutant is likely not functional[167]. In a talin-1 mutant additionally lacking ABS2 (Tln1-950), however, transfer rates were further increased, indicating that in Tln1-1330 cells few sensor molecules are still under tension, most probably mediated by f-actin connection to ABS2. Thus, ABS2 linkage might either not reach the threshold to open VBS 1-5 or collapse before efficient vinculin recruitment can occur. This theory is supported by data from Yao et al. that show stable vinculin binding to R3 at forces above 7 pN[130].

Recent studies on vinculin's regulatory role in talin-1 actin binding suggested distinct roles for ABS2 and ABS3 in adhesion reinforcement and maturation[167]. Expressing truncated talin-1 isoforms in cells indicated that ABS3 might play a major role in nascent adhesion formation, as cells carrying point mutations in ABS3 were not able to form nascent adhesions in many cases and showed clear polarization defects. However, loss of ABS3 association with f-actin could be compensated by expression of a constitutive active vinculin mutant, suggesting that both, f-actin binding and vinculin association play a cooperative, regulatory role in FA

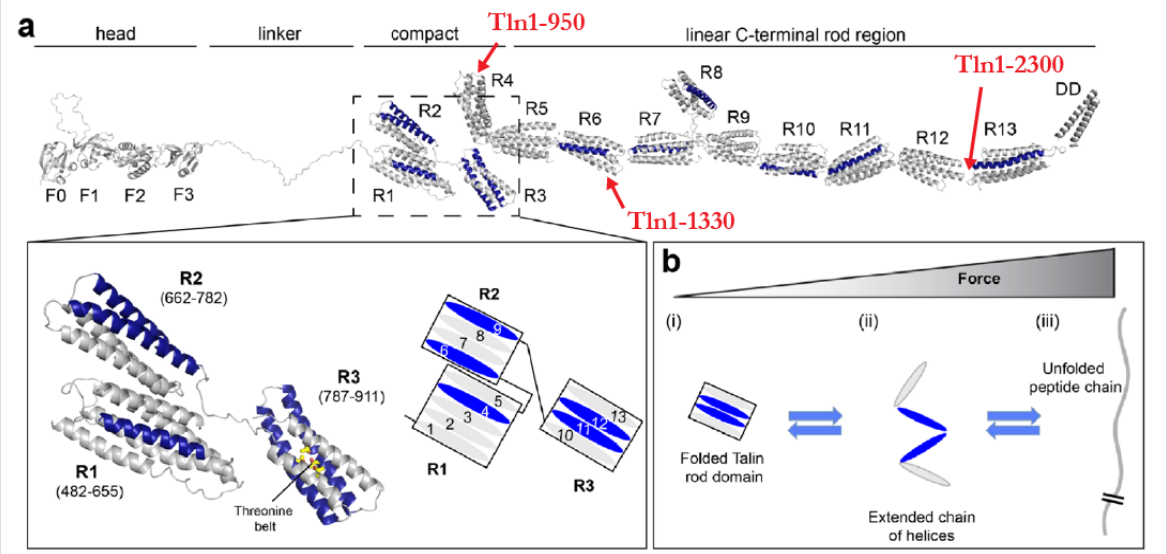

Figure 3.2: Proposed structure of talin-1 and force induced accessibility of VBSs in R1-R3 domains from [130]. (**a**) Structural model of talin-1. The talin-1 head is comprised of an atypical FERM domain (F0-F3), the talin-1 rod contains 13 helix bundles of 4-5 individual helices as well as a DD. The rod domain is structurally divided into a compact (R1-R3, insert) and a linear (R4-DD) region. Potential VBS are marked in blue. Red arrows indicate approximate ends in deletion mutants Tln1-950, Tln1-1330 and Tln1-2300. (**b**) Three potential force-dependent conformations of the rod subdomains. (i) F<5 pN: Without force applied, helix bundles are in an entirely folded conformation. (ii) F~5 pN: Intermediate forces separate the helices and expose cryptic VBSs. (iii) F>5 pN: Under high forces, the polypeptide chain is entirely unfolded and devoid of any structural components.

assembly. The data of the Tln1-2300 mutant supports this hypothesis, as it could be shown that mechanical resilient linkages between talin-1 and f-actin can be established even in the absence of ABS3. However, the Tln1-2300 mutant FA formation was not as impaired as in the published mutant (Figure 2.46).

ABS2, in cooperation with vinculin, on the other hand was shown in FLAP (fluorescent loss after photoactivation) experiments to regulate talin dynamics in FAs and play an important role in force transmission and traction force generation. These findings match the results on talin-1 950 mutants, where cells lacking vinculin and f-actin association to talin-1 were incapable of traction force generation and FA maturation (chapter 2.4.4) (Figure 3.3).

Taken together, the current model of talin-1 association to f-actin suggests a force-dependent recruitment of vinculin to VBS 1-5. The forces are generated by f-actin binding to ABS2 and ABS3 as well as vinculin recruitment to the C-terminal VBS (6-11) in the talin-1 rod. These findings partially elucidate the functional role of f-actin and vinculin association to talin-1 in talin-1 force transduction.

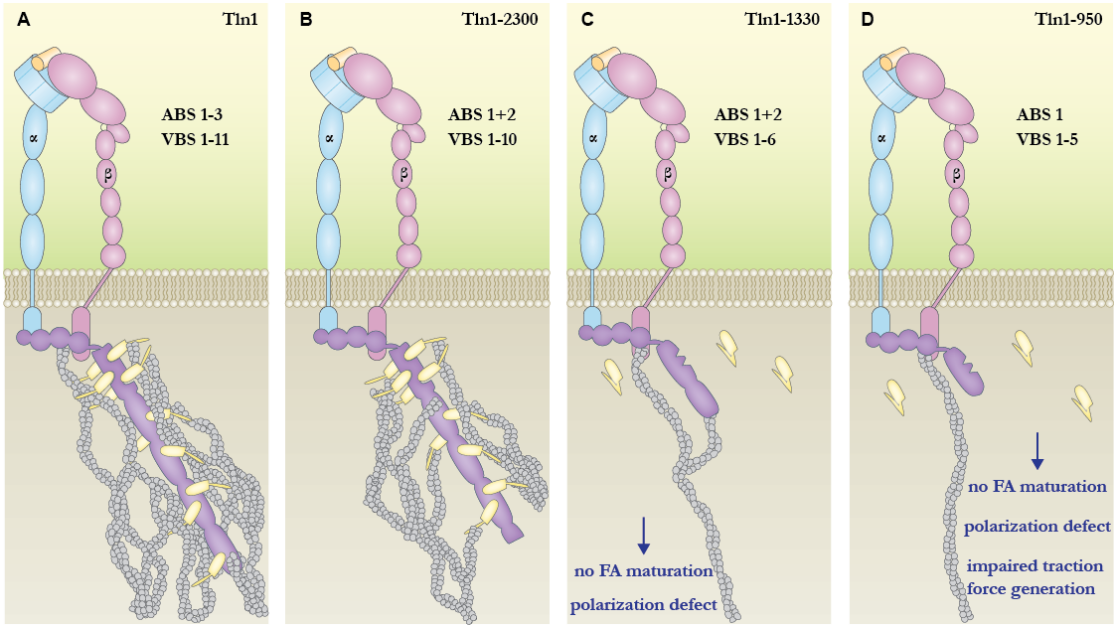

Figure 3.3: Schematic illustration of supposed f-actin recruitment to talin-1 (mutant) proteins. (**A**) In full length talin-1, all ABS and VBS establish the connection between talin-1 and the cytoskeleton. (**B**) Without ABS 3 and VBS 11, VBS 6-10 and ABS 2 enable initial forces across Tln1-2300 and (**C**) Even though f-actin association to ABS 1 + 2 is still possible in Tln1-1330 mutant expressing cells, forces are insufficient to open cryptic VBS 1-5. As a consequence cells display defects in polarization and FA maturation. (**D**) In addition to FA maturation and polarization defects, Tln1-950 cells, where no force generation through f-actin and vinculin can be established, show impaired traction force generation.

Analysis of the functionality of individual ABS and VBS in the talin-1 rod by point mutations would be the next step towards a deeper understanding about the functional role of vinculin and actin association to talin-1 at specific binding sites. The VBS 1-5 in the N-terminal rod

domain (R1-R3) are of special interest in this case. It would be interesting to investigate if constitutive accessibility of these sites (e. g. by mutations that reduce the hydrophobicity of the helices) could – at least partially – rescue the phenotype of the Tln1-950 cells. This would indicate that indeed missing vinculin and thus f-actin association to talin-1 is responsible for the defects of these cells.

Additionally, the existing truncated talin-1 versions could be used to further analyze the role of talin-1 association with the cytoskeleton in FA-dependent downstream signaling. For example, analysis of the phosphorylation state of proteins downstream of potential effector kinases in cells seeded on substrates of varying stiffness in cells expressing Tln1 or Tln1-950 could provide insight in the role of talin-1 in force transduction pathways.

However, it would be also important to understand the full process of force induced adhesion maturation. For example, the role of the talin-1 binding protein RIAM would be of interest, as it was suggested earlier that RIAM binding competes with vinculin association to talin-1 in nascent adhesions[136]. During adhesion maturation RIAM is supposedly displaced by vinculin upon force applied on talin-1[137]. Thus, the interaction between RIAM and talin-1 and its role in talin-1 force transduction and adhesion maturation would be interesting to study.

3.5.4 Mechanical engagement of talin-1 is important for cellular rigidity sensing

Experiments on the Tln1-950 cells revealed a characteristic phenotype for cells lacking mechanically engaged talin-1: Cell spreading (Figure 2.53) and polarization, FA maturation and traction force generation (Figure 2.59) were strongly impaired, even though integrin β1 activation was unaffected (Figure 2.51). Furthermore, FA strengthening did not follow increased actomyosin contractility triggered by active RhoA (Figure 2.55). All these processes require mechanical stabilization of FAs, a process that was also supposed to be required in extracellular rigidity sensing[36]. Extracellular physical stimuli, like for example substrate rigidity, are epigenetic factors that trigger important cellular processes, for example stem cell fate decision and differentiation[186,187]. To test whether mechanical engagement of talin-1 is required in this essential cellular process, Tln-1 and Tln1-950 cells were seeded on substrates with specified rigidity indices. Surprisingly, Tln1-950 did not respond to changes in stiffness, whereas Tln1 cells showed the expected stiffness-dependent increase in surface area (Figure 2.56 and Figure 2.57). Taken together, these data suggest that mechanical engagement of talin-1 plays a major role in extracellular rigidity sensing and that f-actin association to talin-1 is indispensable for adhesion dependent processes like cell spreading and traction force generation.

As integrin mediated adhesion is widespread throughout different cell types and tissues, it will be interesting to understand if talins play a regulatory role in organ function and development. In a first attempt, talin-1 tension sensors could be expressed in various cell types to investigate whether forces in talin-1 alter in a tissue-specific manner. Furthermore, it could be shown that integrin mediated adhesion is talin isoform dependent[154]. Talin-2, the second talin isoform is, in contrast to the ubiquitously expressed talin-1, restricted to a limited set of tissues, including heart- and skeletal muscle as well as brain and testis[103]. Still, the function of talin-2 expression in those tissues it not yet clarified, but talin-2 bears – in average – significantly higher forces as compared to talin-1 when expressed in fibroblasts. These differences were mediated by the talin rod, specifically through differential vinculin recruitment to the R1-R3 domains. In addition to these findings, cells expressing talin-2 were shown to spread more efficient on soft substrates (1-2 kPa), indicating that rigidity sensing might be regulated by specific talin isoform expression[154]. Intriguingly, neurons were shown to branch on very soft substrates and only apply very mild traction on their substrates whereas astrocytes are shown to be sensitive to more rigid substrates[188,189]. When seeded on soft hydrogels, astrocytes failed to form f-actin stress fibers on soft gels whereas neurons showed significantly more f-actin structures on soft gels along with enhanced neurite branching[190]. As f-actin anchorage in FAs seems talin-isoform dependent, it would be interesting to investigate whether differential isoform expression is responsible for altered rigidity sensing in these two cell types. After lesion of spinal cord tissue, glial scar tissue is formed that circumvents cellular and axonal repair. These scar tissues are characterized by a higher elastic modulus, suggesting that neuronal growth and growth cone formation might be inhibited through substrate rigidity[191]. Understanding of how neuronal growth can be regulated on a cellular level could for example help to develop treatments for traumatic injuries in the central nervous system.

3.6 Outlook

In this study, two novel talin-1 tension sensors have been developed and evaluated. It could be shown that talin-1 bears mechanical tension of 7-10 pN in cells and that this tension is modulated by vinculin and f-actin association. Furthermore, mechanical resilient linkages between talin-1 and the cytoskeleton are important for FA maturation, polarization and cellular rigidity sensing.

In the future, it would be interesting to analyze forces not only across talin-1 but also characterize other candidate proteins using the VH based tension sensor under *in vivo* conditions to learn more about the functional purpose of forces across certain proteins. Here, various biological processes are of special interest as they have been described to be force dependent. For example it could be shown that traction forces generated by fibroblasts play a critical role in wound healing processes[192]. Here, the mechanosensitive function of talin-1 but also other proteins, e. g. ECM components, could play central role. Furthermore it has been described that forces are important for many developmental processes[170]. Examples are rigidity-dependent stem cell differentiation[187] or mechanical regulation of gene-expression that controls differentiation during gastrulation[193]. The tension sensors described in this study could be used to analyze force transduction across key regulators of these processes. As conventional confocal microscopy is unsuitable to analyze living animals, FRET analysis using two-photon microscopy could be used to study the tension sensors *in vivo*.

Even more interesting for the field would be the analysis of forces across single molecules. A major disadvantage of this study is that information about local force transduction is lost due to limited resolution of the imaging techniques. Here, signals from thousands of talin-1 proteins were pooled in one FRET value of the cell that allows assumptions about the overall state of all talin-1 molecules within the cell but neglects information on the molecular level. High resolution approaches using for example STORM (stochastic optical reconstruction microscopy) or PALM (photo-activated localization microscopy) are nowadays used in many fields to overcome the conventional Abbe resolution limit. However, the tension sensors used here will need to be modified for this approach. Especially the fluorophores (YPet and mCherry) are not suitable in this approach and would have to be exchanged for other fluorescent probes to perform single molecule FRET experiments[194].

In addition to single molecule approaches, the toolkit of tension sensors used for the analysis of forces acting intra- and extracellularly needs to be broadened in the future. The sensors used in this study (F40, VH and stVH) can be used for a wide range of biological processes, but do not cover forces beyond 10 pN. Still, some molecules might bear higher forces, e. g.

single αvβ3 integrins were demonstrated to be subject to forces in the 40 pN range[73]. Single molecule calibrated tension sensors will be required for the analysis of these forces in living cells in the future. Furthermore, switch-like sensors in the low pN range (1-6 pN) would significantly increase the validity of measurements in this force area, as the F40 sensor seems not sufficient to visualize small differences in this regime. Thus, the development of new tension sensor probes is an important part for future analysis of cellular mechanotransduction. Altogether, the VH based tension sensors are not only an appropriate tool to study force transduction across talin-1, but also enable investigation of force propagation across other proteins of interest and the impact of mechanical engagement of proteins in many regulatory processes in the future.

4 Materials and Methods

4.1 Molecular biological Methods

4.1.1 Generation of expression constructs

All talin-1 constructs were based on the published murine talin-1 cDNA with the accession number X56123. The pLPcXmod vector was used for all mammalian expression constructs. Insertion of the tension sensor was achieved by the introduction of a 5' SalI/3' NotI site into the talin-1 linker region between aa 447 and 448 of talin-1 via overlap extension PCR (4.1.2.2.3). Fluorophores or the tension sensor motives were inserted as described in [154]. Point mutations were introduced using a site directed mutagenesis kit by amplification of the corresponding DNA plasmid (4.1.2.2.4). Deletion mutants were generated through amplification of shorter fragments of the original talin-1 cDNA.

4.1.2 Cloning methods

4.1.2.1 Media and reagents

LB medium

NaCl	10 g
Trypton	10 g
Yeast extract	5 g
H_2O, autoclaved	filled up to 1000 ml

LB plates

LB medium	1000 ml
Agar-Agar	15 g
autoclaved, poured into 100 mm Petri dishes,	

Additives

Ampicillin	50µg/ml
Kanamycin	25µg/ml
Tetracycline	10µg/ml

4.1.2.2 Polymerase Chain Reaction (PCR)

The PCR is among the most frequently used methods in molecular biology as it allows the amplification of specific DNA fragments even from small amounts of starting material. The DNA polymerase of a thermophilic organism (Thermus aquaticus; taq polymerase) has a temperature optimum at 72 °C and only needs few additives for its reaction: a template DNA strand, 2 primers (forward and reverse) as well as specific buffer conditions (dNTPs, Mg2+). The reaction is characterized by three repetitively successive steps; denaturation at 95 °C, primer annealing to the template at 58-68 °C and DNA synthesis at 72 °C. Freshly synthesized DNA products serve as a template in the next cycle of the reaction and therefore lead to a fast amplification of the required DNA sequence. All primers were purchased from Eurofins Genomics GmbH (Ebersberg, Germany). Depending on the PCR approach, different polymerases and PCR programs were used. For genotyping PCRs, a Taq polymerase was used in order to control for efficient knockout of the gene of interest. For cloning purposes, a Pfu Ultra II (NEB biolabs) polymerase was used, carrying an intrinsic proof-reading activity to reduce the probability of spontaneous mutations during the PCR runs.

4.1.2.2.1 Genotyping PCR

This PCR method was used to control the efficiency of Cre mediated knockout of talin-1 in *talin-1 f/f* cell lines. DNA was isolated from various cell lines using a mammalian mini prep kit (Sigma-Aldrich) according to manufacturer's information. In brief, cells were seeded in growth medium and lyses with the supplied buffer system. Subsequently, PCR was performed.

Genotyping PCR	
DNA template	5 µl
Primer 1	0.2 µl
Primer 2	0.2 µl
Taq Polymerase	0.2 µl
dNTPs (10mM)	0.4 µl
MgCl2	0.6 µl
10x PCR buffer	2 µl
dd H_2O	Filled up to 20 µl

Genotyping PCR program				
Step	**time [sec]**	**Temperature [°C]**		
1	300	94		
2	30	94	-1 °C	9x
3	30	63		
4	30	72		
5	30	94	35x	
6	30	53		
7	30	72		
8	300	72		
9	∞	4		

4.1.2.2.2 Cloning PCR

This method was primarily used to generate expression constructs for mammalian cell culture. PCR's were performed for 30 cycles (step 5-7), touch down from 70 °C - 60 °C in 9 cycles by sequential reduction of the annealing temperature (-1 °C / cycle) (step 2-4). DNA synthesis step (72 °C) was adjusted according to construct length (ca. 30 sec per Kb).

Cloning PCR	
DNA template	~ 1-5 µl
Primer 1 (20 pmol)	1 µl
Primer 2 (20 pmol)	1 µl
Pfu Ultra Polymerase	1 µl
dNTPs (10 mM)	3 µl
10x PCR buffer	5 µl
dd H_2O	Filled up to 50 µl

Cloning PCR program

Step	**time [sec]**	**Temperature [°C]**		
1	300	95		
2	30	95		
3	30	70	-1 °C	10x
4	60	72		
5	30	95		30x
6	30	60		
7	60	72		
8	300	72		
9	∞	4		

4.1.2.2.3 Overlap extension PCR

Overlap extension PCR is a PCR variant of the normal cloning PCR, used to insert small DNA fragments into a region of interest in a target DNA sequence. The reaction is divided into three separate PCR reactions: in a first round of two PCRs two fragments of the target sequence are generated, one reaching from 5' end to the insertion site, the other from the insertion site to the 3' end. The overhang of both primers annealing to the insertion sites hereby encode for the inserted DNA fragment. In a third PCR, both products of the initial PCRs are used as template with only the 5' and 3' primers. As a result, the DNA fragment is introduced into the region of interest.

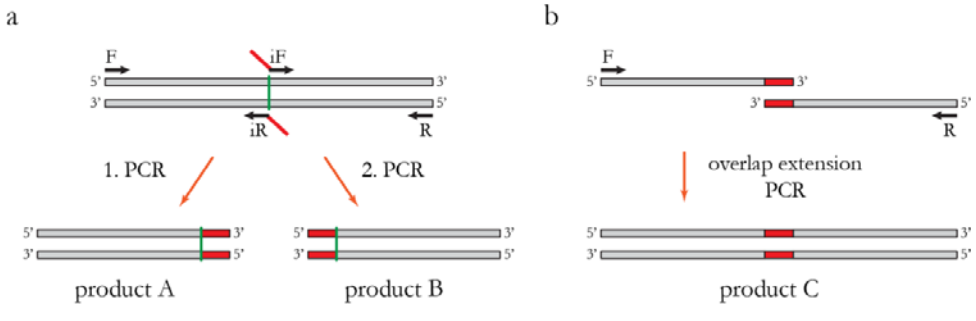

Figure 4.1: principle of the overlap extension PRC method.
(a) In the first step, two separate PCRs from the template of interest are performed, using two different primer pairs with overhangs encoding for the insertion sequence. (b) In the second step, both products with and the flanking primers are used to amplify the final DNA product. (Figure adapted from [202])

4.1.2.2.4 Mutagenesis PCR

In order to manipulate only few basepairs of a DNA sequence, a mutagenesis PCR was performed, using the QuikChange II Site-Directed Mutagenesis PCR kit (Agilent Technologies; Santa Clara, USA). The QuikChange II Site-Directed Mutagenesis kit is based on the function of the Dpn I endonuclease that targets parental methylated and hemi-methylated DNA after the PCR reaction and only leaves functional, mutated strands for transformation of competent bacteria (4.1.2.8). Oligonucleotides were designed individually for every desired mutation and according to company instructions (primer design tool: www.agilent.com/genomics/qcpd). The primers carry the sequence of the desired mutation and anneal on opposite strands of the plasmid to the same sequence.

Mutagenesis PCR	
DNA template	2 µl
Primer 1 (20 pmol)	1 µl
Primer 2 (20 pmol)	1 µl
Pfu Ultra Polymerase	1 µl
dNTPs (10 mM)	1 µl
10x reaction buffer	5 µl
dd H_2O	Filled up to 50 µl

Mutagenesis PCR program

Step	**time [sec]**	**Temperature [°C]**
1	30	95
2	30	95
3	60	55
4	60 / kb	68
5	∞	4

PCR's were performed for 12-18 cycles (step 2-4), depending on the putative mutation sites (12 cycles for point mutations, 16 for single amino acid changes and 18 for multiple amino acid changes). DNA synthesis step size needed to be adjusted depending on the plasmid length (60 sec per kb of plasmid length).

4.1.2.2.5 Sequencing PCR

This PCR variant was used to check PCR products from cloning PCR to ensure correct DNA sequences. All sequencing PCRs were performed by Eurofins Genomics GmbH (Ebersberg, Germany). Here, premixed DNA template and sequencing primers were added to barcode labeled tubes and sent for sequencing.

sequencing PCR	
DNA template	~ 1 µg DNA
Primer 1 (20 pmol)	2 µl
Primer 2 (20 pmol)	2 µl
dd H_2O	Filled up to 17 µl

4.1.2.2.6 PCR Primer list

Name	Alternate Name/ Additional Info	Sequence (5' —> 3')
TalinR2526G_Cla	Primer for Dimerization mutant + Cla restriction side_rev	TAT ATC GAT TTA GTG CTC GTC TCG AAG CTC TGA AGG CAA GAA CTT GTA CTG CTG CTG CCC GAT CTG GG
Tal1_Seq_1	Talin-1 Sequencing	ATG GTT GCG CTT TCG CTG
Tal1_Seq_2	Talin-1 Sequencing	GAT GGA AGA AAA GAA AGA TGA GG
Tal1_Seq_3	Talin-1 Sequencing	GCC CAA GGA GTA TGT GAA GCA G
Tal1_Seq_4	Talin-1 Sequencing	ATT GCT GGC TAC ATA GAT ATC ATC
Tal1_Seq_5	Talin-1 Sequencing	GGC GTA AGA ACA AGA TGG ATG
Tal1_Seq_6	Talin-1 Sequencing	GGA TGT TCT AAT GCA GCT AGC
Tal1_Seq_7	Talin-1 Sequencing	GAC CAA GCC ACT GAT ACC ATC C
Tal1_Seq_8	Talin-1 Sequencing	GCT GCA GCC CAA CAT GCA GCC
Tal1_Seq_9	Talin-1 Sequencing	GCA GCA GCT CGA GAT GGC AAG C
Tal1_Seq_10	Talin-1 Sequencing	GTG TCA GCT GCC TGC CTG GCC
Tal1_Seq_12	Talin-1 Sequencing	GTT TGC CCG TGC AAA CCA GGC
Tal1_Seq_13	Talin-1 Sequencing	GTA ATC TCT GCT AAG ACA ATG
Tal1_Seq_14	Talin-1 Sequencing	CCA AAT GGC CCA GTA CTT TG
Tal1_Seq_15	Talin-1 Sequencing	ACT GTT CAG GAG ATG GTA ACC AAG
Tal1_Seq_16	Talin-1 Sequencing	CTG CTG GCA CAC TTA ACC GTG
Tal1_Seq_17	Talin-1 Sequencing	GGC TGT GGA AGA TGA GGC CAC C
Tal1_Seq_18	Talin-1 Sequencing	CAG CAG CTA ACT GGA CAC TCA AAG
Tal1_Seq_19	Talin-1 Sequencing	GGC TGC GGC CAC CAA CAA TCT G
Tal_dim_not_rev	Talin dimerization mutant pr. Rev. + Not site N-term	ATA AGC GGC CGC TTA GTG CTC GTC TCG AAG CTC TGA AGG CAA GAA CTT GTA CTG CTG CTG CCC GAT CTG GG
tal_Xho_inter_f	Talin internal Xho site forward	CAG CTC GAG ATG GCA AGC TTA AGC CCT TAC
tal_Xho_inter_r	Talin internal Xho site reverse	CAT CTC GAG CTG CTG CTT TTA TTT CCT G
tal_wt_rev_not	Talin WT reverse_ + Not Restriction site N-term	ATA AGC GGC CGC TTA GTG CTC GTC TCG AAG CTC TG
talin_c2019g	talin mutagenesis forward for bp 2019	GAT GTT CTA ATG CAG CTA GCA AAG GCA GTG GCA AGT
tal_c2019g_rev	talin mutagenesis reverse for bp 2019	ACT TGC CAC TGC CTT TGC TAG CTG CAT TAG AAC ATC
talin_t3680c	talin mutagenesis forward for bp 3680	GCA AGC GAC TCC TGA GTG ACT CGC TTC CTC CAA
tal_t3680c_rev	talin mutagenesis reverse for bp 3680	TTG GAG GAA GCG AGT CAC TCA GGA GTC GCT TGC
cherry_Eco_for	fluorophore elongation	ATA GAA TTC ATG GTG AGC AAG GGC GAG GAG GAT AAC ATG GCC AT
cherry_Eco_rev	fluorophore elongation	ACA GAA TTC ACC ACC CTT GTA CAG CTC GTC CAT GCC G
cherry_sal_for	fluorophore elongation	GTC GAC ATG GTG AGC AAG GGC GAG GAG G
R358W forw	Talin-1 f-actin binding mutant forward	CAC CAA CAT CAA ACA GTG GGC TGC CTC TCC CAA G
R358W rev	Talin-1 f-actin binding mutant reverse	CTT GGG AGA GGC AGC CCAC TGT TTG ATG TTG GTG
M319A forw	constitutive active talin-1 mutation forward	CTA GTC AAG GAA AAG GCC AAG GGG AAG AAT AAA C
M319A rev	constitutive active talin-1 mutation reverse	GTT TAT TCT TCC CCT TGG CCT TTT CCT TGA CTA G
tal Δ7485 NotI	Talin-1 deletion mutant for dimerization helix (7486-7626)	CGG GCG GCC GCA ACC ATT TTC TCC TTC ACC ACC ACC
tal Δ6900 NotI	Talin-1 deletion mutant for dimerization helix and actin binding domain (6900-7626)	CGG GCG GCC GCC TCT GGG TCC ACC CAC TCT GTT CC
Ypet_Eco_f_n	fluorophore elongation	ATT GAA TTC ACC ATG GTG AGC AAA GGC GAA GAG CTG TTC
Ypet(s)StEco r	fluorophore elongation	TAT GAA TTC TTA GGC GGC GGT CAG GAA CTC CAG CAG C
Ypet(s)Eco r	fluorophore elongation	TAT GAA TTC ACC ACC GGC GGC GGT CAG GAA CTC CAG CAG C
T7 Primer	sequencing for pBSK	TAA TAC GAC TCA CTA TAG GG

Name	Alternate Name/ Additional Info	Sequence (5' —> 3')
T3 Primer	sequencing for pBSK	AAT TAA CCC TCA CTA AAG GG
Cherry_Hind_f	fluorophore	CGC AAG CTT ACC ATG GTG AGC AAG GGC GAG GAG G
Cherry_Apa_r	fluorophore	CAT GGG CCC CTT GTA CAG CTC GTC CAT GCC
Tal_EcorI_for	SalI-NotI linker introduction	GCG AAT TCA CCA TGG TTG CGC TTT CGC TGA AGA TTA GC
Tal_Xho_rev	SalI-NotI linker introduction	CG CTCGAG CTG CTG CTT TTA TTT CCT GTA GGT CTT TC
Tal447_salnot_f	SalI-NotI linker introduction	CAT CTC GAG CTG CTG CTT TTA TTT CCT G
Tal447_salnot_r	SalI-NotI linker introduction	AGC GGC CGC TAT TAT GTC GAC AGA GCC GTG CTC CAC TTT CCC CAC TCG GTT GTA CTG CTG
pLPCX_seq_f	Sequencing for pLPCX	AGC TCG TTT AGT GAA CCG TCA GAT C
pLPCX_seq_r	sequencing for pLPCX	ACC TAC AGG TGG GGT CTT TCA TTC CC
LZ_Bgl_f	linker amplification	CAG AGA TCT GCC TTG AAG AAG GAG CTT CAG
LZ_Bam_r	linker amplification	TAT GGA TCC GCC CGC CAG TTT CTT CTC CAG
Tal_nstp_Not_r	Talin1 amplification	ATA AGC GGC CGC TCC GTG CTC GTC TCG AAG
Cherry_NotI_f	fluor. ampl.	ATA AGC GGC CGC AGG TGT GAG CAA GGG CGA GGA G
Cherry_stp_Cla_r	fluor. ampl.	ATA ATC GAT TTA CTT GTA CAG CTC GTC CAT GCC GCC GG
YPet_Not_f	fluor. ampl.	ATA AGC GGC CGC AGG AGT GAG CAA AGG CGA AGA GC
YPet(s)stp_Cla_r	fluor. ampl.	ATA ATC GAT TTA GGC GGC GGT CAG GAA CTC CAG
Villinhead_f	annealing; TS linker	aat tca gat etC TCT CCG ATG AGG ACT TCA AAG CTG TGT TTG GCA TGA CCA GGA GCG CAT TTG CCA ACC TTC CTC TGT GGA AAC AGC AAC ACC TGA AGA AGG AAA AGG GAC TGT TCg
Villinhead_r	annealing; TS linker	gat ccG AAC AGT CCC TTT TCC TTC TTC AGG TGT TGC TGT TTC CAC AGA GGA AGG TTG GCA AAT GCG CTC CTG GTC ATG CCA AAC ACA GCT TTG AAG TCC TCA TCG GAG AGa gat ctg
delYpet_Not_r	fluor. ampl.	ATA AGC GGC CGC GCC GGC GGC GGT CAG GAA CTC CAG
Tal1_seq_20	talin1 sequencing	AGC TCG CCC AGA TCC GGC AGC
Tal1_seq_11n	talin1 sequencing	TTG TCC ACA GAC CCT GCT TCT CCC
Cherry_BamHI_r	fluor. ampl.	ATA GGATCC CTT GTA CAG CTC GTC CAT GCC G
Ypet_BamHI_f	fluor. ampl.	ATA GGATCC GTG AGC AAA GGC GAA GAG CTG
YPet(s)stp_Not_r	fluor. ampl.	ATA A GCGGCCGC TTA GGC GGC GGT CAG GAA CTC CAG
YPet(s)stp_Xho_r	fluor. ampl.	ATA CTCGAG TTA GGC GGC GGT CAG GAA CTC CAG
LZ_SacI_f	linker amplification	ATA GAG CTC GCC TTG AAG AAG GAG CTT CAG
LZ_KpnI_r	linker amplification	ATA GGT ACC GCC CGC CAG TTT CTT CTC CAG
TagBFP_Hind_f	fluor. ampl.	CCA AGC TTA CCA TGA GCG AGC TGA TTA AGG AGA AC
TagBFP_Ecor_r	fluor. ampl., HindIII site removal	ATG AAT TCA TTA AG**T** TTG TGC CCC AGT TTG CTA GGG
sVillin_SDM_f	Villin linker SDM; to stable version	TCCTCTGTGGAAACAACAGGCCCTGATGAAGGAAAAGGGACTCTTC
sVillin_SDM_r	Villin linker SDM; to stable version	GAAGAGTCCCTTTTCCTTCATCAGGGCCTGTTGTTTCCACAGAGGA
Chry_stp_Cla_02	fluor. ampl., reverse	TAT ATA ATC GAT TTA CTT GTA CAG CTC GTC CAT GCC GCC GG
TagBFP_NotI_f	Gly linker	ATATTGCGGCCGCA GGA AGC GAG CTG ATT AAG GAG AAC ATG CAC ATG AAG C
TagBFP_HA_ClaI_r		ATAAATCGATTTAAGCGTAATCTGGAACATCGTATGGGTATCCATTAAGCTTGTGCCCCA GTTTGCTAGGGAGGTCGCAGTATCTGG
mT1_SDM_AA_f	Leu2094Ala, Ile2095Ala	CCAAGGCCCTGGGTGACGCCGCCAGCGCTACGAAGGCTG
mT1_SDM_AA_r	Leu2094Ala, Ile2095Ala	CAGCCTTCGTAGCGCTGGCGGCGTCACCCAGGGCCTTGG
Villin_BamHI_r		ATAGGATCCGAAGAGTCCCTTTTCCTTCTTCAGG
YPet_BamHI_f		ATA GGATCC ATG GTG AGC AAA GGC GAA GAG C
YPet_Cys_XhoI_r		ATAACTCGAGACATTTGGCGGCGGTCAGGAACTC
mT1_R358A_f	SDM; Arg358Ala	GCC TCA CCA ACA TCA AAG CCT GGG CTG CCT CTC CC
mT1_R358A_r	SDM; Arg358Ala	GGGAGAGGCAGCCCAGGCTTTGATGTTGGTGAGGC
mT1(1-2299)_stp_NotI_r	dimerization & actin binding domains deletion	ATAAGCGGCCGCTTACTCTGGGTCCACCCACTCTGTTCC
mT1(1-2495) _stp_NotI_r	dimerization domain deletion	ATAAGCGGCCGCTTAAACCATTTTCTCCTTCACCACCACC
mT1(dIBS2)_PCR1r	OE-PCR inner for removal of IBS2	GGTCCTCTGGGTCCACCCACTCACGATTCCCAGCCTGGAGTGCAGC

Name	Alternate Name/ Additional Info	Sequence (5' —> 3')
mT1(dIBS2)_PCR2f	OE-PCR inner for removal of IBS2	CTGCACTCCAGGCTGGGAATCGTGAGTGGGTGGACCCAGAGGACC
mT1_K324D_f	SDM; Lys324Asp	GGAAAAGATGAAGGGGAAGAATGATCTGGTGCCCAGGCTG
mT1_K324D_r	SDM; Lys324Asp	CAGCCTGGGCACCAGATCATTCTTCCCCTTCATCTTTTCC
mT1_E1770A_f	SDM; Glu1770Ala	GACTAAAACGTTGGCAGCGTCTGCCTTGCAGTTGC
mT1_E1770A_r	SDM; Glu1770Ala	GCAACTGCAAGGCAGACGCTGCCAACGTTTTAGTC
mT1_EcoRI_f		ATAAGAATTCACCATGGTTGCGCTTTCGCTGAAGATTAGC
mT1_950_Not_r		ATAATGCGGCCGCTCCGGGCTGGGGGCCCGCAGAGGCC
mT1_950_s_Xho_r		ATAACTCGAGTTAGGGCTGGGGGCCCGCAGAGGCC
mT1_1330_sCla_r		ATAAATCGATTTAGTTGGGAGAAGCAGGGTCTGTGG
mT1_1330_Not_r		ATAATGCGGCCGCTCCGTTGGGAGAAGCAGGGTCTGTGG

4.1.2.3 Agarose gel electrophoresis

Analysis of DNA fragment size after PCR or enzymatic digestion occurred by agarose gel electrophoresis. Here, negatively charged DNA fragments were separated according to their length, as they run with different velocities in the gel. A standard of 1% agarose gels was used, that was, in some cases, adjusted to 0.2 – 2 %, depending on the expected fragment length. In order to prepare the gels, the desired amount of agarose (life technologies) was boiled in the microwave in 1xTAE buffer. Successively, 5 µl ethidium bromide (Roth) per 100 ml gel were added and the solution was poured into a casting tray and hardened at RT. Samples were prepared with 6x DNA loading buffer and applied on the gel in a electrophoresis chamber filled with 1x TAE buffer. Gels run at 40-120 V at RT, depending on fragment size and visualized in a UV light transilluminator at 366 nm wavelength. As a standard marker, the 1 Kb DNA Ladder (Invitrogen) was used.

50x TAE buffer

Tris-base	242 g
EDTA	37.2 g
Glacial acetic acid	57.1 ml
H_2O, autoclaved filled up to	1000 ml

6x DNA loading buffer

Glycerol	60 % (v/v)
EDTA	60 mM
Bromphenol blue	0.1 % (w/v)
Orange G	0.2 % (w/v)
Xylene cyanol FF	0.1 % (w/v)
Tris-HCl, pH 7.6	10 mM

4.1.2.4 DNA extraction from agarose gels

The extraction of separated DNA fragments was performed using a Nucleo Spin Gel and PCR cleanup kit (Marchery Nagel) according to manufacturer's instructions.

4.1.2.5 Enzymatic DNA-manipulation

A wide range of enzymes, called restriction endonucleases, from bacterial and eukaryotic origin are binding DNA in a sequence-specific manner. Endonucleases cut DNA, retaining defined overhangs of various length. Those restriction enzymes are widely used in molecular biology to manipulate DNA fragments at defined sites and can be divided in 3 subgroups:
Type I restriction enzymes are multi-subunit protein complexes, cutting DNA sequence-unspecific far from their recognition sites. Type II enzymes are most frequently used as they bind to specific, often palindromic DNA recognition sites and cut within or close by this sequence. In contrast, type III enzymes, just like type I enzymes, are cleaving outside their recognition sequence.
According to manufacturers' instructions (New England Biolabs) type II restriction enzymes were used in provided buffer systems. Multi-enzyme digestion cocktails were prepared according to double digest finder software on the NEB website (https://www.neb.com/tools-and-resources/interactive-tools/double-digest-finder).

DNA digestion reaction

DNA	3 – 5 µg
NEB buffer (+/- BSA)	25 µg/ml
Restriction enzyme	5 – 10 U
Filled up to 30 µl with H_2O	

The reaction was incubated according to enzyme preferences, in most cases at 37 °C, for at least 2 h.

4.1.2.6 Dephosphorylation of plasmid DNA

The DNA overhangs created by restriction enzymes have a reactive 5'-phosphate group and a 3'-hydroxyl group with the intrinsic capacity to re-ligate during the following ligation reaction. Freshly digested plasmid DNA was therefore treated with 2 x 30 min at 37 °C with CiP (alkaline phosphatase, New England Biolabs, 5 U directly added into digestion mix) to remove the 5'-phosphate group.

4.1.2.7 Ligation

Ligation of DNA fragments generates a new phosphodiester bond between a 3' –hydroxyl group and a 5'–phosphate group of a backbone DNA fragment and the DNA insert of interest. Ligation mix was incubated at RT for 45 min. Previous dephosphorylation of the vector DNA reduced the probability of religation of the vector without insert.

Ligation mixture	
DNA backbone	0.5 – 1 µl
DNA insert	5 µg PCR product or digested DNA
T4 ligase buffer	1.5 µl
T4 ligase	1 µl
H_2O	filled up to 15µl

10 µl of the ligation mixture was used for transformation in competent bacteria (100 µl).

4.1.2.8 Competent bacteria

The synthesis of recombinant plasmids was performed in an E.coli (XL-1 blue) strand. To enhance the plasmid uptake of the bacteria, starter culture of competent cells was shaken O/N in 10ml Tet-LB Medium with one colony of bacteria at 37 °C/200 rmp. 1 ml of the O/N starter culture was added to 100 ml pre-warmed LB Medium and shaken at 200 rpm / 37 °C until an OD_{550} of ~0.5 was reached. The suspension was cooled down 10 min on ice, subsequently centrifuged for 15 min at 4 °C/1100 g and resuspended in 10 ml ice cold TSS buffer. 2.5 ml of sterile 87 % glycerol were added, bacteria were aliquoted in volumes of 50-200 µl and immediately shock frozen in liquid nitrogen.

Long time storage for several month occurred at -80 °C.

TSS (500ml)	
Polyethylenglycol	50 g
Tryptone	5 g
Yeast extract	2.5 g
NaCl	2.5 g
DMSO	25 ml
MgCl2 1 M	25 ml
filtrated and stored at 4°C	

4.1.2.9 Transformation

Plasmid DNA uptake in competent bacteria was induced by heat-shock transformation. 10 µl of ligation mix were added to 100 µl of freshly thawed competent bacteria and incubated for 30 min on ice. As a control, plasmid-only ligation mix was introduced to bacteria. Heat-shock was performed for 45 sec in a 42 °C water bath. Subsequently cell suspension was cooled down on ice for 5 min, supplemented with 1 ml LB medium (w/o antibiotics) and incubated 45 min at 37 °C / 200 rpm in an Eppendorf Thermomixer to allow regeneration after heat-shock. After centrifugation at 6000 g for 3 min in a microcentrifuge (Eppendorf Centrifuge 5417) and resuspension in 50 µl LB-medium, cells were plated on LB-Agar plates containing an appropriate antibiotic (concentrations see chapter 4.1.2.1) and incubated at 37 °C O/N.

4.1.2.10 Cryo-preservation of bacteria

Cryo–preservation of competent bacteria was achieved by addition of 250 µl glycerol to 750 µl bacteria O/N-culture and storage at -80 °C.

4.1.2.11 Plasmid DNA preparation

In order to isolate plasmid DNA from bacteria, single colonies were picked, using a sterile pipette tip and incubated O/N at 37 °C / 200 rpm in LB-Amp medium. Cell suspension was transferred into a 1.5 ml reaction tube and centrifuged at 6000 g for 3 min. Plasmid isolation was performed using a NucleoSpin Plasmid Easy Pure (Macherey-Nagel) kit according to manufacturer's instructions. For higher concentrations of plasmid DNA, cells were grown in 250 ml LB-Amp medium and plasmid isolation occurred using the NucleoBond Xtra Midi Plus kit (Macherey-Nagel) after centrifugation 15 min/6000 g/4 °C in a Eppendorf centrifuge (5417R, Eppendorf).

4.2 Cell culture methods

4.2.1 Cell culture material

Plastic material		
Name	Company	Catalog Number
5ml Pipette, Costar Stripette	Corning Inc.	4487
15ml Pipette, Costar Stripette	Corning Inc.	4488
25ml Pipette, Costar Stripette	Corning Inc.	4489
50ml Pipette, Costar Stripette	Corning Inc.	4490
96-well plate, round bottom	Corning Inc.	35 3799
96-well plate, flat bottom	Corning Inc.	35 3596
24 well plate	Corning Inc.	35 3524
12 well plate	Corning Inc.	35 3043
6 well plate	Corning Inc.	35 3046
15 ml Falcon tube	Corning Inc.	43 0791
50 ml Falcon tube	Corning Inc.	43 0829
Cryogenic vials	Corning Inc.	43 0489
100mm dish	Corning Inc.	353003
140mm dish	NUNC	168381
Cell culture flask 75 mm²	Corning Inc.	35 3136
Cell culture flask 175 mm²	Corning Inc.	35 3118
FN coated patterned substrates	CYTOO	10-031-10-18
Soft substrate dishes 25 kPa	Matrigen	SV3520-EC-25
Soft substrate dishes 12 kPa	Matrigen	SV3520-EC-12
Soft substrate dishes 4 kPa	Matrigen	SV3520-EC-4
Soft substrate dishes 2 kPa	Matrigen	SV3520-EC-2
Soft substrate dishes 1 kPa	Matrigen	SV3520-EC-1
Soft substrate dishes 0.5 kPa	Matrigen	SV3520-EC-0.5
Soft substrate dishes 0.2 kPa	Matrigen	SV3520-EC-0.5
Cell scraper	Sarstedt	4142400
Steriflip-GP 0.22µm filter	Merck	SCGP00525
Syringes		
Microscope slides	Gerhard Menzel GmbH	J1800AMNZ
Glass coverslips #1.5	Gerhard Menzel GmbH	0284

Medium and additives, Reagents Name	Company	Catalog Number
Dulbecco's Modified Eagle Medium (D-MEM):		
1. D-MEM, high Glucose, GlutaMAX, Pyruvate	Life Technologies	31966047
2. D-MEM, high glucose, HEPES, no phenol red	Life Technologies	21063045
Opti-MEM I Reduced Serum, GlutaMAX	Life Technologies	51985026
Fetal bovine serum	Gibco	10270-106
P/S: Penicillin-Streptomycin (10,000 U/mL)	Life Technologies	15140122
Trypsin: 0.5% Trypsin-EDTA (10X)	Life Technologies	15400054
Fibronectin: bovine plasma fibronectin	Merck	341631-5MG
Poly-L Lysine 0.01%	Sigma-Aldrich	P4707
Lipofectamine 2000 Transfection Reagent	Life Technologies	11668027
Puromycin	Sigma-Aldrich	P8833
Y-27632	Sigma-Aldrich	Y0505
Calpain Inhibitor I (N-ACETYL-LEU-LEU-NORLEUCINAL)	Sigma-Aldrich	A6185-5MG
Chloroquine diphosphate crystalline	Sigma-Aldrich	C6628

4.2.2 Sub-culturing of adherent cell lines

Cell lines were grown in uncoated cell culture flasks in growth medium for several weeks under 5 % CO_2 and 37 °C conditions in a standard incubator. For all imaging methods (see chapter 4.5) growth medium was exchanged for imaging medium. Passaging was performed by washing the cell layer with sterile PBS and incubation for 5 min in trypsinization solution. Detached cells were resuspended in growth medium and depending on the desired density, dispensable cells were discarded. Residual cells were further supplemented with growth medium.

Growth medium

D-MEM Glutamax	500 ml
FBS	10 %
P/S	1 %

Imaging medium

D-MEM without phenol red	500 ml
FBS	10 %
P/S	1 %

Trypsinization solution

10x Trypsin /EDTA	10 ml
PBS, pH 7.4	90 ml

4.2.3 Freezing cells

Long time storage of cells was achieved by cryo-preservation in liquid nitrogen. Cells were trypsinized and resuspended in normal growth medium, centrifuged at 500 g, and resuspended in 1.5 ml freezing medium per vial. Cryotubes were immediately transferred to -80°C; after freezing cells were transferred into liquid nitrogen (-196°C).

Freezing Medium

FBS	25 ml
DMSO	5 ml
D-MEM	20 ml

4.2.4 Thawing cells

After long-time storage in freezing medium at -196 °C, cells were quickly thawed in a 37 °C water bath, centrifuged at 500 g and the cell pellet was resuspended in normal growth medium. Cell suspension was transferred to an adequately sized cell culture flask and further cultivated in a 37 °C/5 % CO_2-incubator.

4.2.5 Generation of talin-1 deficient cells

Initially, fibroblastoid cell lines from *Tln1(f/f), Tln2(+/+)* mice were isolated and immortalized via SV40 large T antigen infection. *Tln1* deletion occurred via adenoviral transfection of GFP-Cre recombinase, as described above. GFP-positive cell lines were sorted by FACS-sorting (chapter 4.2.11) and cell lines from single cell clones were generated.

After further analysis of the *Tln1(f/f)* cells, cell lines deficient of both, talin-1 and talin-2, were created. Therefore Tln2 knockout mice (*Tln2-/-*) mice were intercrossed with mice in which the Tln1 gene is marked with loxP sites (*Tln1f/f*) (Figure 4.2). Fibroblasts from adult animals (postnatal day 21) were isolated and immortalized, using the SV40 large T antigen. Furthermore, deletion of Tln1 was achieved by adenoviral infection with a GFP-tagged Cre recombinase; afterwards, single clones were isolated and sub-cultured for further analysis. (*Tln1(f/f)/Tln2(-/-)* mice were generated and parental kidney fibroblasts were isolated by Roy Zent. Moritz Widmaier generated double knockout cells by Cre expression and isolated single cell clones[27].

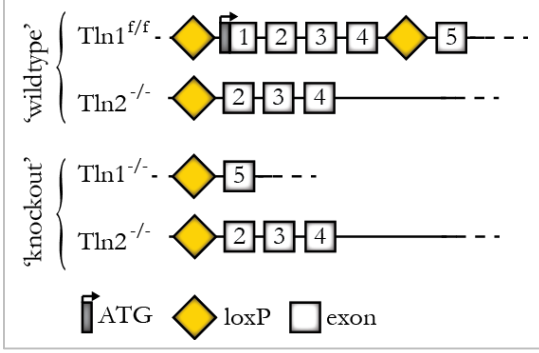

Figure 4.2: Talin-1 and Talin-2 loci in 'wildtype' and 'knockout' animals. Both talin loci are flanked with loxP sites (yellow boxes) in *Tln1(f/f)/Tln2(-/-)* ('wildtype'). In *Tln1(-/-)/Tln2(-/-)* ('knockout') cell lines talin-1 exons 1-4 were deleted. Exons are indicated with white boxes, ATG site is marked by gray box.

4.2.6 Clonal cell lines

In order to isolate clonal cell lines, approximately 100 cells were seeded in a 10 cm plate and kept in culture for several days. Resulting colonies were picked, plated in 48-well plates and sub-cultured in growth medium.

4.2.7 Stable expression of cDNA constructs

Stable cell lines were generated using the Phoenix helper-free retrovirus producer cell system (Nolan Lab, Stanford). Phoenix cells, seeded at 80 % density, were transfected via Calcium chloride Phosphate coprecipitation transfection. While vortexing the DNA mixture, 500 µl of 2x HBS was added drop-wise, subsequently the complete solution was added to the cells. Supplementing the medium with 25 µm chloroquine inhibited the digestion of transfected DNA by lysosomal DNases. The phoenix cells were incubated with the transfection-solution for at least 5 h, afterwards medium was changed to normal growth medium. Target cells were seeded in growth medium to a density of ~50 % and medium was exchanged for filtered supernatant of phoenix cells every 12 h for 3 days. Infected cells were selected by application of 1µg/ml puromycin in the growth medium for 24-48 h.

Na_2HPO_4 (stock solution)

Na_2HPO_4	5.25 g in 500 ml H_2O

2x HBS solution

NaCl	8 g
HEPES	6.5 g
Na_2HPO_4 (stock solution)	10 ml
	pH 7.0

Transfection mix

$CaCl_2$, 2 M	61 µl
DNA	20 µg
H_2O	filled up to 500 µl
2x HBS solution	500 µl

4.2.8 Expression constructs

Abbreviation	Full name	Description / Function
Rho-A Q63L	active Rho-A-BFP	constitutive active Rho-A (Q63L) N terminally tagged to TagBFP
Tln1-1330iTS	Talin-1 1330 tension sensor	Truncation mutant of talin1 tension sensor, lacking ABS 3 VBS 6-11, lacking aa 1331 - aa 2541
Tln1-1330Y	Talin-1 1330 Ypet	Truncation mutant of talin1 tension sensor, lacking ABS 3 and VBS 6-11, lacking aa 1331 - aa 2541, C-terminally tagged with Ypet
Tln1-2300iTS	Talin-1 2300 tension sensor	DD and ABS 3 deletion mutant of talin-1 tension sensor, lacking aa 2301 - aa 2541
Tln1-2300Y	Talin-1 2300 Ypet	DD and ABS 3 deletion mutant of talin-1 tension sensor, lacking aa 2301 - aa 2541, C-terminally tagged with Ypet
Tln1-950cTS	Talin-1 950 zero force control	Zero force control for Tln1-950TS
Tln1-950iTS	Talin-1 950 tension sensor	Truncation mutant of talin-1 tension sensor, lacking ABS 2 and 3 and VBS 6-11, lacking aa 1331 - aa 2541
Tln1-950Y	Talin-1 950 YPet	Truncation mutant of talin1 tension sensor, lacking ABS 2 and 3 and VBS 6-11, lacking aa 1331 - aa 2541, C-terminally tagged with Ypet
Tln1-AAA	Talin-1 AAA tension sensor	Integrin binding deficient mutation at R358A and L2094A, I2095A of talin-1 tension sensor
Tln1C	Talin-1 mCherry	Full length talin-1 C-terminally tagged with mCherry fluorophore, intermolecular FRET control
Tln1C-i	Talin-1 mCherry internal	Full length talin-1 internally tagged with mCherry fluorophore, intermolecular FRET control, insertion between aa 447 and 448
Tln1Con	Talin-1 zero force control	Full length talin-1 C-terminally tagged with VH-based tension sensor module, zero-force control
Tln1-Δ2496	Talin-1 2496 tension sensor	DD deletion mutant of talin-1 tension sensor, lacking aa 2496 - aa 2541
Tln1-EA	Talin-1 E1770A tension sensor	Constitutive active talin-1 tension sensor, E1770A
Tln1-F40-cTS	Talin-1 F40 zero force control	Full length talin-1 C-terminally tagged with F40 based tension sensor module, zero-force control
Tln1-F40-iTS	Talin-1 internal F40 tension sensor	Full length talin-1 F40 based tension sensor
Tln1iTS	Talin-1 (7 pN) internal tension sensor	Full length talin-1 VH based tension sensor, insertion between aa 447 and 448
Tln1-KD	Talin-1 K324D tension sensor	Constitutive active talin-1 tension sensor, K324D
Tln1-LI/AA	Talin-1 LI/AA tension sensor	Integrin binding deficient mutations at L2094A, I2095A of talin1 tension sensor
Tln1-LZ-cTS	Talin-1 LZ zero force control	Full length talin-1 C-terminally tagged with LZ based tension sensor module, zero-force control
Tln1-LZ-iTS	Talin-1 internal LZ tenson sensor	Full length talin-1 LZ based tension sensor
Tln1-MA	Talin-1 M139A tension sensor	Constitutive active talin-1 tension sensor, M319A
Tln1-R2426G	Talin-1 R2526G tension sensor	Dimerization deficient mutation at R2526G of talin-1 tension sensor
Tln1-R358A	Talin-1 R358A tension sensor	Integrin binding deficient mutation at R358A of talin-1 tension sensor
Tln1stiTS	Talin-1 (10 pN) stable internal tension sensor	Full length talin-1 stable (10 pN) VH based tension sensor, insertion between aa 447 and 448
Tln1Y	Talin-1 YPet	Full length talin-1 C-terminally tagged with YPet fluorophore, intermolecular FRET control
Tln1Y-i	Talin-1 YPet internal	Full length talin-1 internally tagged with YPet fluorophore, intermolecular FRET control, insertion between aa 447 and 448

Reconstituted cell lines were named according to the expressed constructs.

4.2.9 Transient transfection

To achieve transient expression of certain proteins, Lipofectamine 2000 transfection was used. According to the manufacturer protocol, 4 µg DNA and 10 µl Lipofectamine 2000 solution were incubated in 250 µl Optimem each for 5 min at RT. Subsequently, both mixtures were merged, vortexed and incubated for 20 min at RT. The DNA-Lipofectamine solution was incubated on cells in antibiotic-free DMEM for 4-6 h. To ensure adequate transcription of the transfected plasmid, cells were incubated O/N in growth medium.

4.2.10 ROCK-inhibitor treatment

Cells were seeded O/N on FN coated glass slides for imaging under normal culture conditions. ROCK inhibitor Y-27632 was added to growth medium to a final concentration of 10 µM and incubated on cells for 1 h. Respectively, medium was exchanged for imaging medium (TCSPC-FLIM experiments, chapter 4.5.5) or cell were washed in PBS and fixed in 4 % PFA (immunostainings, chapter 4.3.3).

4.2.11 FACS sorting

Comparable and physiologically relevant expression levels of stably expressed protein were achieved via fluorescence activated cell sorting (FACS) using a BD FACS CantoTM II instrument (BD Biosciences). Therefore, cells were seeded to 80 % density in normal growth medium and trypsinized as described above (4.2.2). After centrifugation at 600 g, growth medium was exchanged for ~ 500 µl sorting buffer, depending on the pellet size. Prior to the sorting, cells were filtered into a FACS vial to exclude cell aggregates in the system.

Sorting buffer

10 % FBS in PBS

4.2.12 Plate and wash assay

Cell adhesion of cell lines was studied by plate and wash assays. 96 well plates were coated with cell matrix proteins (FN 10 μg/ml) for 4 h at RT and washed with PBS. Incubation of all wells for 1 hour in blocking buffer was used to reduce unspecific binding to the plastic plates. After trypsinization, as described above (4.2.2), 10^5 cells per well were allowed to attach for 15-30 min, subsequently non-attached cells were removed by 3 times carefully washing with PBS. Remaining cells were fixed for 10 min in 70 % Ethanol, 2 times washed in PBS, stained in crystal violet solution and lysed after 3 washing steps in PBS. Absorption of the cell lysate was measured by a plate reader (TECAN, sunrise) at 595 nm wavelength.

Blocking solution (100 ml)	
BSA	1 g
PBS	100 ml

Staining solution (100 ml)	
Crystal violet	0.005 g
PBS	100 ml

Lysis buffer (100 ml)	
Triton-X-100	0.25 μl
PBS	100 ml

4.3 Immunological Methods

4.3.1 Antibodies and Chemicals

Antigene [clone]	Species	Label	Source	Catalog #	IF	WB
Actinin (ACTN1)	rabbit	-	Sigma	HPA006035	1/400	-
FAK	rabbit	-	Millipore	06-543	1/400	1/1000
FAK (pY397)	rabbit	-	Invitrogen	44-624G	1/400	1/1000
GAPDH (6C5)	mouse	-	Calbiochem	-	1/2000	1/10000
GFP	rabbit	-	abcam	ab290	-	1/2000
Integrin β1 [9EG7]	rat	-	BD Pharmingen	550531	1/200	
Integrin β1 [MB1.2]	rat	-	Millipore	MAB1997	1/200	1/1000
Kindlin-2	rabbit	-	Millipore	MAB2617	1/400	-
Mouse IgG (H+L)	donkey	Alexa-647	Invitrogen	A31571	1/500	-
Mouse IgG (H+L)	goat	Alexa-568	Invitrogen	A11004	1/500	-
Mouse IgG (H+L)	chicken	Alexa-488	Invitrogen	A-21200	1/500	-
Mouse IgG (H+L)	goat	HRP	Biorad	170-6516	-	1/20000
Mouse IgG (H+L)	goat	Alexa-405	Invitrogen	A31553	1/500	-
Paxillin	mouse	-	BD Transduction L.	610051	1/200	1/5000
Phalloidin	-	Alexa-488	Invitrogen	A12379	1/400	-
Phalloidin	-	Alexa-647	Invitrogen	A22287	1/200	-
Phalloidin	-	Alexa-568	Invitrogen	A12380	1/200	-
P-Paxillin (Tyr118)	rabbit	-	Millipore	07-1440	-	1/1000
Rabbit IgG (H+L)	goat	Alexa-568	Invitrogen	A11036	1/500	-
Rabbit IgG (H+L)	chicken	Alexa-488	Invitrogen	A-21441	1/500	-
Rabbit IgG (H+L)	goat	HRP	Biorad	170-6515	-	1/20000
Rabbit IgG (H+L)	goat	Alexa-405	Invitrogen	A31556	1/500	-
Rat IgG (H+L)	goat	Alexa-568	Invitrogen	A11077	1/500	-
Rat IgG (H+L)	goat	Alexa-647	Invitrogen	A21247	1/500	-
Talin (8d4)	mouse	-	Sigma-Aldrich	T3287	1/400	1/2000
Talin-1 [mono]	mouse	-	abcam	ab57758	1/1000	1/2000
Talin-2 [68E7]	mouse	-	abcam	ab105458	-	1/2000
Tubulin (DM1A)	mouse	-	Sigma-Aldrich	T9026	-	1/3000
Vinculin (hVIN-1)	mouse	-	Sigma-Aldrich	V9131	1/400	1/4000

ProLong® Gold Antifade Reagent (Molecular Probes, Inc.; Eugene, OR; USA)

4.3.2 Standard solutions

PBS (10x); 1l; pH 7.4

NaCl	1.37 M
Na_2HPO_4	101 mMol
KH_2PO_4	17.5 mM
KCl	27 mM

Fixative (100 ml)

Paraformaldehyde	4 % in PBS pH 7.4

Blocking solution (100 ml)

BSA	2 g
Triton-X100	0.1 ml in PBS pH 7.4

4.3.3 Immunocytochemistry

In order to visualize the subcellular localization of proteins, immunostainings were performed. Therefore, cells were seeded on FN-coated (10 µg/ml) glass slides in normal growth medium O/N or for several h. After washing in PBS, cells were incubated in fixative for 10 min at room temperature and washed again. Blocking of unspecific binding sites (blocking buffer) was performed at RT for one hour previous to primary antibody incubation of one to two h at RT. Secondary antibodies were added after washing in PBS, all antibodies were diluted in blocking buffer. In case of a DNA counterstaining, cells were incubated with 4', 6-Diamidin-2-phenylindol (DAPI) solution (300 nM in PBS) for 5 min. To prevent fluorophore bleaching during image acquisition cells were mounted in Prolong Gold® Antifade Reagent.

4.3.4 Fluorescence activated cell sorting (FACS)

Surface expression of integrin receptors was detected via FACS, using a BD FACS CantoTM II instrument (BD Biosciences). For every cell line, a 75 cm^2 tissue culture plate was cultured to a density of 80%, trypsinized (4.2.2) and centrifuged at 600 g. Stainings were performed in triplicates in a 96 well plate. Primary antibody incubation with anti-integrin antibodies occurred in FACS buffer (100 µl per well) for 1 hour on ice. After at least three washing steps (centrifugation at 2400 rpm for 30 sec), secondary antibody incubation was performed 1 hour on ice. To control for unspecific antibody labelling, cells lacking β1, β2, β3 and β7 integrin were used[158]. Surface expression of integrins was quantitated by geometric mean fluorescence intensity using FlowJo software (Tree Star).

FACS-buffer (in TBS)

BSA	5 %
$MgCl_2$	1 mM
$CaCl_2$	1 mM
sodium azide	0.02 %

4.4 Biochemical methods

Reagents, Consumables Name	Company	Catalog Number
cOmplete ULTRA, mini, EDTA-free EASYpack tablets	Roche	05892791001
PhosStop tablets	Roche	04906837001
Prestained Protein Ladder (10-230 kDa)	NEB	P7710S
BCA Protein Assay Kit	Merck	71285-3
Immobilon Western Chemilumineszenz HRP Substrat	Merck	WBKLS0500
Immobilon-P Rolle (PVDF membrane)	Merck	IPVH00010
Mini-PROTEAN TGX Gels, 4–15%	Biorad	456-1084
µMACS GFP Tagged Protein Isolation Kit	Miltenyi	130-091-125

4.4.1 Hypotonic lysates

For preparation of hypotonic lysates, cells were washed in PBS, detached from the culture plate and collected in a 15 ml tube. After centrifugation (900-1000 rpm for 3 min), PBS was carefully removed and cells were resuspended in hypotonic lysis buffer. Homogenization occurred with a Dounce homogenizer, subsequent to 30 min incubation on ice. Nuclei and remaining intact cells were separated by a second centrifugation step (13,000 rpm for 10 min); the resulting cleared lysate was transferred into a new reaction tube and stored at -80 °C.

Hypotonic lysis buffer

Tris-HCl pH 7.4	10 mM
$MgCl_2$	2 mM
EDTA pH 8.0	0.2 mM
Protease inhibitor cocktail	1 tablet per 10 ml

4.4.2 Total protein lysates

Cells were grown in a 10 cm petri dish O/N at 37 °C, 5% CO_2. After washing in ice-cold PBS, cells were lysed by incubation in 200 µl of lysis buffer for 10 min on ice and scraped off the plate with a cell scraper. Lysates were transferred to reaction tubes and centrifuged 13000 g for 10 min at 4 °C. The supernatant was used for further analysis, pellets containing nuclei, membranes, and other organelles were discarded. Protein concentration was determined by using a BCA solution kit (Merck), protein levels were adjusted and samples were boiled at 95 °C for 5 min with Laemmli buffer, containing sodium dodecyl sulfate (SDS) and 2-Mercaptoethanol to reduce disulfide bonds.

Lysis Buffer		
Tris-HCl	pH 7.4	50 mM
NaCl		150 mM
Triton-X 100		1 %
Protease Inhibitor		1 Tablet for 10 ml
Phosphatase Inhibitor		1 Tablet for 10 ml

Laemmli Buffer (4x)		
Tris-HCl	pH 7.4	4 mM
EDTA		84.5 %
Glycerol		8 %
SDS		4 %
β-Mercaptoethanol		<0.05 %
Bromphenolblue		0.001 %

4.4.3 One-dimensional SDS-polyacrylamid-gelelectrophoresis (SDS-PAGE)

SDS-PAGE is a standard method to analyze protein lysates concerning protein size and concentration under denaturating conditions and is either followed by western blotting, silver staining or visualization with other protein dyes. To analyze protein expression levels, cell lysates were applied on a SDS-PAGE-gel and proteins were separated by application of electric current (120V). To facilitate protein separation in the gel, a stacking gel and a separating gel are poured on top of each other; in the stacking gel proteins accumulate at the gel interface to synchronize the running process and are then separated in the separating gel according to their molecular size. In this study, the Mini Protean III System (BioRad) was used with either self-made or commercially available gels (BioRad). In both cases, lysates were applied to the stacking gel and electrophoresis was performed in SDS-PAGE running buffer at 120 V at RT.

Stacking Gel (5 %)	
H_2O	3.4 ml
30% ProtoGel	0.83 ml
1.5M Tris-HCl pH 6.8	0.63 ml
10% SDS	0.04 ml
10% APS	0.04 ml
TEMED	0.004 ml

10x SDS-PAGE running buffer (1l)	
Glycine	144 g
Tris-HCl	30.3 g
SDS	10 g

4.4.4 Western blotting and Immunodetection

Analysis of protein expression levels of specific proteins of interest after SDS-PAGE was performed with polyclonal and monoclonal antibodies after western blotting. Using wet blot systems, separated proteins were transferred electrically onto a polyvinylide fluoride (PVDF) membrane and visualized by immunodetection methods. To assemble the blotting sandwich, the stacking gel was removed from the SDS-PAGE Gel and the separating gel was placed on top of a methanol-activated PVDF membrane in blotting buffer. On both sides, Whatman paper and sponges were added and the full sandwich was squeezed into a special clip to apply mechanical pressure on the gel and the membrane to facilitate protein transfer (Figure 4.3). This setup was placed in blotting buffer and electric current of 25 V was applied O/N at 4 °C or 100 V for 3-4 h at 4 °C.

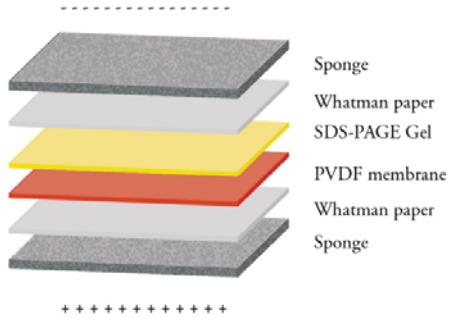

Figure 4.3: Assembly of western blot sandwich.
The SDS-PAGE Gel is tightly placed on the PDVF membrane and assembled between Whatman paper and sponges. Negatively charged proteins are transported to the plus pole onto the membrane by electric current.

After blotting, membranes were washed in TBS-T buffer and blocked in blocking buffer for 1 h at RT. Subsequently, primary antibody solution (in blocking buffer) was incubated on the membranes O/N at 4 °C or for 3-4 h at RT. After 3 washing steps in TBS-T for 5 min, secondary antibody solution was applied to the membrane and incubated 2 h at RT. Washing steps were repeated as before and chemiluminescence signal from HRP reaction was detected using a Fujifilm LAS-4000 Luminescent image analyzer. The staining procedure was eventually repeated after incubating the membrane in Restore Plus Western Blot Stripping Buffer (Fisher Scientific).

Western blot transfer buffer (1l)		
Tris-HCl	pH 7.4	6g
Glycine		28,8g
Methanol		200ml

TBS (10x; 1l)		
Tris-HCl	pH 7.4	24.3g
NaCl		80g

TBS-T (1l)	
10x TBS	100 ml
Tween-20	1 ml

Blocking buffer	
Skim milk powder	5% in TBST

4.5 Microscopy methods and evaluation processes

4.5.1 Image acquisition for Immunostainings

Immunofluorescence images were captured with a LSM780 confocal scanning microscope (Zeiss) using a 100x oil objective (αPlan-APOCHROMAT, NA=1.46). For image acquisition of cells on soft substrates, a Leica TCS SP5 X confocal microscope (Leica Microsystems) equipped with a 40x long-distance water objective (HC PL APO 40x/1.10 W CORR C S2) was used.

4.5.2 Fluorophores

Different fluorophores were tested to establish optimal conditions for tension sensor experiments. Criteria of suitability were quantum yield, brightness, and photostability. Furthermore, only monomeric fluorophores were appropriate candidates for the tension sensor approach, as the direct transfer from one donor fluorochrome to only one acceptor fluorochrome is critical to determine energy transfer between the two. Several fluorophores were tested to achieve a decent FRET pair for FLIM analysis.

In a previously used tension sensor[12], he teal-venus FRET pair was used but exchanged for YPet-mCherry in this study. YPet is a derivate of the GFP variant YFP (yellow fluorescent protein), engineered especially for FRET purposes (YPet = YFP for energy transfer). It is brighter than other YFP variants, gives a higher quantum yield and was demonstrated to be more photostable[195]. The RFP variant mCherry was used as a compatible FRET acceptor for YPet. With an excitation maximum at 596, the mCherry excitation spectrum has a large overlap with the YPet emission spectrum[196].

In addition to fluorophores suitable for the tension sensor approach, a TagBFP was used for labeling of additional proteins in life-cell microscopy. The expression of TagBFP-tagged proteins did not change the lifetime of YPet and therefore did not interfere with FRET measurements. Its excitation and emission properties enable the parallel application TagBFP and YPet, even though BFP variants are less photostable than other fluorescent proteins.

Fluorophore properties[196,197 ,198,199]

	Ex [nm]	Em [nm]	QY	BR	
TagBFP	399	456	0.63	33	monomer
YPet	517	530	0.77	80	Weak dimer
mCherry	587	610	0.22	16	monomer

Ex: Peak excitation wavelength (nm) Em: Peak emission wavelength (nm) QY: Quantum yield BR: Brightness; Extinction coefficient * Quantum yield / 1000

4.5.3 Fluorescence recovery after Photobleaching (FRAP)

4.5.3.1 Image acquisition

Protein turnover rates were determined by fluorescence recovery after photobleaching (FRAP), using a SP8 confocal laser scanning microscope equipped with a 63x water objective (HCX PL APO, NA=1.2). To achieve comparable FA sizes in non-migrating states, cells were seeded for at least 4 h on FN-coated micro-patterned substrates (CYTOO). Imaging was obtained at 37 °C and 5 % CO_2 in imaging medium with a laser intensity of 5 % at 514 nm; the emission signal was recorded at wavelengths between 530-570 nm using a HyD detector. Previous to bleaching with 100 % laser power for about 1 sec, two pre-bleach images were recorded; post-bleach images were recorded every 20 sec up to 300 sec after initial bleaching.

4.5.3.2 Evaluation FRAP

FRAP intensity data were analyzed using the 'FRAP profiler' plugin (http://imagej.nih.gov/ij/plugins/mbf/) of the ImageJ software; data of cells with comparable initial mean intensities and sufficient initial photo-bleaching, were imported into MATLAB for further analysis. Mean values and variance of normalized data were calculated and plotted against time after photo-bleaching. According to $f(t) = A\,(1 - e^{-k_{off}\,t})$, a reaction-dominated model was assumed to determine fluorescence recovery[200]. In this equation, k_{off} is the rate constant and A the mobile fraction of the protein. The recovery half-time $\tau_{1/2}$ was calculated according to: $\tau_{1/2} = \frac{\ln(2)}{k_{off}}$, where t is time.

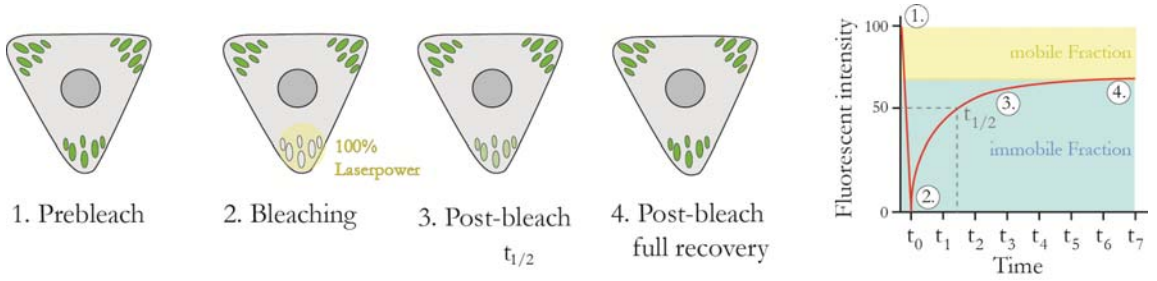

Figure 4.4 Schematic illustration of FRAP principle in cells seeded on micropatterned substrates. (1) Prior to image acquisition, cells adopt a regular shape on the FN coated pattern with equally formed adhesion sites. (2) High laser power bleaches all fluorophores within a distinct area of the cell. (3) The halftime of recovery defines the time when 50 percent of initial fluorescent intensity is regained. (4) Complete recovery is defined by a flat line and therefore steady state conditions. The immobile fraction is defined as the difference in intensity between initial pre-bleach (1) and the steady state intensity (4), whereas the mobile fraction is defined by steady-state (4) and bleach (2) intensity.

4.5.4 Traction force microscopy

To acquire information of the executed force cells apply on their substrates, traction force microscopy was used. Fluorescent beads were incorporated into elastic polyacrylamide (PAA) gels of different stiffness and their position was evaluated before and after the removal of the cells.

4.5.4.1 Preparation of microscopic slides

To achieve PAA gels of even and comparable thickness, polymerization of the gels occurred between two coverslips (25 mm diameter). Activation through amination of one glass slide led to the attachment of the gel to the respective surface, hydrophobic passivation of the other slide surface facilitated the removal of the coverslip. For amination, coverslips were incubated for 10 min in 2 % 3-amino-propyl-trimethoxysilane, washed three times 10 min in dd H_2O and dried at 37°C for at least 30 min. Next, the coverslips were incubated 10 min in 0.5 % glutaraldehyde solution, again washed three times 10 min and dried at RT. Preparation of the hydrophobic surfaces was achieved by treatment with Rain-X solution after washing in EtOH.

4.5.4.2 Preparation of PAA gels

Depending on the required substrate stiffness, PAA and BisAA were mixed in the ratios shown in table (x) and supplemented with dd H_2O to a total volume of 4450 µl stock solution. 445 µl of this stock solution were mixed with 10 µl fluorescent bead solution (FluoSheres® molecular probes carboxylate, 0.2 µm, crimson [625/645]) and 42 µl dd H_2O. Subsequent to degassing of the gels for 20 min, the solution was supplied with 2.5 µl APS and 0.5 µl TEMED to initialize polymerization. 15 µl of the gel solution were applied between a hydrophobic and an aminated coverslip and the resulting sandwich was kept for 20 min at RT to ensure polymerization. Using a razorblade, the hydrophobic slide was detached and PAA gels were stored in dd H_2O at 4°C.

TFM-Gels

Gel stiffness	PAA (%)	BisAA (%)
2.058 kPa	4	0.1
4.363 kPa	4	0.225
7.939 kPa	5	0.225
11.614 kPa	10	0.1
23.838 kPa	10	0.225

4.5.4.3 Activation of PAA surface

As PAA surfaces are inert for cell spreading, the gel surface needed to be activated and covalently bound to FN. For this purpose, Sulfo-SANPAH solution was used in a final concentration of 12.5 µg/ml. After application of the Sulfo-SANPAH on the gels, surfaces were exposed to a strong UV light source at a distance of 8 cm (Hanau Quarzlampe Typ 5261 Fluotest UV 210 W) for 5 min. After brief washing in dd H_2O, slides were inverted on a 50 µl drop of FN (1mg/ml) and incubated at 4 °C for 6 h.

4.5.4.4 Traction force microscopy

Cells were seeded O/N to a confluence of less than 50% in normal growth medium on FN coated PAA gels that were glued onto a microscopic dish (20 mm bottom hole). Prior to imaging, growth medium was exchanged to 750 µl imaging medium. Image acquisition occurred using a Leica SP8 confocal laser scanning microscope (Leica Microsystems) equipped with a 63x glycerol objective (HC PL APO, NA=1.3) at 37°C. All images were recorded with a resolution of 2048x2048 pixels, 12 bit and 60 nm pixel size. FAs were imaged using an excitation wavelength of 514 nm with a scan rate of 100 Hz, fluorescent beads with 633 nm excitation wavelength and 50 Hz. Next, cells were lysed by the application of 1-2 ml cell lysis buffer into the microscopic dish. Post-lysis images of PAA gels were acquired with identical settings as before at the same z-position as the pre-lysis images.

Cell lysis buffer

NaCl	150 mM
Tris-HCL	50 mM
SDS	1 %
Triton-X 100	1 %

4.5.4.5 Image analysis of TFM data

Data analysis was performed by Benedikt Sabass at Princeton University using previously published, custom written analysis software[201,25].

4.5.5 Time-correlated single photon counting - fluorescence lifetime microscopy

Time-correlated single photo counting - fluorescence lifetime microscopy (TCSPC-FLIM) is a method allowing quantitative evaluation of FRET, as the lifetime of a fluorescent protein (donor) is directly depended on the abundance of other fluorophores (acceptor) in close proximity. In this study, TCSPC-FLIM experiments were executed on a confocal microscope (Leica TCS SP5 X) equipped with a pulsed white light laser (WLL, 80 MHz repetition rate, NKT Photonics), a FLIM X16 TCSPC detector (LaVision Biotech, Germany) and a 63x water objective (HCX PL APO CS, NA=1.2); a bandpass filter 545/30 (AHF Analysentechnik, Germany) was used to block photons emitted by the acceptor fluorophore. Images of 512x512 pixels were acquired with a scanning velocity of 400 Hz and field coverage of 123.02 x 123.02 μm^2. 12.24 ns after excitation pulse were covered with a temporal resolution of 0.08 ns. Emitted photons from the sample were passing an emission filter to arrive at the detector that recorded arrival time and spatial information for each photon. As a result, a 'photon count' histogram is calculated for each pixel, which could be converted into fluorescence lifetime of the sample via a mono-exponential decay fit.

4.5.6 Evaluation of TCSPC-FLIM data

Signals specifically localized in FAs were isolated (Figure 4.5) and further evaluated using a custom-written MATLAB R2013a (Mathworks, USA) software, calculating the FRET efficiency E according to $E = 1 - \frac{\tau_{DA}}{\tau_D}$, where τ_D is the mean donor lifetime and τ_{DA} is the lifetime of the donor in presence of an acceptor fluorophore. The data analysis was performed using a custom-written software (by Carleen Kluger, MPI of Biochemistry) as described in[202].

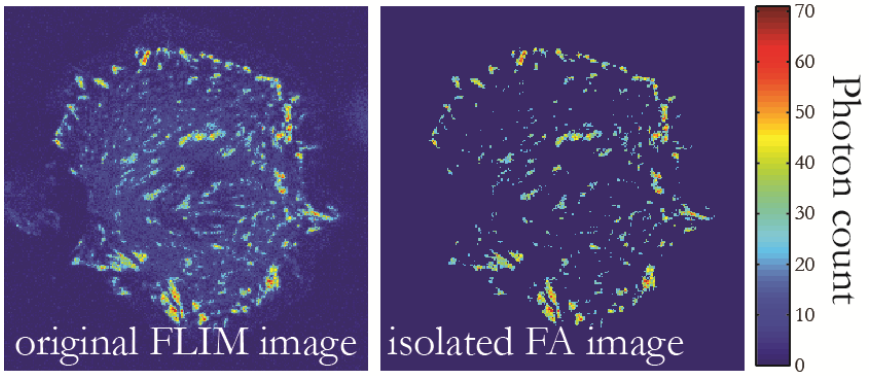

Figure 4.5: Feature extraction from FLIM images. Photon count in cell before and after feature isolation by custom-written MATLAB software. (**A**) original FLIM photon count image (**B**) Photon count in FAs

4.5.7 Evaluation co-localization

To evaluate the colocalization of two proteins, cells were fixed and stained with two spectrally distinguishable dyes as described above (Chapter 4.3.3); next, images of both proteins were acquired by using a confocal microscope (4.5.1) and exported for data analysis in a LIF format. Intensity line plots were defined for at least 25 FAs per condition in ImageJ and further evaluated in MATLAB. By applying a Gaussian fit to one channel, a local maximum was identified and averaged intensity values in the local maximum ±2 pixels in all channels were measured.

4.5.8 Evaluation cell and FA size

In order to acquire data on cell size, polarization and FA size, cells were seeded on FN-coated glass coverslips or substrate dishes (Matrigen Life Technologies) for the indicated times, fixed and stained (Chapter 4.3.3). For cell size, shape and orientation analysis, an Otsu threshold was applied to the phalloidin images, binarized into cellular shape masks and evaluated for the criteria of interest. Subsequently, FAs were analyzed according to their quantity per cell, size, eccentricity and orientation relative to the cells major principal axis using a custom-written program (by Dr. Christoph Klingner, MPI of Biochemistry) as described in[154].

4.5.9 Ratiometric FRET

TCSPC-FLIM offers many advantages for the analysis of FRET data but also holds limitations. A relatively high laser power and subsequent bleaching as well as the lack of spatial-temporal resolution are two obvious draw backs of this particular technique. Therefore, the data obtained with TSCSP-FLIM were confirmed by a ratiometric FRET approach. Images were recorded using the Leica SP8 confocal microscope (Leica Microsystems) at 37 °C. Data were exported and analyzed using a custom-written software (Christoph Klingner, MPI of Biochemistry) as described in [154]. In brief, the FA signal was isolated (Chapter 4.5.8) to exclude cytoplasmic background by a multi-Otsu thresholding algorithm. The resulting FA masks were applied to both images (donor and acceptor) to calculate a mean FRET efficiency per cell. Convolution of the image (Gaussian structure element; width: 25 and height: 2) and application of a top-hat filtering step (disk SE, radius: 7 pixel) was performed in order to reduce cytosolic background. The FA masks were applied to donor and acceptor channel and FRET signals for individual FAs was achieved by acceptor/donor division.

4.5.10 Statistical analyses

For the statistical analysis of data, several tests were performed. All TCSPC-FLIM data were evaluated by the Kolmogorov-Smirnov test with a default significance level of $\alpha = 0.05$. Data acquired for the morphological analysis of cells were tested by a two sited t-test. Error bars in figures represent the standard error of the mean (s.e.m.), if not indicated otherwise. To confirm the normal distribution of data, the Lilliefors test was performed. The following nomenclature was used in all figures: ***: $p<0.001$; **: $p<0.01$; *: $p<0.05$; not significant (n.s.): $p > 0.05$. Boxplots were generated using the MATLAB function boxplot() or the boxplot function in the OriginPro 9.1.0 software (OriginLab Corporation), indicating the median as well as 25th and 75th percentiles; whiskers reach out to 2.7 standard deviations (σ).

References

1 Ingber, D. E. Mechanobiology and diseases of mechanotransduction. *Annals of medicine* 35, 564-577 (2003).

2 Sachs, F. Stretch-Activated Ion Channels: What Are They? *Physiology* 25, 50-56, doi:10.1152/physiol.00042.2009 (2010).

3 Lumpkin, E. A. & Caterina, M. J. Mechanisms of sensory transduction in the skin. *Nature* 445, 858-865, doi:10.1038/nature05662 (2007).

4 Christensen, A. P. & Corey, D. P. TRP channels in mechanosensation: direct or indirect activation? *Nature reviews. Neuroscience* 8, 510-521, doi:10.1038/nrn2149 (2007).

5 Jaalouk, D. E. & Lammerding, J. Mechanotransduction gone awry. *Nature reviews. Molecular cell biology* 10, 63-73, doi:10.1038/nrm2597 (2009).

6 Harris, A. K., Wild, P. & Stopak, D. Silicone rubber substrata: a new wrinkle in the study of cell locomotion. *Science* 208, 177-179 (1980).

7 Szafranski, J. D. *et al.* Chondrocyte mechanotransduction: effects of compression on deformation of intracellular organelles and relevance to cellular biosynthesis. *Osteoarthritis and cartilage / OARS, Osteoarthritis Research Society* 12, 937-946, doi:10.1016/j.joca.2004.08.004 (2004).

8 Holle, A. W. & Engler, A. J. More than a feeling: discovering, understanding, and influencing mechanosensing pathways. *Current opinion in biotechnology* 22, 648-654, doi:10.1016/j.copbio.2011.04.007 (2011).

9 Polacheck, W. J., German, A. E., Mammoto, A., Ingber, D. E. & Kamm, R. D. Mechanotransduction of fluid stresses governs 3D cell migration. *Proceedings of the National Academy of Sciences of the United States of America* 111, 2447-2452, doi:10.1073/pnas.1316848111 (2014).

10 Halder, G., Dupont, S. & Piccolo, S. Transduction of mechanical and cytoskeletal cues by YAP and TAZ. *Nature reviews. Molecular cell biology* 13, 591-600, doi:10.1038/nrm3416 (2012).

11 Schoen, I., Pruitt, B. L. & Vogel, V. The Yin-Yang of Rigidity Sensing: How Forces and Mechanical Properties Regulate the Cellular Response to Materials. *Annu Rev Mater Res* 43, 589-618, doi:10.1146/annurev-matsci-062910-100407 (2013).

12 Grashoff, C. *et al.* Measuring mechanical tension across vinculin reveals regulation of focal adhesion dynamics. *Nature* 466, 263-266, doi:10.1038/nature09198 (2010).

13 Hytonen, V. P. & Vogel, V. How force might activate talin's vinculin binding sites: SMD reveals a structural mechanism. *PLoS computational biology* 4, e24, doi:10.1371/journal.pcbi.0040024 (2008).

14 Sawada, Y. *et al.* Force sensing by mechanical extension of the Src family kinase substrate p130Cas. *Cell* 127, 1015-1026, doi:10.1016/j.cell.2006.09.044 (2006).

15 Baneyx, G., Baugh, L. & Vogel, V. Fibronectin extension and unfolding within cell matrix fibrils controlled by cytoskeletal tension. *Proceedings of the National Academy of Sciences of the United States of America* 99, 5139-5143, doi:10.1073/pnas.072650799 (2002).

16 Zamir, E. & Geiger, B. Molecular complexity and dynamics of cell-matrix adhesions. *Journal of cell science* 114, 3583-3590 (2001).

17 Iwamoto, D. V. & Calderwood, D. A. Regulation of integrin-mediated adhesions. *Current opinion in cell biology* 36, 41-47, doi:10.1016/j.ceb.2015.06.009 (2015).

18 Campbell, I. D. & Humphries, M. J. Integrin structure, activation, and interactions. *Cold Spring Harbor perspectives in biology* 3, doi:10.1101/cshperspect.a004994 (2011).

19 Calderwood, D. A. *et al.* Integrin beta cytoplasmic domain interactions with phosphotyrosine-binding domains: a structural prototype for diversity in integrin signaling. *Proceedings of the National Academy of Sciences of the United States of America* 100, 2272-2277, doi:10.1073/pnas.262791999 (2003).

20 Legate, K. R. & Fassler, R. Mechanisms that regulate adaptor binding to beta-integrin cytoplasmic tails. *Journal of cell science* 122, 187-198, doi:10.1242/jcs.041624 (2009).

21 Kim, C., Ye, F., Hu, X. & Ginsberg, M. H. Talin activates integrins by altering the topology of the beta transmembrane domain. *The Journal of cell biology* 197, 605-611, doi:10.1083/jcb.201112141 (2012).

22 R&D Systems, I. (ed Integrin subunit interactions) (R&D Systems, Inc., https://www.rndsystems.com/resources/posters/integrin-subunit-interactions, 2015).

23 Hynes, R. O. Integrins: bidirectional, allosteric signaling machines. *Cell* 110, 673-687 (2002).

24 Lee, J. O., Rieu, P., Arnaout, M. A. & Liddington, R. Crystal structure of the A domain from the alpha subunit of integrin CR3 (CD11b/CD18). *Cell* 80, 631-638 (1995).

25 Plotnikov, S. V., Sabass, B., Schwarz, U. S. & Waterman, C. M. High-resolution traction force microscopy. *Methods in cell biology* 123, 367-394, doi:10.1016/B978-0-12-420138-5.00020-3 (2014).

26 Critchley, D. R. Biochemical and structural properties of the integrin-associated cytoskeletal protein talin. *Annual review of biophysics* 38, 235-254, doi:10.1146/annurev.biophys.050708.133744 (2009).

27 Theodosiou, M. *et al.* Kindlin-2 cooperates with talin to activate integrins and induces cell spreading by directly binding paxillin. *eLife* 5, doi:10.7554/eLife.10130 (2016).

28 Montanez, E. *et al.* Kindlin-2 controls bidirectional signaling of integrins. *Genes & development* 22, 1325-1330, doi:10.1101/gad.469408 (2008).

29 Moser, M., Nieswandt, B., Ussar, S., Pozgajova, M. & Fassler, R. Kindlin-3 is essential for integrin activation and platelet aggregation. *Nature medicine* 14, 325-330, doi:10.1038/nm1722 (2008).

30 Takagi, J., Petre, B. M., Walz, T. & Springer, T. A. Global conformational rearrangements in integrin extracellular domains in outside-in and inside-out signaling. *Cell* 110, 599-511 (2002).

31 Luo, B. H., Carman, C. V. & Springer, T. A. Structural basis of integrin regulation and signaling. *Annual review of immunology* 25, 619-647, doi:10.1146/annurev.immunol.25.022106.141618 (2007).

32 Kong, F., Garcia, A. J., Mould, A. P., Humphries, M. J. & Zhu, C. Demonstration of catch bonds between an integrin and its ligand. *Journal of Cell Biology* 185, 1275-1284, doi:10.1083/jcb.200810002 (2009).

33 Wehrle-Haller, B. & Imhof, B. A. Integrin-dependent pathologies. *J Pathol* 200, 481-487, doi:10.1002/path.1399 (2003).

34 Shattil, S. J. & Newman, P. J. Integrins: dynamic scaffolds for adhesion and signaling in platelets. *Blood* 104, 1606-1615, doi:10.1182/blood-2004-04-1257 (2004).

35 Oppenheimermarks, N., Davis, L. S., Bogue, D. T., Ramberg, J. & Lipsky, P. E. Differential Utilization of Icam-1 and Vcam-1 during the Adhesion and Transendothelial Migration of Human Lymphocytes-T. *Journal of immunology* 147, 2913-2921 (1991).

36 Geiger, B., Spatz, J. P. & Bershadsky, A. D. Environmental sensing through focal adhesions. *Nat Rev Mol Cell Bio* 10, 21-33, doi:10.1038/nrm2593 (2009).

37 Geiger, T. & Zaidel-Bar, R. Opening the floodgates: proteomics and the integrin adhesome. *Current opinion in cell biology* 24, 562-568, doi:10.1016/j.ceb.2012.05.004 (2012).

38 Berginski, M. E., Vitriol, E. A., Hahn, K. M. & Gomez, S. M. High-resolution quantification of focal adhesion spatiotemporal dynamics in living cells. *PloS one* 6, e22025, doi:10.1371/journal.pone.0022025 (2011).

39 Giannone, G. Super-resolution links vinculin localization to function in focal adhesions. *Nature cell biology* 17, 845-847, doi:10.1038/ncb3196 (2015).

40 Kratimenos, P. *et al.* Multi-targeted molecular therapeutic approach in aggressive neuroblastoma: the effect of Focal Adhesion Kinase-Src-Paxillin system. *Expert opinion on therapeutic targets* 18, 1395-1406, doi:10.1517/14728222.2014.952280 (2014).

41 Kanchanawong, P. *et al.* Nanoscale architecture of integrin-based cell adhesions. *Nature* 468, 580-584, doi:10.1038/nature09621 (2010).

42 Egelman, E. H., Francis, N. & DeRosier, D. J. F-actin is a helix with a random variable twist. *Nature* 298, 131-135 (1982).

43 Moore, P. B., Huxley, H. E. & DeRosier, D. J. Three-dimensional reconstruction of F-actin, thin filaments and decorated thin filaments. *Journal of molecular biology* 50, 279-295 (1970).

44 Dominguez, R. Actin filament nucleation and elongation factors--structure-function relationships. *Critical reviews in biochemistry and molecular biology* 44, 351-366, doi:10.3109/10409230903277340 (2009).

45 Carlier, M. F. & Pantaloni, D. Control of actin dynamics in cell motility. *Journal of molecular biology* 269, 459-467, doi:10.1006/jmbi.1997.1062 (1997).

46 Wallar, B. J. & Alberts, A. S. The formins: active scaffolds that remodel the cytoskeleton. *Trends in cell biology* 13, 435-446 (2003).

47 Naruse, K., Yamada, T. & Sokabe, M. Involvement of SA channels in orienting response of cultured endothelial cells to cyclic stretch. *The American journal of physiology* 274, H1532-1538 (1998).

48 Shirinsky, V. P. *et al.* Mechano-chemical control of human endothelium orientation and size. *The Journal of cell biology* 109, 331-339 (1989).

49 Pollard, T. D. & Borisy, G. G. Cellular motility driven by assembly and disassembly of actin filaments. *Cell* 112, 453-465 (2003).

50 Giannone, G. *et al.* Periodic lamellipodial contractions correlate with rearward actin waves. *Cell* 116, 431-443 (2004).

51 Ponti, A., Machacek, M., Gupton, S. L., Waterman-Storer, C. M. & Danuser, G. Two distinct actin networks drive the protrusion of migrating cells. *Science* 305, 1782-1786, doi:10.1126/science.1100533 (2004).

52 Case, L. B. & Waterman, C. M. Integration of actin dynamics and cell adhesion by a three-dimensional, mechanosensitive molecular clutch. *Nature cell biology* 17, 955-963, doi:10.1038/ncb3191 (2015).

53 Wu, Y. I. *et al.* A genetically encoded photoactivatable Rac controls the motility of living cells. *Nature* 461, 104-108, doi:10.1038/nature08241 (2009).

54 Howard, J. *Mechanics of motor proteins and the cytoskeleton*. (Sinauer Associates, Publishers, 2001).

55 Kneussel, M. & Wagner, W. Myosin motors at neuronal synapses: drivers of membrane transport and actin dynamics. *Nature reviews. Neuroscience* 14, 233-247, doi:10.1038/nrn3445 (2013).

56 Totsukawa, G. *et al.* Distinct roles of MLCK and ROCK in the regulation of membrane protrusions and focal adhesion dynamics during cell migration of fibroblasts. *The Journal of cell biology* 164, 427-439, doi:10.1083/jcb.200306172 (2004).

57 Salhia, B. *et al.* Role of myosin II activity and the regulation of myosin light chain phosphorylation in astrocytomas. *Cell motility and the cytoskeleton* 65, 12-24, doi:10.1002/cm.20240 (2008).

58 Riento, K. & Ridley, A. J. Rocks: multifunctional kinases in cell behaviour. *Nature reviews. Molecular cell biology* 4, 446-456, doi:10.1038/nrm1128 (2003).

59 Wechezak, A. R., Viggers, R. F. & Sauvage, L. R. Fibronectin and F-actin redistribution in cultured endothelial cells exposed to shear stress. *Laboratory investigation; a journal of technical methods and pathology* 53, 639-647 (1985).

60 Hirata, H., Tatsumi, H. & Sokabe, M. Dynamics of actin filaments during tension-dependent formation of actin bundles. *Biochimica et biophysica acta* 1770, 1115-1127, doi:10.1016/j.bbagen.2007.03.010 (2007).

61 Janmey, P. A. The cytoskeleton and cell signaling: component localization and mechanical coupling. *Physiological reviews* 78, 763-781 (1998).

62 Pavalko, F. M. *et al.* Fluid shear-induced mechanical signaling in MC3T3-E1 osteoblasts requires cytoskeleton-integrin interactions. *The American journal of physiology* 275, C1591-1601 (1998).

63 Toma, C. D., Ashkar, S., Gray, M. L., Schaffer, J. L. & Gerstenfeld, L. C. Signal transduction of mechanical stimuli is dependent on microfilament integrity: identification of osteopontin as a mechanically induced gene in osteoblasts. *Journal of bone and mineral research : the official journal of the American Society for Bone and Mineral Research* 12, 1626-1636, doi:10.1359/jbmr.1997.12.10.1626 (1997).

64 Gupta, M. *et al.* Adaptive rheology and ordering of cell cytoskeleton govern matrix rigidity sensing. *Nature communications* 6, 7525, doi:10.1038/ncomms8525 (2015).

65 Shafrir, Y. & Forgacs, G. Mechanotransduction through the cytoskeleton. *Am J Physiol-Cell Ph* 282, C479-C486 (2002).

66 Letort, G. *et al.* Geometrical and mechanical properties control actin filament organization. *PLoS computational biology* 11, e1004245, doi:10.1371/journal.pcbi.1004245 (2015).

67 Wozniak, M. A., Modzelewska, K., Kwong, L. & Keely, P. J. Focal adhesion regulation of cell behavior. *Bba-Mol Cell Res* 1692, 103-119, doi:10.1016/j.bbamcr.2004.04.007 (2004).

68 Maheshwari, G., Brown, G., Lauffenburger, D. A., Wells, A. & Griffith, L. G. Cell adhesion and motility depend on nanoscale RGD clustering. *Journal of cell science* 113, 1677-1686 (2000).

69 Coussen, F., Choquet, D., Sheetz, M. P. & Erickson, H. P. Trimers of the fibronectin cell adhesion domain localize to actin filament bundles and undergo rearward translocation. *Journal of cell science* 115, 2581-2590 (2002).

70 Cavalcanti-Adam, E. A. *et al.* Cell spreading and focal adhesion dynamics are regulated by spacing of integrin ligands. *Biophysical journal* 92, 2964-2974, doi:10.1529/biophysj.106.089730 (2007).

71 Han, S. J., Oak, Y., Groisman, A. & Danuser, G. Traction microscopy to identify force modulation in subresolution adhesions. *Nature methods* 12, 653-656, doi:10.1038/nmeth.3430 (2015).

72 Rossier, O. *et al.* Integrins beta1 and beta3 exhibit distinct dynamic nanoscale organizations inside focal adhesions. *Nature cell biology* 14, 1057-1067, doi:10.1038/ncb2588 (2012).

73 Wang, X. & Ha, T. Defining single molecular forces required to activate integrin and notch signaling. *Science* 340, 991-994, doi:10.1126/science.1231041 (2013).

74 Finer, J. T., Simmons, R. M. & Spudich, J. A. Single myosin molecule mechanics: piconewton forces and nanometre steps. *Nature* 368, 113-119, doi:10.1038/368113a0 (1994).

75 Yu, C. H., Law, J. B. K., Suryana, M., Low, H. Y. & Sheetz, M. P. Early integrin binding to Arg-Gly-Asp peptide activates actin polymerization and contractile movement that stimulates outward translocation. *Proceedings of the National Academy of Sciences of the United States of America* 108, 20585-20590, doi:10.1073/pnas.1109485108 (2011).

76 Amano, M. *et al.* Phosphorylation and activation of myosin by Rho-associated kinase (Rho-kinase). *The Journal of biological chemistry* 271, 20246-20249 (1996).

77 Kimura, K. *et al.* Regulation of myosin phosphatase by Rho and Rho-associated kinase (Rho-kinase). *Science* 273, 245-248 (1996).

78 Hirata, H., Tatsumi, H. & Sokabe, M. Mechanical forces facilitate actin polymerization at focal adhesions in a zyxin-dependent manner. *Journal of cell science* 121, 2795-2804, doi:10.1242/jcs.030320 (2008).

79 Gupton, S. L., Eisenmann, K., Alberts, A. S. & Waterman-Storer, C. M. mDia2 regulates actin and focal adhesion dynamics and organization in the lamella for efficient epithelial cell migration. *Journal of cell science* 120, 3475-3487, doi:10.1242/jcs.006049 (2007).

80 Riveline, D. *et al.* Focal contacts as mechanosensors: externally applied local mechanical force induces growth of focal contacts by an mDia1-dependent and ROCK-independent mechanism. *The Journal of cell biology* 153, 1175-1186 (2001).

81 Colombelli, J. *et al.* Mechanosensing in actin stress fibers revealed by a close correlation between force and protein localization. *Journal of cell science* 122, 1665-1679, doi:10.1242/jcs.042986 (2009).

82 Drees, B. *et al.* Characterization of the interaction between zyxin and members of the Ena/vasodilator-stimulated phosphoprotein family of proteins. *The Journal of biological chemistry* 275, 22503-22511, doi:10.1074/jbc.M001698200 (2000).

83 Drees, B. E., Andrews, K. M. & Beckerle, M. C. Molecular dissection of zyxin function reveals its involvement in cell motility. *The Journal of cell biology* 147, 1549-1560 (1999).

84 Chrzanowska-Wodnicka, M. & Burridge, K. Rho-stimulated contractility drives the formation of stress fibers and focal adhesions. *The Journal of cell biology* 133, 1403-1415 (1996).

85 Gingras, A. R. *et al.* The structure of the C-terminal actin-binding domain of talin. *The EMBO journal* 27, 458-469, doi:10.1038/sj.emboj.7601965 (2008).

86 Vogel, V. & Sheetz, M. Local force and geometry sensing regulate cell functions. *Nature reviews. Molecular cell biology* 7, 265-275, doi:10.1038/nrm1890 (2006).

87 Blakely, B. L. *et al.* A DNA-based molecular probe for optically reporting cellular traction forces. *Nature methods* 11, 1229-1232, doi:10.1038/nmeth.3145 (2014).

88 Monkley, S. J. *et al.* Disruption of the talin gene arrests mouse development at the gastrulation stage. *Developmental dynamics : an official publication of the American Association of Anatomists* 219, 560-574, doi:10.1002/1097-0177(2000)9999:9999<::AID-DVDY1079>3.0.CO;2-Y (2000).

89 Monkley, S. J. *et al.* Endothelial cell talin1 is essential for embryonic angiogenesis. *Developmental biology* 349, 494-502, doi:10.1016/j.ydbio.2010.11.010 (2011).

90 Zou, W. *et al.* Talin1 and Rap1 are critical for osteoclast function. *Molecular and cellular biology* 33, 830-844, doi:10.1128/MCB.00790-12 (2013).

91 Conti, F. J. *et al.* Progressive myopathy and defects in the maintenance of myotendinous junctions in mice that lack talin 1 in skeletal muscle. *Development* 135, 2043-2053, doi:10.1242/dev.015818 (2008).

92 Zhang, X. *et al.* Talin depletion reveals independence of initial cell spreading from integrin activation and traction. *Nature cell biology* 10, 1062-1068, doi:10.1038/ncb1765 (2008).

93 Kopp, P. M. *et al.* Studies on the morphology and spreading of human endothelial cells define key inter- and intramolecular interactions for talin1. *European journal of cell biology* 89, 661-673, doi:10.1016/j.ejcb.2010.05.003 (2010).

94 Calderwood, D. A., Campbell, I. D. & Critchley, D. R. Talins and kindlins: partners in integrin-mediated adhesion. *Nature reviews. Molecular cell biology* 14, 503-517, doi:10.1038/nrm3624 (2013).

95 Ratnikov, B. *et al.* Talin phosphorylation sites mapped by mass spectrometry. *Journal of cell science* 118, 4921-4923, doi:10.1242/jcs.02682 (2005).

96 Rees, D. J., Ades, S. E., Singer, S. J. & Hynes, R. O. Sequence and domain structure of talin. *Nature* 347, 685-689, doi:10.1038/347685a0 (1990).

97 Goult, B. T. *et al.* Structure of a double ubiquitin-like domain in the talin head: a role in integrin activation. *The EMBO journal* 29, 1069-1080, doi:10.1038/emboj.2010.4 (2010).

98 Tadokoro, S. *et al.* Talin binding to integrin beta tails: a final common step in integrin activation. *Science* 302, 103-106, doi:10.1126/science.1086652 (2003).

99 Lee, H. S. *et al.* Characterization of an actin-binding site within the talin FERM domain. *Journal of molecular biology* 343, 771-784, doi:10.1016/j.jmb.2004.08.069 (2004).

100 de Pereda, J. M. *et al.* Structural basis for phosphatidylinositol phosphate kinase type Igamma binding to talin at focal adhesions. *The Journal of biological chemistry* 280, 8381-8386, doi:10.1074/jbc.M413180200 (2005).

101 Wegener, K. L. *et al.* Structural basis for the interaction between the cytoplasmic domain of the hyaluronate receptor layilin and the talin F3 subdomain. *Journal of molecular biology* 382, 112-126, doi:10.1016/j.jmb.2008.06.087 (2008).

102 Frame, M. C., Patel, H., Serrels, B., Lietha, D. & Eck, M. J. The FERM domain: organizing the structure and function of FAK. *Nature reviews. Molecular cell biology* 11, 802-814, doi:10.1038/nrm2996 (2010).

103 Debrand, E. *et al.* Talin 2 is a large and complex gene encoding multiple transcripts and protein isoforms. *The FEBS journal* 276, 1610-1628, doi:10.1111/j.1742-4658.2009.06893.x (2009).

104 Manso, A. M. *et al.* Talin1 has unique expression versus talin 2 in the heart and modifies the hypertrophic response to pressure overload. *The Journal of biological chemistry* 288, 4252-4264, doi:10.1074/jbc.M112.427484 (2013).

105 Debrand, E. *et al.* Mice carrying a complete deletion of the talin2 coding sequence are viable and fertile. *Biochemical and biophysical research communications* 426, 190-195, doi:10.1016/j.bbrc.2012.08.061 (2012).

106 Molony, L., McCaslin, D., Abernethy, J., Paschal, B. & Burridge, K. Properties of talin from chicken gizzard smooth muscle. *The Journal of biological chemistry* 262, 7790-7795 (1987).

107 Calderwood, D. A. *et al.* The phosphotyrosine binding-like domain of talin activates integrins. *The Journal of biological chemistry* 277, 21749-21758, doi:10.1074/jbc.M111996200 (2002).

108 Goksoy, E. *et al.* Structural basis for the autoinhibition of talin in regulating integrin activation. *Molecular cell* 31, 124-133, doi:10.1016/j.molcel.2008.06.011 (2008).

109 Goult, B. T. *et al.* Structural studies on full-length talin1 reveal a compact auto-inhibited dimer: implications for talin activation. *Journal of structural biology* 184, 21-32, doi:10.1016/j.jsb.2013.05.014 (2013).

110 Legate, K. R. *et al.* Integrin adhesion and force coupling are independently regulated by localized PtdIns(4,5)2 synthesis. *The EMBO journal* 30, 4539-4553, doi:10.1038/emboj.2011.332 (2011).

111 Lee, H. S., Lim, C. J., Puzon-McLaughlin, W., Shattil, S. J. & Ginsberg, M. H. RIAM activates integrins by linking talin to ras GTPase membrane-targeting sequences. *The Journal of biological chemistry* 284, 5119-5127, doi:10.1074/jbc.M807117200 (2009).

112 Golji, J. & Mofrad, M. R. The talin dimer structure orientation is mechanically regulated. *Biophysical journal* 107, 1802-1809, doi:10.1016/j.bpj.2014.08.038 (2014).

113 Srivastava, J. *et al.* Structural model and functional significance of pH-dependent talin-actin binding for focal adhesion remodeling. *Proceedings of the National Academy of Sciences of the United States of America* 105, 14436-14441, doi:10.1073/pnas.0805163105 (2008).

114 Muguruma, M., Matsumura, S. & Fukazawa, T. Direct interactions between talin and actin. *Biochemical and biophysical research communications* 171, 1217-1223 (1990).

115 Muguruma, M., Nishimuta, S., Tomisaka, Y., Ito, T. & Matsumura, S. Organization of the functional domains in membrane cytoskeletal protein talin. *Journal of biochemistry* 117, 1036-1042 (1995).

116 Hemmings, L. *et al.* Talin contains three actin-binding sites each of which is adjacent to a vinculin-binding site. *Journal of cell science* 109 (Pt 11), 2715-2726 (1996).

117 Peng, X., Nelson, E. S., Maiers, J. L. & DeMali, K. A. New insights into vinculin function and regulation. *International review of cell and molecular biology* 287, 191-231, doi:10.1016/B978-0-12-386043-9.00005-0 (2011).

118 Winkler, J., Lunsdorf, H. & Jockusch, B. M. The ultrastructure of chicken gizzard vinculin as visualized by high-resolution electron microscopy. *Journal of structural biology* 116, 270-277, doi:10.1006/jsbi.1996.0042 (1996).

119 Bakolitsa, C. *et al.* Structural basis for vinculin activation at sites of cell adhesion. *Nature* 430, 583-586, doi:10.1038/nature02610 (2004).

120 Volberg, T. *et al.* Focal adhesion formation by F9 embryonal carcinoma cells after vinculin gene disruption. *Journal of cell science* 108 (Pt 6), 2253-2260 (1995).

121 Rodriguez Fernandez, J. L. *et al.* Suppression of tumorigenicity in transformed cells after transfection with vinculin cDNA. *The Journal of cell biology* 119, 427-438 (1992).

122 Izard, T. & Vonrhein, C. Structural basis for amplifying vinculin activation by talin. *The Journal of biological chemistry* 279, 27667-27678, doi:10.1074/jbc.M403076200 (2004).

123 Bois, P. R., O'Hara, B. P., Nietlispach, D., Kirkpatrick, J. & Izard, T. The vinculin binding sites of talin and alpha-actinin are sufficient to activate vinculin. *The Journal of biological chemistry* 281, 7228-7236, doi:10.1074/jbc.M510397200 (2006).

124 Golji, J., Wendorff, T. & Mofrad, M. R. Phosphorylation primes vinculin for activation. *Biophysical journal* 102, 2022-2030, doi:10.1016/j.bpj.2012.01.062 (2012).

125 Bass, M. D. *et al.* Further characterization of the interaction between the cytoskeletal proteins talin and vinculin. *The Biochemical journal* 362, 761-768 (2002).

126 Bass, M. D., Smith, B. J., Prigent, S. A. & Critchley, D. R. Talin contains three similar vinculin-binding sites predicted to form an amphipathic helix. *The Biochemical journal* 341 (Pt 2), 257-263 (1999).

127 Gingras, A. R. *et al.* Mapping and consensus sequence identification for multiple vinculin binding sites within the talin rod. *The Journal of biological chemistry* 280, 37217-37224, doi:10.1074/jbc.M508060200 (2005).

128 Humphries, J. D. *et al.* Vinculin controls focal adhesion formation by direct interactions with talin and actin. *The Journal of cell biology* 179, 1043-1057, doi:10.1083/jcb.200703036 (2007).

129 Yan, J., Yao, M., Goult, B. T. & Sheetz, M. P. Talin Dependent Mechanosensitivity of Cell Focal Adhesions. *Cell Mol Bioeng* 8, 151-159, doi:10.1007/s12195-014-0364-5 (2015).

130 Yao, M. *et al.* Mechanical activation of vinculin binding to talin locks talin in an unfolded conformation. *Scientific reports* 4, 4610, doi:10.1038/srep04610 (2014).

131 Gingras, A. R. *et al.* The structure of the C-terminal actin-binding domain of talin. *Embo Journal* 27, 458-469, doi:10.1038/sj.emboj.7601965 (2008).

132 del Rio, A. *et al.* Stretching single talin rod molecules activates vinculin binding. *Science* 323, 638-641, doi:10.1126/science.1162912 (2009).

133 Pasapera, A. M., Schneider, I. C., Rericha, E., Schlaepfer, D. D. & Waterman, C. M. Myosin II activity regulates vinculin recruitment to focal adhesions through FAK-mediated paxillin phosphorylation. *The Journal of cell biology* 188, 877-890, doi:10.1083/jcb.200906012 (2010).

134 Margadant, F. *et al.* Mechanotransduction in vivo by repeated talin stretch-relaxation events depends upon vinculin. *PLoS biology* 9, e1001223, doi:10.1371/journal.pbio.1001223 (2011).

135 Lee, S. E., Kamm, R. D. & Mofrad, M. R. Force-induced activation of talin and its possible role in focal adhesion mechanotransduction. *Journal of biomechanics* 40, 2096-2106, doi:10.1016/j.jbiomech.2007.04.006 (2007).

136 Goult, B. T. *et al.* RIAM and vinculin binding to talin are mutually exclusive and regulate adhesion assembly and turnover. *The Journal of biological chemistry* 288, 8238-8249, doi:10.1074/jbc.M112.438119 (2013).

137 Lee, H. S., Anekal, P., Lim, C. J., Liu, C. C. & Ginsberg, M. H. Two modes of integrin activation form a binary molecular switch in adhesion maturation. *Molecular biology of the cell* 24, 1354-1362, doi:10.1091/mbc.E12-09-0695 (2013).

138 Lagarrigue, F. *et al.* A RIAM/lamellipodin-talin-integrin complex forms the tip of sticky fingers that guide cell migration. *Nature communications* 6, 8492, doi:10.1038/ncomms9492 (2015).

139 Carisey, A. *et al.* Vinculin regulates the recruitment and release of core focal adhesion proteins in a force-dependent manner. *Current biology : CB* 23, 271-281, doi:10.1016/j.cub.2013.01.009 (2013).

140 Gosse, C. & Croquette, V. Magnetic tweezers: micromanipulation and force measurement at the molecular level. *Biophysical journal* 82, 3314-3329, doi:10.1016/S0006-3495(02)75672-5 (2002).

141 Tan, J. L. *et al.* Cells lying on a bed of microneedles: an approach to isolate mechanical force. *Proceedings of the National Academy of Sciences of the United States of America* 100, 1484-1489, doi:10.1073/pnas.0235407100 (2003).

142 Balaban, N. Q. *et al.* Force and focal adhesion assembly: a close relationship studied using elastic micropatterned substrates. *Nature cell biology* 3, 466-472, doi:10.1038/35074532 (2001).

143 Cost, A. L., Ringer, P., Chrostek-Grashoff, A. & Grashoff, C. How to Measure Molecular Forces in Cells: A Guide to Evaluating Genetically-Encoded FRET-Based Tension Sensors. *Cell Mol Bioeng* 8, 96-105, doi:10.1007/s12195-014-0368-1 (2015).

144 Baneyx, G., Baugh, L. & Vogel, V. Coexisting conformations of fibronectin in cell culture imaged using fluorescence resonance energy transfer. *Proceedings of the National Academy of Sciences of the United States of America* 98, 14464-14468, doi:10.1073/pnas.251422998 (2001).

145 Meng, F., Suchyna, T. M. & Sachs, F. A fluorescence energy transfer-based mechanical stress sensor for specific proteins in situ. *The FEBS journal* 275, 3072-3087, doi:10.1111/j.1742-4658.2008.06461.x (2008).

146 Iwai, S. & Uyeda, T. Q. Visualizing myosin-actin interaction with a genetically-encoded fluorescent strain sensor. *Proceedings of the National Academy of Sciences of the United States of America* 105, 16882-16887, doi:10.1073/pnas.0805513105 (2008).

147 Borghi, N. *et al.* E-cadherin is under constitutive actomyosin-generated tension that is increased at cell-cell contacts upon externally applied stretch. *Proceedings of the National Academy of Sciences of the United States of America* 109, 12568-12573, doi:10.1073/pnas.1204390109 (2012).

148 Morimatsu, M., Mekhdjian, A. H., Adhikari, A. S. & Dunn, A. R. Molecular tension sensors report forces generated by single integrin molecules in living cells. *Nano letters* 13, 3985-3989, doi:10.1021/nl4005145 (2013).

149 Kotecki, M., Zeiger, A. S., Van Vliet, K. J. & Herman, I. M. Calpain- and talin-dependent control of microvascular pericyte contractility and cellular stiffness. *Microvascular research* 80, 339-348, doi:10.1016/j.mvr.2010.07.012 (2010).

150 Becker, N. *et al.* Molecular nanosprings in spider capture-silk threads. *Nature materials* 2, 278-283, doi:10.1038/nmat858 (2003).

151 Moll, J. R., Ruvinov, S. B., Pastan, I. & Vinson, C. Designed heterodimerizing leucine zippers with a ranger of pIs and stabilities up to 10(-15) M. *Protein science : a publication of the Protein Society* 10, 649-655, doi:10.1110/ps.39401 (2001).

152 Alber, T. Structure of the leucine zipper. *Current opinion in genetics & development* 2, 205-210 (1992).

153 Gebhardt, J. C., Bornschlogl, T. & Rief, M. Full distance-resolved folding energy landscape of one single protein molecule. *Proceedings of the National Academy of Sciences of the United States of America* 107, 2013-2018, doi:10.1073/pnas.0909854107 (2010).

154 Austen, K. *et al.* Extracellular rigidity sensing by talin isoform-specific mechanical linkages. *Nature cell biology*, doi:10.1038/ncb3268 (2015).

155 Pogenberg, V. *et al.* Restricted leucine zipper dimerization and specificity of DNA recognition of the melanocyte master regulator MITF. *Genes & development* 26, 2647-2658, doi:10.1101/gad.198192.112 (2012).

156 Zoldak, G., Stigler, J., Pelz, B., Li, H. & Rief, M. Ultrafast folding kinetics and cooperativity of villin headpiece in single-molecule force spectroscopy. *Proceedings of the National Academy of Sciences of the United States of America* 110, 18156-18161, doi:10.1073/pnas.1311495110 (2013).

157 Freddolino, P. L., Harrison, C. B., Liu, Y. & Schulten, K. Challenges in protein folding simulations: Timescale, representation, and analysis. *Nature physics* 6, 751-758, doi:10.1038/nphys1713 (2010).

158 Schiller, H. B. *et al.* beta1- and alphav-class integrins cooperate to regulate myosin II during rigidity sensing of fibronectin-based microenvironments. *Nature cell biology* 15, 625-636, doi:10.1038/ncb2747 (2013).

159 Goult, B. T. *et al.* The structure of an interdomain complex that regulates talin activity. *The Journal of biological chemistry* 284, 15097-15106, doi:10.1074/jbc.M900078200 (2009).

160 Engler, A. *et al.* Substrate compliance versus ligand density in cell on gel responses. *Biophysical journal* 86, 617-628, doi:10.1016/S0006-3495(04)74140-5 (2004).

161 Elosegui-Artola, A. *et al.* Rigidity sensing and adaptation through regulation of integrin types. *Nature materials* 13, 631-637, doi:10.1038/NMAT3960 (2014).

162 Elosegui-Artola, A. *et al.* Rigidity sensing and adaptation through regulation of integrin populations. *Molecular biology of the cell* 24 (2013).

163 Moes, M. *et al.* The integrin binding site 2 (IBS2) in the talin rod domain is essential for linking integrin beta subunits to the cytoskeleton. *The Journal of biological chemistry* 282, 17280-17288, doi:10.1074/jbc.M611846200 (2007).

164 Ellis, S. J., Pines, M., Fairchild, M. J. & Tanentzapf, G. In vivo functional analysis reveals specific roles for the integrin-binding sites of talin. *Journal of cell science* 124, 1844-1856, doi:10.1242/jcs.083337 (2011).

165 Garcia-Alvarez, B. *et al.* Structural determinants of integrin recognition by talin. *Molecular cell* 11, 49-58 (2003).

166 Wang, P., Ballestrem, C. & Streuli, C. H. The C terminus of talin links integrins to cell cycle progression. *The Journal of cell biology* 195, 499-513, doi:10.1083/jcb.201104128 (2011).

167 Atherton, P. *et al.* Vinculin controls talin engagement with the actomyosin machinery. *Nature communications* 6, 10038, doi:10.1038/ncomms10038 (2015).

168 Calderwood, D. A. *et al.* The talin head domain binds to integrin beta subunit cytoplasmic tails and regulates integrin activation. *Journal of Biological Chemistry* 274, 28071-28074, doi:DOI 10.1074/jbc.274.40.28071 (1999).

169 Heisenberg, C. P. & Bellaiche, Y. Forces in tissue morphogenesis and patterning. *Cell* 153, 948-962, doi:10.1016/j.cell.2013.05.008 (2013).

170 Wozniak, M. A. & Chen, C. S. Mechanotransduction in development: a growing role for contractility. *Nature reviews. Molecular cell biology* 10, 34-43, doi:10.1038/nrm2592 (2009).

171 Lu, P. F., Takai, K., Weaver, V. M. & Werb, Z. Extracellular Matrix Degradation and Remodeling in Development and Disease. *Cold Spring Harbor perspectives in biology* 3, doi:ARTN a00505810.1101/cshperspect.a005058 (2011).

172 Haack, H. & Hynes, R. O. Integrin receptors are required for cell survival and proliferation during development of the peripheral glial lineage. *Developmental biology* 233, 38-55, doi:10.1006/dbio.2001.0213 (2001).

173 Aoudjit, F. & Vuori, K. Integrin signaling in cancer cell survival and chemoresistance. *Chemotherapy research and practice* 2012, 283181, doi:10.1155/2012/283181 (2012).

174 Cukier, R. I. Simulations of Potentials of Mean Force for Separating a Leucine Zipper Dimer and the Basic Region of a Basic Region Leucine Zipper Dimer. *Journal of Physical Chemistry B* 118, 10341-10354, doi:10.1021/jp504723m (2014).

175 Niehorster, T. *et al.* Multi-target spectrally resolved fluorescence lifetime imaging microscopy. *Nature methods*, doi:10.1038/nmeth.3740 (2016).

176 Murakoshi, H., Shibata, A. C. E., Nakahata, Y. & Nabekura, J. A dark green fluorescent protein as an acceptor for measurement of Forster resonance energy transfer. *Scientific reports* 5, doi:Artn 15334

10.1038/Srep15334 (2015).

177 Keppler, A. *et al.* Labeling of fusion proteins of O6-alkylguanine-DNA alkyltransferase with small molecules in vivo and in vitro. *Methods* 32, 437-444, doi:10.1016/j.ymeth.2003.10.007 (2004).

178 Sander, J. D. & Joung, J. K. CRIRISPR-Cas systems for editing, regulating and targeting genomes. *Nature biotechnology* 32, 347-355, doi:10.1038/nbt.2842 (2014).

179 Cho, S. W. *et al.* Analysis of off-target effects of CRISPR/Cas-derived RNA-guided endonucleases and nickases. *Genome research* 24, 132-141, doi:10.1101/gr.162339.113 (2014).

180 Goult, B. T. *et al.* The domain structure of talin: residues 1815-1973 form a five-helix bundle containing a cryptic vinculin-binding site. *FEBS letters* 584, 2237-2241, doi:10.1016/j.febslet.2010.04.028 (2010).

181 Nguyen, A. W. & Daugherty, P. S. Evolutionary optimization of fluorescent proteins for intracellular FRET. *Nature biotechnology* 23, 355-360, doi:10.1038/nbt1066 (2005).

182 Pelham, R. J., Jr. & Wang, Y. Cell locomotion and focal adhesions are regulated by substrate flexibility. *Proceedings of the National Academy of Sciences of the United States of America* 94, 13661-13665 (1997).

183 Discher, D. E., Janmey, P. & Wang, Y. L. Tissue cells feel and respond to the stiffness of their substrate. *Science* 310, 1139-1143, doi:10.1126/science.1116995 (2005).

184 Calderwood, D. A. Integrin activation. *Journal of cell science* 117, 657-666, doi:10.1242/jcs.01014 (2004).

185 Ciobanasu, C., Faivre, B. & Le Clainche, C. Actin dynamics associated with focal adhesions. *International journal of cell biology* 2012, 941292, doi:10.1155/2012/941292 (2012).

186 Engler, A. J., Sen, S., Sweeney, H. L. & Discher, D. E. Matrix elasticity directs stem cell lineage specification. *Cell* 126, 677-689, doi:10.1016/j.cell.2006.06.044 (2006).

187 Engler, A. J., Sweeney, H. L., Discher, D. E. & Schwarzbauer, J. E. Extracellular matrix elasticity directs stem cell differentiation. *Journal of musculoskeletal & neuronal interactions* 7, 335 (2007).

188 Bridgman, P. C., Dave, S., Asnes, C. F., Tullio, A. N. & Adelstein, R. S. Myosin IIB is required for growth cone motility. *The Journal of neuroscience : the official journal of the Society for Neuroscience* 21, 6159-6169 (2001).

189 Flanagan, L. A., Ju, Y. E., Marg, B., Osterfield, M. & Janmey, P. A. Neurite branching on deformable substrates. *Neuroreport* 13, 2411-2415, doi:10.1097/01.wnr.0000048003.96487.97 (2002).

190 Georges, P. C., Miller, W. J., Meaney, D. F., Sawyer, E. S. & Janmey, P. A. Matrices with compliance comparable to that of brain tissue select neuronal over glial growth in mixed cortical cultures. *Biophysical journal* 90, 3012-3018, doi:10.1529/biophysj.105.073114 (2006).

191 Woerly, S., Doan, V. D., Sosa, N., de Vellis, J. & Espinosa-Jeffrey, A. Prevention of gliotic scar formation by NeuroGel allows partial endogenous repair of transected cat spinal cord. *Journal of neuroscience research* 75, 262-272, doi:10.1002/jnr.10774 (2004).

192 Li, B. & Wang, J. H. Fibroblasts and myofibroblasts in wound healing: force generation and measurement. *Journal of tissue viability* 20, 108-120, doi:10.1016/j.jtv.2009.11.004 (2011).

193 Farge, E. Mechanical induction of Twist in the Drosophila foregut/stomodeal primordium. *Current biology : CB* 13, 1365-1377 (2003).

194 Roy, R., Hohng, S. & Ha, T. A practical guide to single-molecule FRET. *Nature methods* 5, 507-516, doi:10.1038/nmeth.1208 (2008).

195 Piston, D. C., Nathan *The Fluorescent Protein Color Palette*, <http://www.olympusconfocal.com/applications/fpcolorpalette.html> (2004).

196 Shaner, N. C. *et al.* Improved monomeric red, orange and yellow fluorescent proteins derived from Discosoma sp. red fluorescent protein. *Nature biotechnology* 22, 1567-1572, doi:10.1038/nbt1037 (2004).

197 Scott, B. L. & Hoppe, A. D. Optimizing fluorescent protein trios for 3-Way FRET imaging of protein interactions in living cells. *Scientific reports* 5, 10270, doi:10.1038/srep10270 (2015).

198 Lin, M. Z. Fluorescent Proteins Illuminate Cell Biology. *Nat Rev Mol Cell Bio* (2010).

199 Greb, C. *Fluorescent Proteins – Introduction and Photo Spectral Characteristics*, <http://www.leica-microsystems.com/science-lab/fluorescent-proteins-introduction-and-photo-spectral-characteristics/> (2012).

200 Sprague, B. L. & McNally, J. G. FRAP analysis of binding: proper and fitting. *Trends in cell biology* 15, 84-91, doi:10.1016/j.tcb.2004.12.001 (2005).

201 Sabass, B., Gardel, M. L., Waterman, C. M. & Schwarz, U. S. High resolution traction force microscopy based on experimental and computational advances. *Biophysical journal* 94, 207-220, doi:10.1529/biophysj.107.113670 (2008).

202 Austen, K., Kluger, C., Freikamp, A., Chrostek-Grashoff, A. & Grashoff, C. Generation and analysis of biosensors to measure mechanical forces within cells. *Methods in molecular biology* 1066, 169-184, doi:10.1007/978-1-62703-604-7_15 (2013).

Publications

Austen, K.; Kluger, C.; Freikamp, A.; Chrostek-Grashoff, A.; Grashoff, C. (2013) "Generation and analysis of biosensors to measure mechanical forces within cells." *Methods in molecular biology* **1066**, 169-184

Austen, K.; Ringer, P.; Mehlich, A.; Chrostek-Grashoff, A.; Kluger, C.; Klingner, C.; Sabass, B.; Zent, R.; Rief, M.; Grashoff, C. (2015) "Extracellular rigidity sensing by talin isoform-specific mechanical linkages." *Nature cell biology*, **17**,1597–1606

Theodosiou, M.; Widmaier M.; Rognoni, E.; Veelders M.; Bharadwaj, M.; Böttcher, R.T.; Lambacher, A.; **Austen, K.**; Müller, D.J.; Zent, R.; Fässler, R. (2016) "Kindlin-2 cooperates with talin to activate integrins and induces cell spreading by directly binding paxillin." *Elife* **5**, doi:10.7554/eLife.10130.

Acknowledgements

First of all, I'd like to thank Dr. Carsten Grashoff for his support and supervision during the last -almost 5- years. In many hours of discussions you taught me to be critical and not be satisfied with hasty explanations and encouraged me to push my own boundaries. Retrospective, the time during my PhD made me a stronger and even more self-confident person and I owe you gratitude for this.

Special thanks to Reinhard Fässler, my 'Doktorvater'. Besides the valuable scientific input he also provided all the materials and support I needed to complete my work without hesitation.

I also want to thank the members of my thesis-committee Prof. Martin Biel, Prof. Tobias Bonhoeffer, Prof. Dietmar Martin, Prof. Christian Wahl-Schott and Prof. Klaus Förstemann for their willingness to examine my work.

Thanks to all my labmembers Andrea Freikamp, Dr. Anna Chrostek-Grashoff, Anna-Lena Cost, Carleen Kluger, Dr. Christoph Klingner and Pia Ringer. I have to point out Pia for the support with my paper and Anna for help wherever it was needed. Christoph, not only thanks for the computing stuff but also for everything else… guess you know what…

Beyond the Grashoff lab are many people how accompanied my during the time of the PhD and whom I'd like to thank for their everyday support and for becoming close friends within the last years: Dr. Christine Bauer, Birgit Blanck, Gisela Beck, Dr. Thomas Hauser, David Ries, Dr. Manuela Weitkunat and Dr. Cornelia Schönbauer. Furthermore, many other people from the Fässler department contributed to this thesis by various means and I only want to point out a few exemplary ones. Here special thanks to Dr. Moritz Widmaier, with whom I was collaborating and Klaus Weber and Dr. Armin Lambacher for all the technical support. Furthermore I'd like to thank Alexander Mehlich and Matthias Rief from the Technical University Munich for the friendly and productive collaboration. Without the single molecule calibrations Alex did, my paper wouldn't have been accepted in such a high ranked journal.

Special thanks go to my 'real friends' Christina, Basti, Oli, Margaux, Alex, Udo. I really enjoyed our 'D-Days' (that were actually transformed into 'W-Days') and the evenings together with fruitful discussions about the things that really matter in life.

Nicht zu vergessen sind meine Volleyball-people, ohne die ich wohl während der letzten Jahre des Öfteren verzweifelt wäre: Allen voran Johannes. Danke für alles was du tust und dafür, dass du so bist wie du bist. Meinen Mädels ein dickes Danke für die tollen Stunden, die ich mit euch verbringen darf - auf dem Feld und nebenher. Und natürlich meine Jungs! Was würde ich nur ohne euch machen? Euch zu begleiten und aufwachsen zu sehen gehört zu den tollsten Erfahrungen, die ich bisher machen durfte.

Danke auch an meine gesamte Familie: Oma Ingelore, Oma Luise und Opa Toni, Madeleine, Michael, Sonja, Petra, Eva und Tante Toni für alles was ihr für mich tut!

Last but most important: Mama und Koko! Eure Unterstützung ist nicht in Worte zu fassen. Danke, dass ihr mir in den letzten Jahre, na ja eigentlich schon immer, Rückendeckung gegeben habt bei allem was ich anstelle. Ihr zwei seid das Beste was mir passieren konnte!